January 2015

IMAGING SPECIFIC ABSORPTION RATE WITH MR THERMOMETRY USING PARAMAGNETIC LANTHANIDE COMPLEXES AND IN VIVO GABA MR SPECTROSCOPY IN MOVEMENT DISORDERS

Shalmali Dharmadhikari
Purdue University

Graduate School Form 30
Updated 1/15/2015

PURDUE UNIVERSITY
GRADUATE SCHOOL
Thesis/Dissertation Acceptance

This is to certify that the thesis/dissertation prepared

By SHALMALI T DHARMADHIKARI

Entitled

IMAGING SPECIFIC ABSORPTION RATE WITH MR THERMOMETRY USING PARAMAGNETIC LANTHANIDE COMPLEXES AND IN VIVO GABA MR SPECTROSCOPY IN MOVEMENT DISORDERS

For the degree of Doctor of Philosophy

Is approved by the final examining committee:

Ulrike Dydak Chair	John Nyenhuis
Chen Lin	
Keith Stantz	
Wei Zheng	

To the best of my knowledge and as understood by the student in the Thesis/Dissertation Agreement, Publication Delay, and Certification Disclaimer (Graduate School Form 32), this thesis/dissertation adheres to the provisions of Purdue University's "Policy of Integrity in Research" and the use of copyright material.

Approved by Major Professor(s): Ulrike Dydak

Approved by: Wei Zheng 4/16/2015

Head of the Departmental Graduate Program Date

IMAGING SPECIFIC ABSORPTION RATE WITH MR THERMOMETRY USING PARAMAGNETIC LANTHANIDE COMPLEXES AND IN VIVO GABA MR SPECTROSCOPY IN MOVEMENT DISORDERS

A Dissertation

Submitted to the Faculty

of

Purdue University

by

Shalmali T Dharmadhikari

In Partial Fulfillment of the

Requirements for the Degree

of

Doctor of Philosophy

May 2015

Purdue University

West Lafayette, Indiana

To my dearest aai, Tanmay and Avni

ACKNOWLEDGEMENTS

As I approach the completion of my Ph.D, I would like to look back on the past and thank everyone who made this possible.

First and foremost, I want to thank my advisor, Dr. Ulrike Dydak, for her incessant support and faith in me. A mentor's role in the academic development of a doctoral student is undeniable but, in my case, Dr. Dydak has provided me much more than that. By giving me the opportunity to continue my Ph.D under her guidance during some uncertain times, she motivated me to successfully complete my Ph.D. I am a better researcher today because she encouraged scientific curiosity and gave me freedom of thought. Her inspiring words, guidance and incredible support were instrumental in helping me successfully achieve my goals. I am deeply touched by all her support and kindness and am very grateful to have her as my mentor and friend. I am greatly obliged to Dr. Jim Murdoch, for his relentless contributions to all "GABA"-related matters, including simulations, basis set generation, data analysis, and proof reading abstracts and manuscripts. He never failed to impress me with his wit and enthusiasm and I thank him for all the enjoyable discussions.

I am appreciative of my former advisor, Dr. Navin Bansal, who encouraged me to pursue a Ph.D in Medical Physics and gave me my first Ph.D project. I am very grateful to Dr. Gary Hutchins for providing the financial support during my Ph.D transition and access

to the facilities at IUPUI for my research and training. I am also thankful to Dr. Wei Zheng, Dr. Keith Stantz, Dr. John Nyenhuis and Dr. Chen Lin for their helpful guidance while serving on my Ph.D committee. For all the interesting research opportunities and discussions, I am thankful to my collaborators Dr. Kenneth Byrd, Dr. Mario Dzemidzic, Dr. Laura Romito, Dr. Elizabeth Zauber and Dr. Christian Beste. My special thanks go to Dr. Yun Liang, Dr. Chen Lin and Dr. Keith Stantz, for the opportunity to get hands-on training on diagnostic imaging equipment. I also want to thank the MR techs, Traci, Michele, Rob and Courtney for their help with data acquisition.

Last but certainly not the least, I want to express my heartfelt gratitude to my exceptionally loving and supportive family. My beloved (late) aji and ajoba, who looked after me while my mom (aai) completed her education, taught me to stay positive during life's hardships. I am indebted to my parents, especially my aai, who worked hard to provide me with the best education and opportunities in life. I would not be what I am today without aai's love, discipline and guidance. I am very grateful to Mohan mama and mami, without whose financial support, my dream to pursue a Masters in the United States would have never been possible. I am very glad to have my sister, Sanika, as a confidante, with whom I had countless conversations sharing all the joys and griefs all these past years. My husband, Tanmay, has been my pillar of strength throughout my studies and I could not have successfully completed my Ph.D without his understanding, love and support. My daughter Avni, who is the apple of my eye, has helped me become a stronger and a better person and I am glad to have her in my life. I truly appreciate my entire family for enduring this long journey with me. Finally, I am thankful to all my friends that are a family away from home, for making these six years of Ph.D memorable.

TABLE OF CONTENTS

Page

Page

LIST OF TABLES

LIST OF FIGURES

Figure Page

Figure Page

Figure Page

LIST OF ABBREVIATIONS

^{1}H	Proton
CHESS	Chemical Shift Selective
Cho	Choline
C_T	Temperature coefficient
DA	Dopamine
DBS	Deep Brain Stimulation
DLPFC	Dorsolateral Prefrontal Cortex
GABA	Gamma-aminobutyric acid
Glu	Glutamate
Gpe	External Globus Pallidus
Gpi	Internal Globus Pallidus
GRE	Gradient Recalled Echo
MEGA-PRESS	Mescher-Garwood Point RESolved Spectroscopy
mIns	myo-Inositol
mM	millimole
MM30	macromolecule at 3 ppm
Mn	Manganese
MRI	Magnetic Resonance Imaging

MRS	Magnetic Resonance Spectroscopy
NAA	N-acetyl aspartate
PD	Parkinson's Disease
ppm	parts per million
preSMA	pre-supplementary motor area
PRESS	Point RESolved Spectroscopy
PRF	Proton Resonance Frequency
RF	Radio frequency
SAR	Specific Absorption Rate
SNR	Signal to Noise Ratio
SB	Sleep Bruxism
SL	Spin Lock
SN	Substantia Nigra
STN	Subthalamic nucleus
tCr	Total creatine
TE	Echo time
TI	Inversion Time
TMD	Temporomandibular disorder
$TmDOTP^{5-}$	Thulium 1,4,7,10-tetraazacyclododecane-1,4,7,10-tetrakis (methylene phosphonate)
TR	Repetition time
UPDRS	Unified Parkinson Disease Rating Scale

ABSTRACT

Dharmadhikari, Shalmali T. Ph.D., Purdue University, May 2015. Imaging Specific Absorption Rate With MR Thermometry Using Paramagnetic Lanthanide Complexes And In Vivo GABA MR Spectroscopy In Movement Disorders. Major Professor: Ulrike Dydak.

Magnetic Resonance Imaging (MRI) is a popular imaging modality due to its ability to provide excellent soft tissue contrast without exposure to ionizing radiation. It can be used for temperature monitoring (thermometry) as well as for assessing the biochemistry *in vivo* (MRS). This dissertation focuses separately on the development, application and quantitation issues of these two aspects of MRI.

Radiofrequency (RF)-induced tissue heating is a concern in MRI. The dosimetric quantity for monitoring RF heating is the Specific Absorption Rate (SAR) defined as the RF power absorbed per unit mass of tissue. A novel approach for imaging SAR from absolute temperature images obtained using a paramagnetic lanthanide complex-Thulium 1,4,7,10-tetraazacyclododecane-1,4,7,10-tetrakis (methylene phosphonate) ($TmDOTP^{5-}$) was developed. The effects of a bare-ended, insulated conductor in a phantom were investigated by 3D SAR imaging. 3D SAR maps were also generated using a high SAR sequence while varying the pulse duration. The high spatial resolution SAR maps correctly identified the local SAR rise near the wire end and also revealed increasing SAR with increasing pulse duration in the high SAR sequence, as expected. These results

demonstrate the potential of MR thermometry with paramagnetic lanthanide complexes for evaluating safety of implants, medical devices as well as different pulse sequences. The second part of the thesis is dedicated to the technique of measuring in vivo levels of the neurotransmitter γ-aminobutyric acid (GABA) using MRS. GABA is an inhibitory neurotransmitter in the brain which is involved in the control of fine movement and balance. GABA MRS with spectral editing was performed and GABA was quantified using custom fitting parameters in the tool LCModel to measure changes in movement disorders – particularly Parkinson's disease (PD) and sleep bruxism. Higher levels of thalamic GABA were detected in PD with correlation to disease severity indicating the possibility to use GABA MRS as a biomarker for PD progression. On the other hand, in the bruxers, lower levels of GABA correlating with higher levels of glutamate in the dorso-lateral prefrontal cortex were detected indicating disturbances in the GABAergic and glutamatergic pathways.

Lastly, since GABA quantification is a much discussed topic in literature with no one, clear and best approach, an effort was made to compare some popular fitting approaches in LCModel. Semi-synthetic simulated GABA spectra were used to test the accuracy, sensitivity and specificity of methods, all of which handled the baseline and macromolecules in the GABA spectra differently. Overall, the approaches using a fully flexible baseline ranked best in the tested aspects.

OUTLINE

This dissertation consists of projects based on two distinct magnetic resonance (MR) methodologies and will be presented in different chapters as outlined below:

Chapter 1. My PhD was started with a focus on development of MR thermometry using paramagnetic lanthanide complexes for evaluation of radio frequency heating in MRI. After two years of progress in this study, the experiments were halted due to the major professor's voluntary retirement from academia. Results from the initial experiments conducted in this project will be presented in this chapter.

Chapter 2. Change in major professor led to a change in my PhD research topic. The focus of my new research was the application of special edited magnetic resonance spectroscopy (MRS) techniques for quantification of gamma-aminobutyric acid (GABA) in movement disorders. This chapter will briefly discuss the role of GABA in movement disorders and the technique and challenges of GABA MRS.

Chapter 3. This chapter will focus on the application of GABA MRS in Parkinson's Disease (PD). Particularly the finding of significantly higher thalamic GABA in PD and its correlation with motor scores will be discussed as a potential biomarker of PD.

Chapter 4. Application of GABA MRS in sleep bruxism, which is also a movement disorder, will be discussed in this chapter. The significant findings of changes in levels of

GABA and glutamate in the dorso-lateral prefrontal cortex will be presented and discussed.

Chapter 5. The concluding chapter will focus on the comparison of GABA quantification strategies using different fitting methods in LCModel to determine their accuracy, sensitivity and specificity. A recommendation based on a current study will be made for future studies using GABA MRS.

CHAPTER 1. IMAGING SPECIFIC ABSORPTION RATE USING HYPERFINE SHIFTED RESONANCE OF PARAMAGNETIC LANTHANIDE COMPLEX

"Evaluation of RF safety by high temperature resolution MR thermometry using a paramagnetic lanthanide complex"

Submitted to Magnetic Resonance in Medicine, Minor revision pending.

1.1 INTRODUCTION

1.1.1 Radio frequency heating in MRI

Magnetic Resonance Imaging (MRI) uses radio-frequency (RF) pulses to excite MR-sensitive nuclei in the body. When RF pulses are used for altering the state of the spins, the energy exchange between the nuclei and pulses causes some power to be deposited in the material being excited. Due to T1 relaxation this absorbed RF power converts to heat inside the patient (M. A. Brown & Semelka, 2011). Moreover, the eddy currents induced due to the RF pulses can cause tissue heating which can become a safety hazard if not monitored. Specific absorption rate (SAR) is a dosimetric measure of the absorption of electromagnetic energy in the body. It is defined as the rate of energy absorbed per unit mass of material and is typically measured in watts per kilogram (W/kg). National and International agencies like the Food and Drug Administration (FDA), American Society

for Testing and Materials (ASTM), International Electrotechnical Commission (IEC) etc. have recommendations and guidelines to ensure that SAR is not exceeded beyond certain limits (ASTM, 2011; FDA, 2014; IEC, 2010). For instance, the current FDA limits for significant risk are as shown in

Table 1.

Table 1. FDA SAR limits for significant risk

Site	Dose	Time (min) equal to or greater than	SAR (W/kg)
whole body	averaged over	15	4
head	averaged over	10	3.2

Specific Absorption Rate (SAR) is a measure of the RF power deposited and is dependent on several factors that affect energy deposition. It depends on the resonance frequency (dependent on the magnetic field strength and the nuclei of interest), the RF pulse characteristics (type, amplitude, duration, duty cycle, etc.), the pulse repetition time, the type of RF coil used (linear vs. quadrature transmission, receive only vs. transmit and receive, etc.), the presence of conducting structures like implants and prosthetic devices and so on (Shellock, 2001). Hence accurate prediction of SAR is highly challenging with so many variables. SAR is used for determination of RF safety in MRI. With the availability of high-field MRI systems, special pulse sequences, and increasing usage of

implanted devices, it is critical to evaluate SAR better so as to increase the benefit to risk ratio to patient population.

1.1.2 SAR measurement concerns

The recommended method to measure SAR is based on measurement of temperature rise induced by the RF field over time. One such recommendation by ASTM, standard F2182-11a, describes a test procedure for evaluating the RF-induced temperature rise associated with an MR procedure that involves irradiation of an implant. This is done by applying an RF field capable of producing SAR of 2 W/kg or more for about 15 min and using fiber optic probes to measure implant heating. The local SAR is then estimated based upon the local temperature change measurements according to the equation

$$SAR = c\,\Delta T/\Delta t \qquad [1]$$

where c is the specific heat capacity of the phantom material (4,160 J/kg °C for water) and ΔT is the change in temperature (°C) over time Δt (s). The SAR is determined by calculating $\Delta T/_{\Delta t}$ using a linear fit over the 15 min period.

Although this method offers a straightforward way of measuring SAR, it is limited to a local measurement. Temperature measurements made with temperature probes suffer from several drawbacks including the effect of probe sensitivity on the measurement, probe area in contact with material, probe location, etc. as shown in earlier studies (Bassen, Kainz, Mendoza, & Kellom, 2006; Mattei et al., 2007). Hence local measurements of temperature using physical probes may not be adequate in the presence of hotspots or large temperature gradients. Studies have shown that local SAR increases

can be as high as 14% for high-field systems (Wolf, Diehl, Gebhardt, Mallow, & Speck, 2013) and hence spatial SAR information is crucial for comprehensive determination of RF safety. The current recommended calorimetric methods based on temperature probe measurements do not have sufficient spatial resolution. Similarly, the RF dosimeters that use transducers for measuring SAR are limited to whole body SAR measurement and are incapable of identifying local SAR increase (Qian, El-Sharkawy, Bottomley, & Edelstein, 2013). Lack of spatial temperature information could potentially miss hotspots leading to an underestimated SAR.

While simulation and numerical modeling methods like Finite Difference Time Domain (FDTD) may provide the needed spatial temperature distribution (Cao, Park, Cho, & Collins, 2014; Jin & et al., 1996; S.-M. Park, Kamondetdacha, & Nyenhuis, 2007; S. M. Park, Kamondetdacha, Amjad, & Nyenhuis, 2005), accurate computation of the fields near the implants is a challenging task due to the presence of extremely high spatial gradients at these locations and the need for very fine computational structures (Bassen et al., 2006). Methods based on temperature dependence of T1 have good temporal resolution but the temperature sensitivity is only ~10 ms/K making it challenging to detect small changes in temperature in the T1 maps (Gensler et al., 2012). MR thermometry methods based on water proton frequency shift have been proposed for temperature mapping (Ishihara et al., 1995; Liu et al., 2014; Poorter et al., 1995; Rieke & Butts Pauly, 2008). These methods can provide high spatial and temporal resolution, but still do not have enough temperature resolution necessary for evaluation of RF heating during MRI. Since water proton chemical shift sensitivity is only ~0.01 ppm/°C, such

small temperature changes produce very small changes in chemical shifts (~0.0022 ppm) which can be challenging to measure.

1.1.3 MR Thermometry using Paramagnetic Lanthanide Complex for measurement of SAR

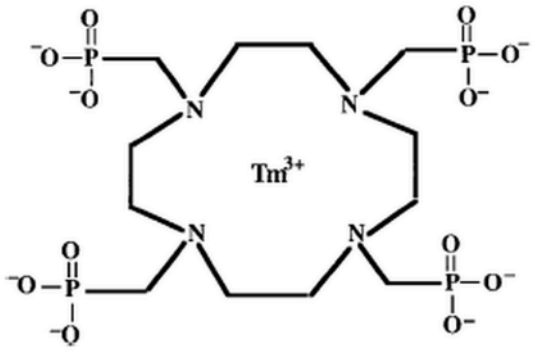

Figure 1.1 Structure of $TmDOTP^{5-}$ molecule

MR Thermometry using paramagnetic lanthanide complexes can provide the high spatial and temperature resolution needed for SAR measurement. One of the complexes of interest to MR thermometry is Thulium 1,4,7,10-tetraazacyclododecane-1,4,7,10-tetrakis (methylene phosphonate) or $TmDOTP^{5-}$. $TmDOTP^{5-}$ has six magnetically non-equivalent groups of protons (H_1-H_6) and four magnetically equivalent phosphorus atoms due to its fourfold symmetry as depicted in (C. S. Zuo, Metz, Sun, & Sherry, 1998). All the six groups of protons have different chemical shifts and sensitivity to temperature as shown in Table 2 . The chemical shift of a proton signal H_6 at -155.7 ppm is much more sensitive to temperature (0.87 ppm/°C) than the water proton chemical shift (0.01 ppm/°C) (Hindman, 1966; Schneider, Bernstein, & Pople, 1958; C S. Zuo et al., 1996).

Additionally, MR thermometry with the paramagnetic lanthanide complexes is less susceptible to magnetic field inhomogeneity and instrumental instabilities compared to water and can provide absolute temperature measurements using water as reference (James, Gao, Miller, Babsky, & Bansal, 2009; C S. Zuo et al., 1996; C. S. Zuo et al., 1998). All these properties make MR thermometry using $TmDOTP^{5-}$ well-suited for SAR measurement. Furthermore, the current methods of SAR calculation do not account for any heat losses that may contribute to the temperature changes occurring during MRI. Hence, there is a critical need for a method that can provide sufficient temperature and spatial resolution, and model the heat exchange effectively.

Table 2. Chemical shift and temperature co-efficient (C_T) of $TmDOTP^{5-}$ proton groups (adapted from (C. S. Zuo et al., 1998))

	H1	H2	H3	H4	H5	H6
Shift (ppm) at 25 °C	-193.7	92.8	72.7	513.6	-398.9	-155.7
C_T (ppm/°C)	1.08	-0.54	-0.42	-2.88	2.19	0.87

The overall goal of this project was to develop, validate and apply a MR thermometry technique using a paramagnetic lanthanide complex Thulium 1, 4, 7, 10-tetraazacyclododecane-1, 4, 7, 10-tetrakis (methylene phosphonate) ($TmDOTP^{5-}$) for evaluation of SAR.

The specific aims of this project were:

Aim 1(a): To develop a high temperature and high spatial resolution MR thermometry technique using the paramagnetic lanthanide complex $TmDOTP^{5-}$ for imaging absolute temperature in phantoms.

Hypothesis 1(a): 3D absolute temperature images with high spatial and temperature resolution can be obtained using $TmDOTP^{5-}$ which can be further used to accurately meassure SAR with high spatial resolution.

Aim 1(b): To develop and apply a mathematical model for imaging SAR from absolute temperature images obtained in phantoms.

Hypothesis 1(b): The temperature change produced in phantoms during MRI is a combined effect of RF heating as well as heat loss due to heat dissipation. Use of high resolution absolute temperature images with an improved model accounting for heat dissipation for SAR calculation will enable accurate and high resolution imaging of SAR.

Aim 2: To apply the SAR imaging method to determine the effects of a) a metallic wire (conductor) and b) a SAR-intensive pulse sequence, in a phantom for evaluating RF safety.

Hypothesis 2: Introduction of a metal conductor perturbs the electric field in the phantom causing localized areas of heating (hot-spots). Pulse sequences that have intrinsically high SAR need to be evaluated for RF safety. The ability to image SAR will provide knowledge of the spatial heating patterns produced in these cases.

1.2 MATERIALS AND METHODS

1.2.1 MR System and phantom

MR experiments were performed on a Varian 9.4 T, 31-cm diameter horizontal bore system (*Varian, Palo Alto, CA, USA*) using a quadrature birdcage RF coil (40-mm

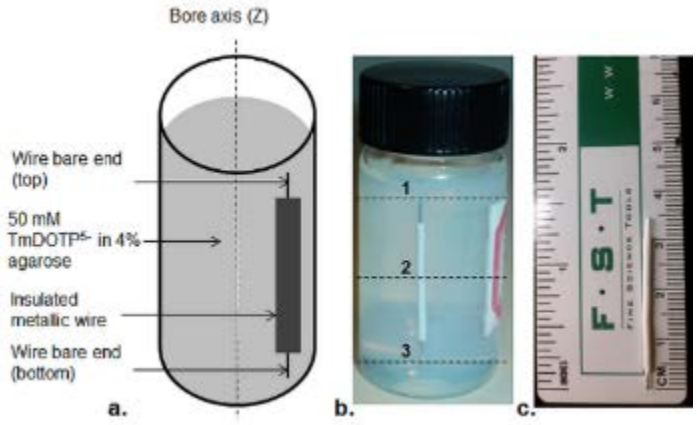

Figure 1.2 a) Schematic of phantom setup and b) actual photo 50 mM $TmDOTP^{5-}$ in 4% agarose gel with c) bare-ended insulated wire inserted in it. The dashed lines in (b) show three representative regions for comparison of SAR.

diameter, 80-mm length) dual tuned to 400 MHz for ^{1}H and 106 MHz for ^{23}Na. A 30-ml cylindrical vial (25-mm diameter and 6 mm in length) filled with 50 mM $TmDOTP^{5-}$ (formula: $TmC_{12}H_{24}N_4O_{12}P_4Na_5 \bullet 5H_2O$) (*Macrocyclics, Dallas, TX, USA*) in 4% agarose gel prepared in normal saline was used as the phantom.

1.2.2 Set-up and data acquisition

The phantom was equilibrated to the scanner temperature by keeping it in the magnet bore overnight before the experiment. A temperature probe taped outside the phantom was used to monitor the ambient temperature throughout the experiment. The phantom

was firmly wrapped in paper to minimize losses to surrounding. Before each experiment, the magnet was shimmed to a line width of ≈100 Hz for water resonance (4.7 ppm).

1.2.3 Calibration of temperature coefficient of $TmDOTP^{5-}$

$TmDOTP^{5-}$ contains six magnetically non-equivalent groups of protons (H_1 to H_6), each of which has a different chemical shift and temperature coefficient (C. S. Zuo et al., 1998). The H_6 resonance from $TmDOTP^{5-}$ was used because of its desirable combination of chemical shift temperature dependence and line width (C. S. Zuo et al., 1998). Temperature dependence of the chemical shift difference between the H_6 proton resonance from $TmDOTP^{5-}$ and water was determined by MR spectroscopy using a phantom inserted with a fiberoptic probe. The fiberoptic probe (*Photon Control Inc., Canada)* used for calibration experiments had an accuracy = ± 0.01 °C. The transmitter offsets (tof) for on-resonance condition for the H_6 resonance from $TmDOTP^{5-}$ (-155 ppm) (C S. Zuo et al., 1996) and water (4.7 ppm) were noted as $tof_{TmDOTP5^-}$ and tof_{H2O}, respectively, and kept constant throughout the experiment. ^1H water and $TmDOTP^{5-}$ spectra were obtained alternatively using a 500 μs sinc-shaped 90° excitation RF pulse followed by acquisition of 2000 data points for $TmDOTP^{5-}$ and 8000 data points for water over a spectral width of 40 kHz. Phantom temperature was recorded from the fiberoptic probe after each $TmDOTP^{5-}$ spectrum. A plot of the difference in chemical shifts of water and $TmDOTP^{5-}$ signals (ΔF (ppm)) as a function of the measured temperature (°C) was made and the intercept (c_0) and the slope (c_1) were obtained from the plot. The calibration constants were used in future imaging experiments to compute absolute temperature images from differences in chemical shifts of $TmDOTP^{5-}$ and water.

1.2.4 Absolute temperature imaging using $TmDOTP^{5-}$

3D MR images were acquired using the same phantom (control) as used in the calibration experiments. Before each experiment, shimming was done to achieve a line width of about 100 Hz for water resonance (4.7 ppm). After shimming, water and $TmDOTP^{5-}$ spectra were obtained and the resonance frequencies were determined. The on-resonance tof_{H2O} and $tof_{TmDOTP5^-}$ were noted and kept constant for water and $TmDOTP^{5-}$ imaging. Phase-sensitive 3D ^1H water and $TmDOTP^{5-}$ images were acquired one after the other using a 3D GRE imaging sequence with a 500 μs sinc-shaped 90° excitation RF pulse and the following parameters: repetition time (TR) = 150 ms, echo time (TE) = 1.1 ms, data matrix = 64 (x-axis) × 64 (y-axis) × 128 (z-axis), and field of view (FOV) = 32 × 32 × 64 mm^3. One transient was collected for each phase-encoding step for water imaging. Weighted signal summation technique was employed in two phase encode directions to improve signal to noise ratio (SNR) during $TmDOTP^{5-}$ imaging (Bansal & Seshan, 1995). In this technique, the number of signal transients summed at different phase-encoding steps are varied such so as to obtain similar signal conditioning effects as produced by apodization with a Gaussian function. The time for acquisition of each 3D ^1H water and $TmDOTP^{5-}$ image pair was approximately 4 min. The average phantom temperature was also monitored by collecting pulse-acquire spectra of water and $TmDOTP^{5-}$ using the same parameters as used in the calibration experiments. Repeated sets of 3D water and $TmDOTP^{5-}$ images and spectra were collected continuously. The ambient temperature was measured using a fiberoptic probe placed in the proximity of the phantom throughout

the experiment. The experiments were conducted until the measured phantom temperature plateaued.

To demonstrate the effects of a bare-ended insulated metallic conductor on SAR distribution, a piece of a coaxial wire (AWG 22, 35-mm in length) was introduced in the control phantom. The outer plastic sheath and metallic shield were completely removed and 3-4 mm of the inner electric insulation at the ends was stripped to expose bare ends. The wire was placed in the phantom along the long axis away from the center as shown in Figure 1.2. 3D ^{1}H water and TmDOTP^{5-} images were acquired using the same imaging parameters and repeating the same steps as described in the above experiment.

Additionally, a high SAR 3D T1rho sequence was used to demonstrate the ability to image the effect of pulse sequence parameters on absolute temperature and SAR. The 3D GRE sequence for water was modified by addition of a pre-encoded pulse cluster consisting of a pair of non-selective 90° pulses separated by an on-resonance, long duration spin lock (SL) pulse cluster. The same control phantom as used in calibration experiments was used. 3D ^{1}H water and TmDOTP^{5-} images and spectra were acquired continuously using the same parameters as used in the above experiments, in addition to the SL pulse cluster in the ^{1}H MRI experiment. Separate experiments were conducted to evaluate the effect of increasing SL pulse duration (0 (equivalent to conventional GRE), 50 and 100 ms) on SAR.

All the data processing and analysis was done using MATLAB (*ver. R2009b, Mathworks, Natick, MA, USA*). 3D images of difference in chemical shifts of water and TmDOTP^{5-}

(ΔF) were calculated from the differences in phase shifts (ΔΦ) of the collected 3D water and $TmDOTP^{5-}$ images, using the relationship (James et al., 2009)

$$\Delta F = \frac{1}{f_0}\left[(tof_{water} - tof_{TmDOTP5-}) + \left(\frac{\Delta\phi}{360*\tau}\right) + \left(\frac{n_{wrap}}{\tau}\right)\right] \quad [2]$$

where f_0= 400.395 MHz was the spectrometer frequency, tof_{H2O} and tof_{TmDOTP}^{5-} were the transmitter offsets used for collecting water and $TmDOTP^{5-}$ images, respectively, t was the echo time for imaging sequence and n_{wrap} = 0, 1, 2,...n was the number of phase wraps. 3D absolute temperature images were calculated from the ΔF images using the relationship

$$T = (c1 * \Delta f) + c0 \quad [3]$$

where c0 and c1 were the calibration constants derived from calibration experiments.

1.2.5 Calculation of SAR from absolute temperature images

The temperature changes in the phantom are due to the competing mechanisms of RF heat deposition and heat loss to the environment (Gorny & et al., 2008). Hence, to compute the SAR images from the absolute temperature images, a cooling term was also incorporated in the model in addition to the RF heat deposition. The recommended model as in Eq. [1] was modified to the form

$$\frac{dT(t)}{dt} = -k * (T(t) - T_a) + \frac{SAR}{c} \quad [1]$$

where $dT(t)/dt$ is the rate of change in temperature (°C/s), *T(t)* is the measured phantom temperature (°C), T_a is the ambient temperature (°C), *k* is a cooling constant (s^{-1}), and *c* is

the specific heat capacity of water (4186 J/kg °C) (Gorny & et al., 2008).

A voxel-by-voxel fitting of the change in absolute temperature in consecutive images over time ($dT(t)/dt$) as a function of difference between the sample and ambient temperature ($T(t)-T(a)$) was performed using the above model and 3D SAR and cooling constant images were obtained.

1.3 RESULTS

1.3.1 Calibration experiment

In our experiments, a temperature co-efficient (C_T) of 1.03 ppm/°C, almost 10^2 times that of water was obtained for $TmDPTP^{5-}$ (Figure 1.3) similar to that obtained by others (Sun

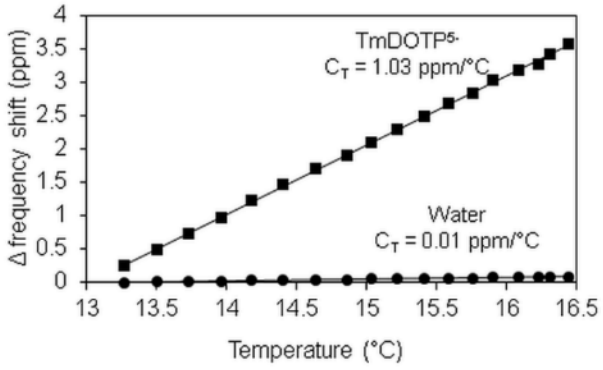

Figure 1.3 Change in ^1H chemical shift of water and $TmDOTP^{5-}$ signal with temperature. The chemical shift of $TmDOTP^{5-}$ is $\approx 10^2$ times more sensitive than water.

et al., 2000). The difference in chemical shifts of water and $TmDOTP^{5-}$ (ΔF, ppm) were plotted against the phantom temperatures measured using fiberoptic probe (T, °C) as seen

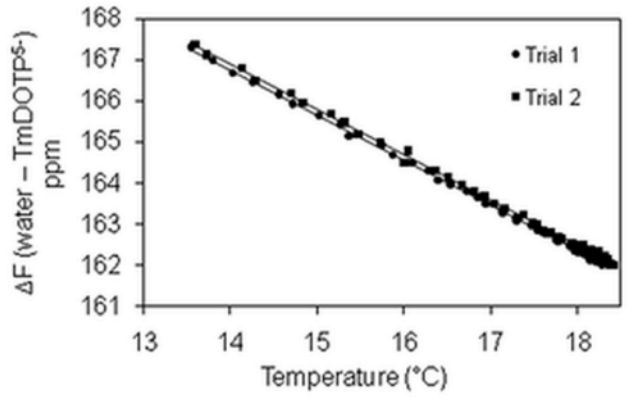

Figure 1.4 Plot for obtaining calibration constants between difference in chemical shift of $TmDOTP^{5-}$ and water and measured temperature.

in Figure 1.4 and calibration constants were obtained by repeating the experiments twice. The plots yielded a slope (c_1) of −1.1035 (± 0.0005) ppm/°C, and an intercept (c_0) of 182.25 (± 0.0005) which were then used to compute the absolute temperature images as per Eq. [3].

1.3.2 Effect of an insulated bare-ended metallic conductor on SAR

Figure 1.5 shows the computed 3D absolute temperature and SAR images in a control phantom (top row) and a phantom with a wire (bottom row) acquired using a 3D GRE sequence. The SAR of the control phantom was seen to be more or less homogenous except slightly higher SAR near the top of the phantom and sides compared to the bottom and center of phantom. Introduction of a conductive wire to the phantom altered the SAR distribution and a sharp local SAR increase was seen near the exposed ends of the wire (Figure 1.5).

The average SAR profile was computed in a 3 x 3 voxel neighborhood along the phantom's long axis where a wire was be inserted later as shown in Figure 1.6. About 29%

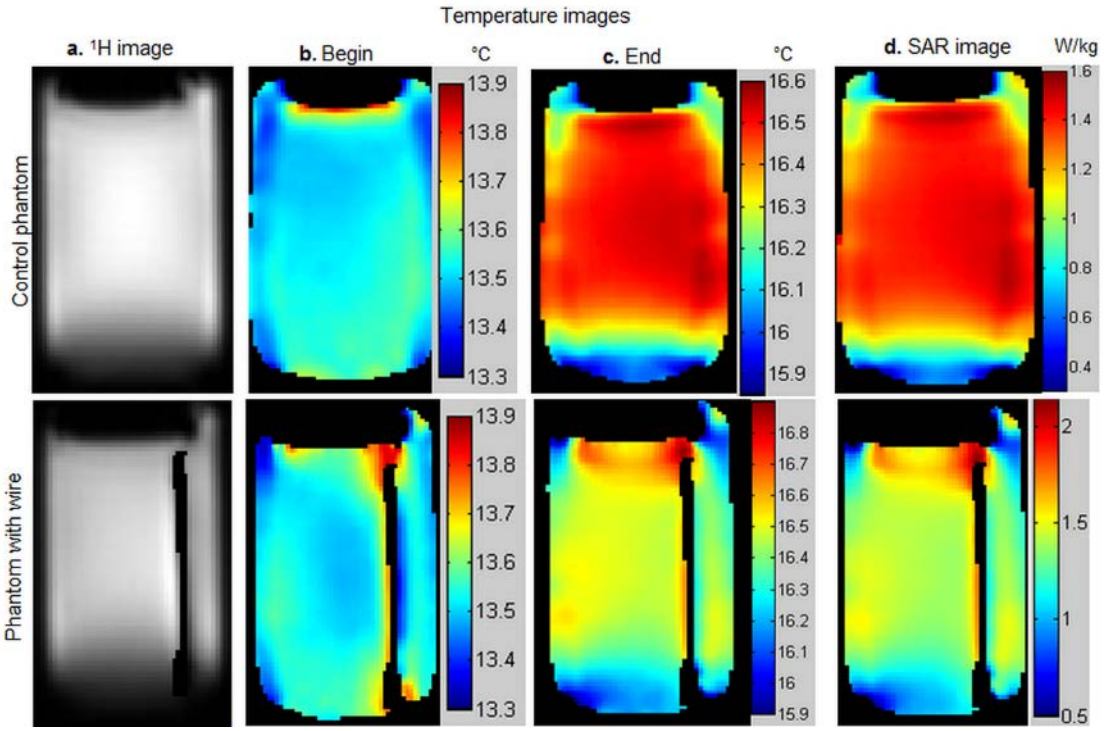

Figure 1.5 Representative sagittal slices of a phantom without (top) and with (bottom) a bare-ended insulated wire, acquired using a 3D GRE sequence. Figure shows a) ^{1}H image, b) and c) temperature images at the start and end of experiment, and d) SAR image.

elevation in average SAR was observed around the exposed end of the wire (1.8 W/g), compared to the rest of the phantom (1.4 W/kg) and at same location in the control phantom (1.4 W/kg). The average SAR profile was also computed along the phantom's diameter (x-y plane) in a 3 x 3 voxel neighborhood at three axial slice locations as represented in Figure 1.7 in both the phantoms. At region 1, which was the axial slice corresponding to the top exposed end of the wire, and along the diameter, the average SAR in the control phantom and the phantom with wire had a similar distribution with slightly higher SAR in phantom with wire (Figure 1.7a). However, along a plane through the wire, an elevation in average SAR (1.8 W/kg) was observed compared to the center (1.6 W/kg) as well as to the control phantom in same plane (1.4 W/kg) (Figure 1.7b).

At region 2, which corresponded to the central axial slice, the average SAR in the

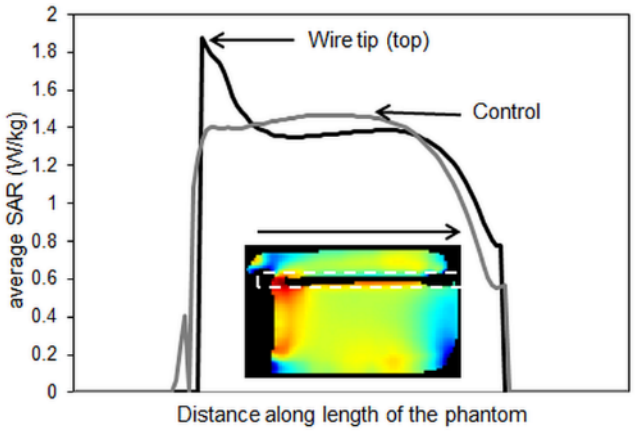

Figure 1.7 A plot of average SAR, computed in a 3 x 3 voxel neighborhood around the length of the wire as seen in the representative slice (inset) in control phantom (gray) and phantom with wire (black).

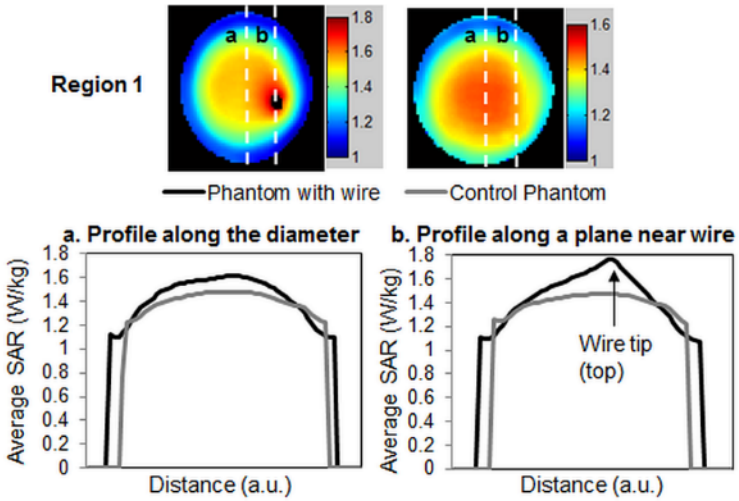

Figure 1.6 Average SAR profile in the top axial slice of the phantom (near the top exposed end) computed in a 3x3 voxel neighborhood along a) phantom diameter and b) off-set from phantom diameter near wire exposed end in the phantom with wire (black) and control phantom (gray).

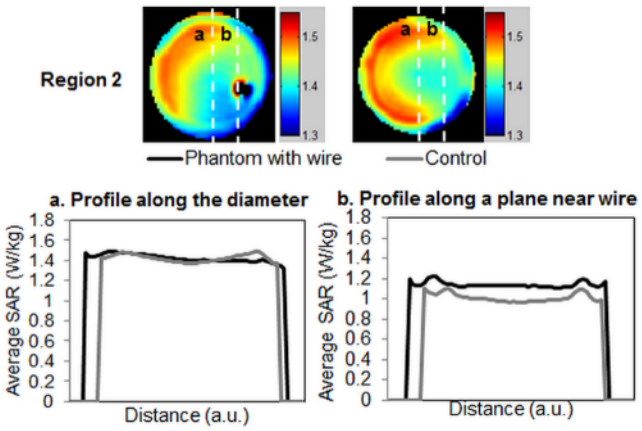

Figure 1.9 Average SAR profile in the middle axial slice of the phantom (away from the exposed ends) computed in a 3x3 voxel neighborhood along a) phantom diameter and b) off-set from phantom diameter near wire exposed end in the phantom with wire (black) and control phantom (gray).

phantom with wire as well as control phantom was higher along the edges compared to the center (Figure 1.8). At region 3, which was the axial slice corresponding to the lower exposed end of the wire, along the diameter, the average SAR in the control was higher at the surface and lower in the middle whereas in the phantom with the wire, it was higher in the center (Figure 1.9a). However, along a plane through the wire, an elevation in

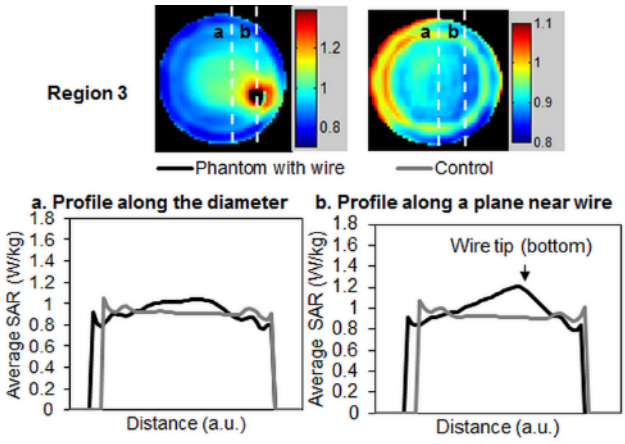

Figure 1.8 Average SAR profile in the bottom axial slice of the phantom (near the bottom exposed end) computed in a 3x3 voxel neighborhood along a) phantom diameter and b) off-set from phantom diameter near wire exposed end in the phantom with wire (black) and control phantom (gray).

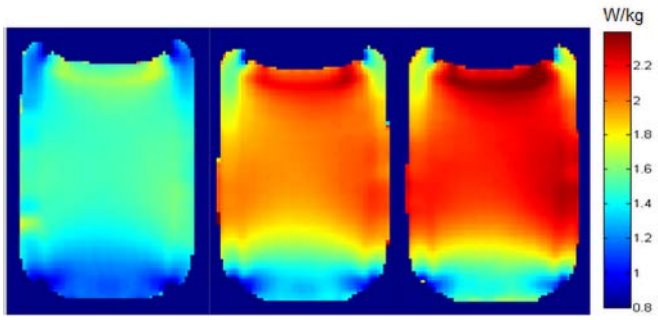

Figure 1.10 Left to right, representative SAR images of a control phantom acquired with 3D T_1rho sequence and SL pulse duration of 0, 50 and 100 ms, respectively.

average SAR (1.2 W/kg) was observed compared to the same location in the control (0.9 W/kg) (Figure 1.9b). The overall average SAR of the entire phantom with the wire was higher than that of the control (wire=1.42 ± 0.13 W/kg vs control= 1.3 ± 0.03 W/kg).

1.3.3 Effect of SAR-intensive pulse sequence on SAR

Figure 1.10 shows representative sagittal SAR images computed in the control phantom for increasing pulse duration. The T1rho sequence revealed small but higher overall average SAR with increasing SL pulse duration. For SL = 0, 50, and 100 ms, average SAR was 1.3 ± 0.03, 1.79 ± 0.26, and 1.97 ± 0.17 W/kg, respectively.

1.4 DISCUSSION AND CONCLUSION

The computed temperature and SAR images were found to be sensitive to small spatial variations in temperature and SAR. The insulated metallic wire with bare ends was used to simulate the presence of a lead-wire or implant in the phantom. It was used mainly to demonstrate the feasibility of detecting RF heating effects of such a conducting wire inside a phantom during MRI and did not necessarily cause maximal heating condition.

Nevertheless, high temperature and elevated SAR at the wire exposed end was identified, which is in agreement with the previously shown higher rate of temperature change produced at the implant lead (Mohsin, Nyenhuis, & Masood, 2010; S.-M. Park et al., 2007; Yeo, Wang, Loew, Vogel, & Hancu, 2011). The SAR of the control phantom was higher at the top compared to the bottom (Figure 6a and 8a). Similarly, the SAR at the top exposed end of the wire was higher than that at the lower exposed end (Figure 6b and 8b) indicating a difference in energy deposition of the coil itself. This RF coil energy deposition heterogeneity may be attributed to the presence of capacitors gaps on that part of the RF coil. To investigate the effects of a high-SAR sequence, the T1rho sequence was chosen due to its high SAR characteristic, simplicity and similarity to a GRE. T1rho pulse sequences require more RF power than the conventional sequences due to the addition of a long duration SL pulse (Regatte, Akella, Borthakur, Kneeland, & Reddy, 2003; Wheaton, Borthakur, Corbo, Charagundla, & Reddy, 2004) and the computed SAR images were sensitive to detect small changes in SL duration.

In our proposed model, heat losses to the environment were accounted for by including a general cooling term. However, it is possible that certain heat losses occurred within the phantom as a result of longer imaging times due to thermal diffusion, although heating as a result of imaging was continuous. Since RF heating is dependent on the pulse sequence parameters, different temperature and SAR patterns could emerge if different parameters were adopted (lower flip angle, low-resolution imaging plane resulting in shorter scan times, etc). Furthermore, due to the complexity involved in estimating the heat

dissipation by different mechanisms like perfusion, perspiration, etc. in actual patients, it may be reasonable to exclude such heat losses and to calculate the worst-case SAR.

A few limitations of the study include low temporal resolution of SAR images, the development of the technique on an ultra-high field system and the use of $TmDOTP^{5-}$ among other Tm^{3+} complexes. Due to the pilot nature of this study, the imaging parameters were optimized for obtaining 3D images with good SNR and spatial resolution. This resulted in a temporal resolution of 4 min for the computed temperature and SAR images.Although the current study was conducted only on a preclinical, high field strength scanner, earlier studies by Coman et. al and Zuo et. al. have shown that the lanthanide complexes of Thulium retain their high chemical shift sensitivity to temperature even at clinically relevant field strengths with only nominal SNR loss (Coman, Trubel, & Hyder, 2010; Chun S Zuo, Mahmood, & Sherry, 2001). Further experiments are needed to evaluate and establish this technique at a clinical field strength.

One of the advantages of using $TmDOTP^{5-}$ for SAR measurement is the high temperature sensitivity of ^{1}H chemical shift compared to other Tm^{3+} complexes. In addition, ^{31}P chemical shifts in $TmDOTP^{5-}$ also exhibit high temperature sensitivity and hence can be used for testing ^{31}P coils and pulse sequences (C S. Zuo et al., 1996). $TmDOTP^{5-}$ has been used to induce temperature-dependent hyperfine shifts in ^{23}Na signals for MR thermometry (Shapiro, Borthakur, & Reddy, 2000) and hence may also be used for testing ^{23}Na coils and sequences. These were the primary reasons for selection of $TmDOTP^{5-}$ in our study. Currently, the use of $TmDOTP^{5-}$ is limited to phantom experiments due to its possible toxic effect in animals. However, the same technique may

be applied in vivo using another paramagnetic lanthanide complex, $TmDOTMA^-$, which is ≈60 times more sensitive to temperature than water and which has been used for absolute temperature measurements.

The presence of a large number of variables influencing the RF heating process makes it tedious to perform extensive and exhaustive experimental measurements. While simulation approaches based on numerical tools may be useful to limit the actual number of experimental measurements required, such methods need appropriate experimental validation to get reliable results (Mattei, Calcagnini, Censi, Triventi, & Bartolini, 2010). This can be facilitated by using MR thermometry with paramagnetic lanthanide complexes. While MRI artifacts were not detected for the specific conductor used, some metal implants may cause substantial image artifacts including signal loss. Careful selection of parameter and pulse sequences can be used to avoid or reduce such artifacts, thus, enabling the use of the proposed method for evaluation of heating due to implant (Hargreaves et al., 2011; Lu, Pauly, Gold, Pauly, & Hargreaves, 2009).

We propose a novel method for calorimetric measurement of SAR using hyperfine shifted resonance from $TmDOTP^{5-}$. The developed MR technique for imaging of absolute temperature and SAR with a superior temperature and spatial resolution will have great potential in providing accurate understanding of RF heating during MRI and can be of significant interest for evaluation of RF coils, medical implants and devices and new pulse sequences.

CHAPTER 2. GAMMA-AMINOBUTYRIC ACID (GABA) MR SPECTROSCOPY IN MOVEMENT DISORDERS

2.1 GABA AND ITS LINK TO MOVEMENT DISORDERS

Gamma-aminobutyric acid (GABA) is an important inhibitory neurotransmitter in the mammalian brain. It is synthesized from glutamate by the enzyme glutamic acid decarboxylase in the GABAergic neurons. Although the typical GABA concentration in the brain is only approximately 1 millimolar (mM), it plays a vital role in the control of movement. Alterations in GABA levels have been linked to several movement

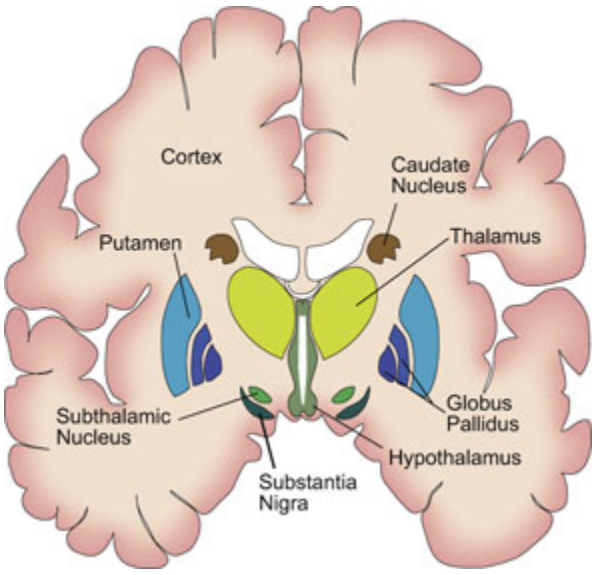

Figure 2.1 Representation of basal ganglia and surrounding structures involved in motor control.

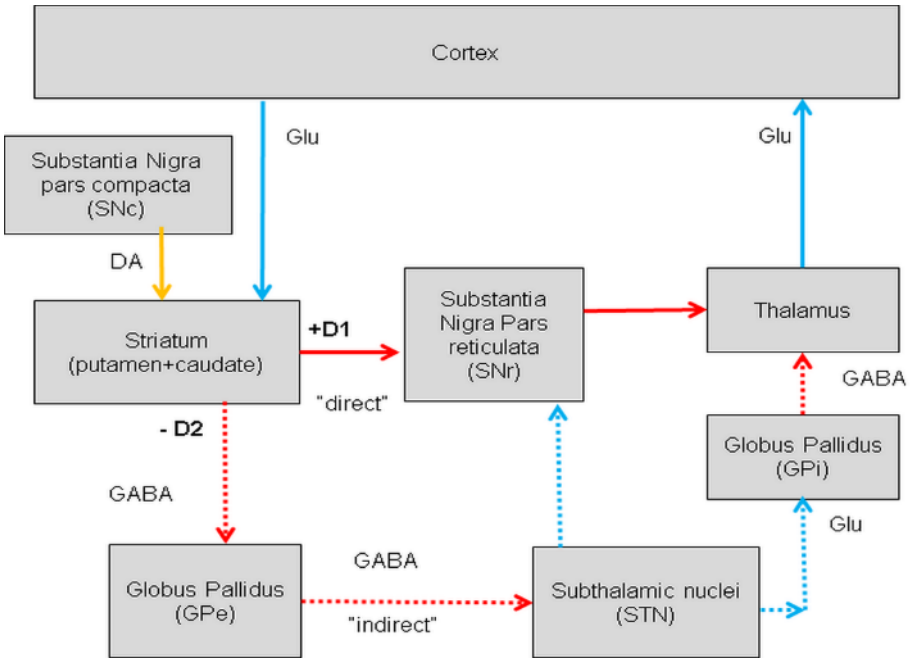

Figure 2.2 Direct and indirect pathway of basal-ganglia.

and psychiatric disorders (Emir, Tuite, & Öz, 2012; Z Long et al., 2013; Öngür, Prescot, McCarthy, Cohen, & Renshaw, 2010; Öz et al., 2006; Isabelle M Rosso et al., 2013).

The basal ganglia (BG) are a group of structures in the brain that are involved in motor and cognitive processing and are part of a neuronal network organized in parallel circuits (Obeso, Rodríguez-Oroz, Rodríguez, Arbizu, & Giménez-Amaya, 2002). The BG comprise the caudate nucleus and putamen (neostriatum), the ventral striatum, the external and internal pallidal segment (GPe and GPi, respectively), the subthalamic nucleus (STN), and the substantia nigra with its pars reticulata and pars compacta (SNr and SNc, respectively) (Galvan & Wichmann, 2007) (Figure 2.1). The BG are components of larger circuits (motor circuit) that involve thalamus and cortex whose major inhibitory and excitatory neurotransmitters are GABA and glutamate (Glu),

respectively. The motor circuit is most relevant to the pathophysiology of movement. Motor control is governed by basal ganglia-thalamocortical circuits via two major pathways – the direct pathway and the indirect pathway. The direct pathway involves sequential GABAergic inhibitory synapses in the SNr and the thalamic nuclei, releasing excitatory glutaminergic thalamo-cortical projections (P. Brown & Marsden, 1998). The direct pathway, therefore, results in the excitation of the motor cortex by the thalamus. Once stimulated, the cortex projects its own excitatory outputs to the brain stem and ultimately muscle fibers via the lateral corticospinal tract. The indirect route, on the other hand, facilitates suppression of thalamo-cortical activity via the STN and the GPi/SNr (P. Brown & Marsden, 1998). This results in decreased stimulation of the motor cortex by the thalamus and reduced muscle activity (Galvan & Wichmann, 2007). Thus, the indirect and direct pathways have opposite and highly balanced effects on motor activity. These pathways are illustrated in Figure 2.2.

Both the BG pathways are modulated by the SNc, which produces the neurotransmitter dopamine (DA). DA has an excitatory effect on the direct pathway (causing movement) but an inhibitory effect on the indirect pathway (preventing movement). Thus, in the presence of DA, D1-receptors in the basal ganglia stimulate the GABAergic neurons increasing movement, while the D2-receptors in the basal ganglia inhibit these GABAergic neurons, reducing the inhibitory effect of the indirect pathway. The control of movement is thus achieved via interactions between the direct and indirect pathways (Wichmann & Delong, 2007). Abnormal increment or reduction in the inhibitory output

activity of BG gives rise, respectively, to poverty and slowness of movement (i.e., Parkinson's disease) or dyskinesias (Obeso et al., 2002).

2.2 DETECTION OF GABA USING MRS

^{1}H magnetic resonance spectroscopy (MRS) is a very useful tool for the in vivo study of brain metabolism and physiology. It provides information about energy metabolism (in the form of creatine, phosphocreatine, etc.), about neurotransmission (through the detection of glutamate, GABA, etc.), neuronal integrity (through measurement of N-acetylaspartate) and about membrane metabolism and integrity via choline detection. The signal amplitudes of an MRS acquisition and the resultant peaks in the reconstructed spectrum are directly related with the number of resonating nuclei and the amount of substance seen by the MRS experiment. Thus the spectral peaks and patterns provide a direct, but not absolute, measure for the concentration of the metabolites (Stagg & Rothman, 2013). Figure 2.3 shows a such representative ^{1}H brain spectrum at 7T.

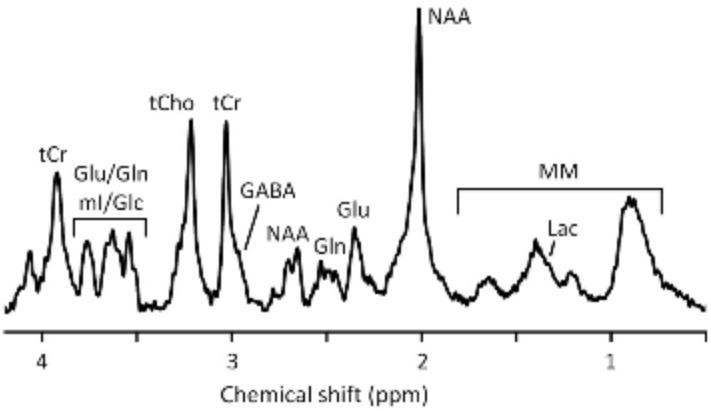

Figure 2.3 A representative short echo time brain spectrum acquired at 7 T.

However, in vivo brain MRS has some challenges. At lower field strengths, one prominent limitation is the spectral overlap that can hinder the identification of individual components. Peak broadening due to field inhomogenities and the millimolar concentrations of metabolites, which can be difficult to detect in low signal to noise spectra are some of the other challenges that need to be overcome for successful in vivo acquisition. Detection of low concentration GABA is, thus, difficult by conventional MRS at a field strength of 3T since the NMR-detectable GABA peak at 3 ppm is overlapped by the much larger creatine peak, and is not well resolved at lower field strengths and in the presence of magnetic field inhomogenities.

A special editing technique based on the spin-spin coupling of the molecules was introduced by Rothman and has become popular for GABA spectroscopy (D L Rothman, Behar, Hetherington, & Shulman, 1984) (D. L. Rothman, Petroff, Behar, & Mattson, 1993). Spectral editing is typically defined as a technique that utilizes scalar coupling to achieve spectral simplification (de Graaf, 2014). The electronic shielding of a nucleus depends on the chemical bonding and its perturbation by the spins of neighboring nuclei. Nuclei in a molecule may not only couple directly, but also indirectly via their chemical bindings. Since the linkage of these nuclear spins is provided by their binding electrons, the interaction has been named J-coupling. Coupling constants of this weak scalar interaction are in the range of 1–15 Hz for ^{1}H–^{1}H couplings, and the corresponding shifts split the individual resonances into characteristic multiplet structures (Stagg & Rothman, 2013). Unlike absolute values of the chemical shift, J-couplings do not depend on the

magnetic field strength. Many ^{1}H brain metabolites exhibit J-couplings and one such example is GABA.

The GABA molecule (molecular formula: $C_4H_9NO_2$) is made of six NMR observable protons in three methylene groups (H2, H3 and H4) (Figure 2.4). At lower magnetic field strengths, the GABA-H4 is strongly coupled to two protons of GABA-H3. The triplet resonances for GABA-H4 and H2 appear at 3.01 ppm and 2.28 ppm while the GABA-H3 quintet appears at 1.89 ppm (Figure 2.5). During a Hahn-spin echo sequence, the spins evolve in the transverse plane, termed phase evolution or J-modulation. This J-modulation depends on TE and gives rise to distinct resonance patterns. In the GABA spin system, the outer resonances of GABA-H4 and H2 undergo modulation (completely inverted at TE=1/2J = 68 ms) while the inner resonance does not undergo modulation. Spectral editing, by alternately allowing and inhibiting the spin evolution, makes use of this coupling difference to differentiate between scalar-coupled and uncoupled spin systems (de Graaf, 2014).

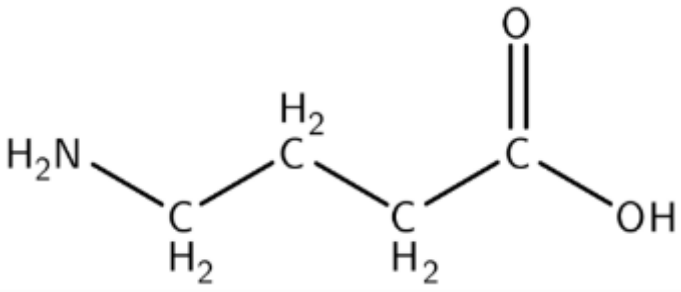

Figure 2.4 Representative structure of GABA molecule.

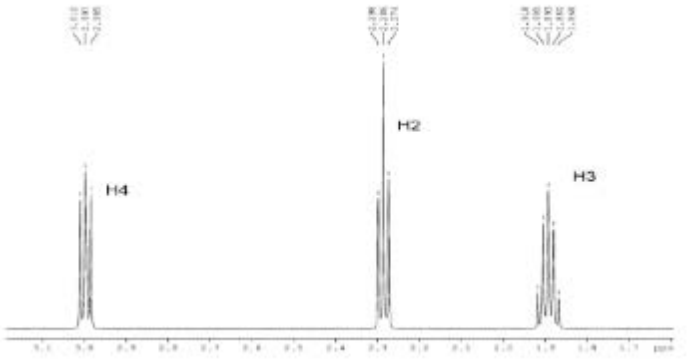

Figure 2.6 Three methylene groups provide three GABA resonances

A popular pulse sequence for J-editing of GABA is the MEscher-Garwood Point RESolved Spectroscopy (MEGA-PRESS) sequence, as shown below (M Mescher, H Merkle, J Kirsch, M Garwood, & R Gruetter, 1998b). It consists of a conventional PRESS localization with added water suppression pulses (MEGA, Chemical Shift Selective (CHESS) or VAriable Pulse power and Optimized Relaxation (VAPOR)) and dual-banded, narrow, frequency selective pulses. For GABA editing, one band of the frequency selective pulses is placed at the H3 resonance (1.9 ppm) and the other band is placed at water (4.7 ppm) in one scan (ON scan). In the next scan, the double banded editing pulse is turned off/ placed symmetric to water at 7.5 ppm (OFF) and 4.7 ppm. Such spectra are acquired as ON and OFF spectra alternately at TE = 68 ms. The

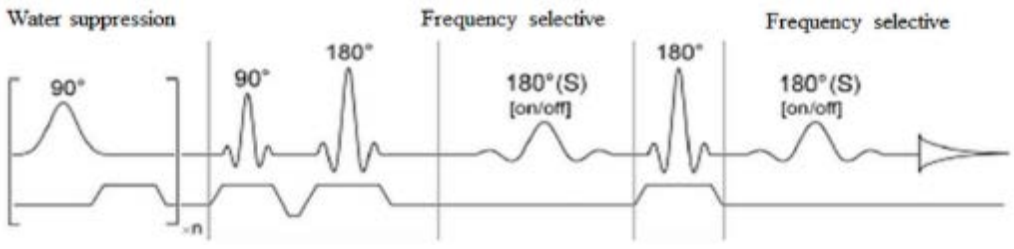

Figure 2.5 MEGA-PRESS pulse sequence representation

subtraction of the ON and OFF spectra gives a GABA difference spectrum which theoretically has only the outer GABA-H4 resonances at 3 ppm, since the inner resonance and overlapping creatine signal is nulled during subtraction. Current implementation of MEGA-PRESS includes addition of two editing pulses to PRESS localization, targeting 1.9 ppm (ON) and 7.5 (or 1.5) ppm.(de Graaf, 2014; Mullins et al., 2014; Puts & Edden, 2012).

2.3 QUANTIFICATION OF GABA MRS

Macromolecules are high molecular weight molecules like protein amino acids or lipids that have shorter relaxation times than the metabolites. These macromolecules contribute to the baseline of in vivo spectra due to their broad resonances and also exhibit coupling effects. One such macromolecule resonance appears at 3 ppm (MM30) and is mainly attributed to lysine. It also has a coupling partner at 1.7 ppm. Due to field drifts and editing inefficiencies, the frequency selective pulses in the MEGA-PRESS sequence, although narrow, are still capable of exciting MM30 by affecting its coupling partner at 1.7 ppm. MM30 can then be co-edited with GABA and appear in the GABA signal at 3ppm. Thus, in reality, the edited GABA signal in the MEGA-PRESS scan with water-symmetric pulses may contain up to 50% contribution from MM30 (Harris, Puts, Barker, & Edden, 2014; Near, Simpson, Cowen, & Jezzard, 2011). In addition, homocarnosine, a dipeptide of GABA and histidine may also be present and contribute to the GABA signal giving rise to a “GABA+” peak in the difference spectra (Puts & Edden, 2012; Douglas L. Rothman, Behar, Prichard, & Petroff, 1997).

While removal of homocarnosine is difficult due to its similarity with the GABA spin structure, several different approaches have been proposed to eliminate the macromolecule contribution to the GABA signal. In the Henry approach (Henry, Dautry, Hantraye, & Bloch, 2001), the MM30 signal is nulled by placing the editing pulses symmetric to the MM30 resonance, which lies at 1.7 ppm, in the OFF scan. The difference spectrum then contains negligible MM30 contribution since MM is affected similarly in the ON and OFF scans. However, due to the necessity of the editing pulse to have sufficient editing efficiency to affect spins only at 1.5 ppm in the OFF scan, this method is limited by the typical pulse duration of ~14 ms at 3 T (Edden, Puts, & Barker, 2012). Another method of handling macromolecules in the GABA spectra includes separately acquiring metabolite-nulled spectra using an inversion recovery sequence with appropriate inversion time (TI) and then subtracting it to get “pure” GABA signal. However, this method increases the acquisition time. It is also dependent on the choice of TI since the relaxation times of different metabolites are different and hence all metabolites cannot be nulled at one TI (Mlynárik, Gruber, & Moser, 2001).

Macromolecule contamination can be also handled during quantification by mathematical estimation of macromolecule resonance. LCModel is one such MRS quantification tool that uses linear combination of basis sets acquired for different metabolites and estimates macromolecules mathematically (S. W. Provencher, 1993; Stephen W Provencher, 2001). In a recent work, mathematical estimation by LCModel has been shown to work equally well as experimentally acquired macromolecule data for estimating in vivo metabolites

(Schaller, Xin, Cudalbu, & Gruetter, 2013). However, for GABA, it was suggested that a more reliable quantification could be possible using a measured macromolecule baseline.

Regardless of these challenges, GABA MRS continues to be a valuable tool for studying several disorders including schizophrenia, panic and anxiety disorder, depression, movement disorders, multiple sclerosis, etc. (Emir et al., 2012; Andrew W Goddard et al., 2001; Gregor Hasler et al., 2007; Mader et al., 2001; Yoon et al., 2010). We used this technique to assess GABA changes in Idiopathic Parkinson's Disease and sleep bruxism as discussed in the following chapters.

CHAPTER 3. GABA MRS IN PARKINSONS DISEASE

"Striatal and thalamic GABA levels in Parkinson's disease and their correlation to disease severity"

Prepared for submission to Movement Disorders

3.1 INTRODUCTION

Idiopathic Parkinson's disease (here onwards referred to as PD) is the second most common progressive neurodegenerative disorder, with an annual incidence of around 16–19 cases per 100,000 (Twelves, Perkins, & Counsell, 2003). Movement abnormalities seen in PD are due to the degeneration of nigrostriatal dopaminergic neurons resulting clinically in the combination of akinesia (poverty of movement), bradykinesia (slowness), rigidity (muscle stiffness) and a 4–6 Hz low frequency tremor at rest (Brooks, 2012; Wichmann & Delong, 2007). PD is classified mainly as a movement disorder but it is also associated with a spectrum of non-motor symptoms like cognitive impairment, depression, etc. which can be debilitating (K. R. Chaudhuri, Healy, & Schapira, 2006).

The basal ganglia are a complex network of neuronal circuits that regulate motor activity. These are comprised of the striatum (caudate and putamen), globus pallidus (internal (GPi) and external (GPe)), subthalamic nucleus, the substantia nigra (pars compacta and pars reticulata) and the pedunculopontine tegmental nucleus (Obeso et al., 2002). The

basal ganglia control movement via two main pathways – direct pathway and indirect pathway. Both nigral and pallidal neurons modulate the activity of the thalamus which acts as a major relay for bringing basal ganglia information back to the cortex, thus completing the cortico-basal ganglia-thalamo-cortical loop (Parent & Hazrati, 1995). The dopaminergic systemexerts control over the motor circuit mainly by inhibiting the indirect pathway and facilitating the direct pathway (Obeso et al., 2002). GABA is the main inhibitory neurotransmitter in the basal ganglia. The striato-pallidal and pallido-thalamic projections of the indirect pathway are GABAergic (Parent & Hazrati, 1995). In PD, loss of dopaminergic modulatory control causes an increase in the neuronal activity of the indirect pathway (Albin, Young, & Penney, 1989; Gerlach et al., 1996; Obeso et al., 2000). This leads to an over inhibition of the thalamo-cortical loop and consequently, a decrease in the neuronal excitation of the cortex (Obeso et al., 2002; Obeso et al., 2000). Thus, loss of DA in PD can been perceived to be causal to an elevation in GABA at the striatal output as well as pallidal (GPi) output going to thalamus.

Increased GABA levels in the basal ganglia are known to be associated with movement disorders (Galvan & Wichmann, 2007). An increase in striatal GABA has been reported in several MRS studies of animal-models of PD (Bagga, Chugani, Varadarajan, & Patel, 2013; Chassain et al., 2008; Coune et al., 2013; Gao et al., 2013; Perry, Javoy-Agid, Agid, & Fibiger, 1983) while human MRS studies have reported higher levels of GABA in the substantia nigra (Gröger, Kolb, Schäfer, & Klose, 2014; Öz et al., 2006), pons as well as the putamen (Emir et al., 2012) in mild-moderate PD patients. Elevated levels of GABA

have also been reported in the striatum and putamen of autopsied PD subjects (Kish et al., 1986; Perry et al., 1983).

There exists another form of Parkinsonism that has been linked to excess exposure to manganese (Mn). Mn is an essential trace metal important for neuronal function, but in high exposure scenarios, Mn can lead to a movement disorder called Mn-induced Parkinsonism or “manganism” which shares some symptoms of PD. Studies of occupational Mn exposure have revealed changes in the levels of GABA. Recently, our group studied workers with high Mn exposure and detected changes in brain chemistry before the onset of clinical symptoms in these workers (Dydak et al., 2010). Some of these workers developed tremor, rigidity, and bradykinesia which resembled PD. Also, one of the recent studies on Mn-exposed welders has shown increase in thalamic GABA in asymptomatic workers which also correlated with subtle measures of motor function suggesting that increased GABA may serve as an early biomarker of motor dysfunction (Long et al., 2014). Due to the similarities between manganism and PD, it is assumed that several pathophysiological pathways are shared between these two disorders.

Besides controlling movement, the basal ganglia along with cerebral cortex also play a role in planning, working memory and emotion (Monchi, Petrides, Mejia-Constain, & Strafella, 2007; Obeso et al., 2000). In PD, early involvement of the cerebral cortex has been shown to contribute to multiple metabolic defects (Ferrer, 2009; Hu et al., 1999). Several MRS studies have investigated cortical regions for neurochemical changes in PD. Some animal studies have reported a decrease in striatal N-acetyl aspartate (NAA) which is a neuronal marker (Brownell et al., 1998; Choi et al., 2011; Coune et al., 2013; Öz et

al., 2006; Pizzi et al., 2013) whereas reduced NAA has been found in cortical structures as well as the substantia nigra and striatum in human studies (K. Chaudhuri et al., 1996; Choe et al., 1998; Holshouser et al., 1995; Nie et al., 2013; Seraji-Bozorgzad et al., 2014; Zhou, Yuan, He, & Tan, 2014). Changes in creatine (Cr) have been reported in the striatum (Hattingen et al., 2009) and substantia nigra (O'Neill et al., 2002), indicating altered metabolism. These findings indicate that the symptoms of PD are linked to alterations in neurochemistry of cortico-basal ganglia-thalamo-cortical loop.

The clinical motor symptoms of PD appear when more than 50% of the striatal dopaminergic neurons have been lost and become more severe with increased neuron loss (Zhou et al., 2014). Hence the identification of sensitive and specific biomarkers that may slow disease progression is important for early and differential diagnosis, and for monitoring disease progression (Ciurleo, Di Lorenzo, Bramanti, & Marino, 2014). Furthermore, in PD, studies of Deep Brain Simulation (DBS) of subthalamic nucleus (STN) have indicated that for an effective therapeutic intervention, it is critical to understand the effect of the basal ganglia output to the thalamus (Alessandro Stefani et al., 2011). It is also of interest to investigate the importance of thalamic and striatal GABA levels for the modulation of sensorimotor integration and response selection processes by proprioceptive information in healthy subjects and PD patients.

Currently, there is a critical unmet need for biomarkers in PD. A desirable marker is one that is non-invasive, improves diagnostic accuracy, facilitates earlier diagnosis, and most importantly, monitors disease progression and responses to therapeutic interventions. The overall objective of this project was to examine neurochemical alterations in different

regions implicated in PD – basal ganglia, thalamus, and regions of cerebral cortex (frontal and motor cortex), and to determine whether GABA levels measured by in vivo MRS could serve as biomarker for PD.

The specific aims of the study were:

Aim 1: To determine the impact of PD on brain GABA levels in the basal ganglia and cortical regions.

Hypothesis: Levels of GABA in thalamus and striatum as measured by MRS will be higher in PD patients compared to controls.

Aim 2: To determine the alterations in NAA in the basal ganglia and cortical regions.

Hypothesis: Due to neuronal loss, PD patients will have lower levels of NAA compared to controls.

Aim 3: To determine the relationship between severity of motor symptoms and basal ganglia, thalamic and frontal GABA levels, in PD.

Hypothesis: GABA levels will be correlated with disease severity as measured by the Unified Parkinson Disease Rating Scale (UPDRS) and motor tests.

3.2 MATERIALS AND METHODS

3.2.1 Subject Recruitment

Nineteen subjects with mild-moderate PD and eighteen age-matched healthy controls were recruited for the study (refer

Table 3). Three PD patients were medication-naïve (i.e. never used any Parkinson's medication) whereas the remaining did not take any Parkinson's medication for at least 12 hours before the study. Subjects with previous history of neurological disorder, dementia or using any GABA-ergic drugs like GABApentin were excluded from the study. Written informed consent approved by the Indiana University Institutional Review Board was obtained from all subjects prior to participation

Table 3. Subject demographics and clinical information.

	PD	**Control**
Age (y)	63.68 ± 9.12	59.63 ± 10.24
Number of subjects and gender	19 (10 males)	18 (11 males)
Disease duration range (yrs)	< 1 - 11	N/A
UPDRS total	33.34 ± 10.9	5.43 ± 3.36
Tremor subscore	4.13 ± 3.62	0.47 ± 0.90
Bradykinesia subscore	1.78 ± 0.71	0.05 ± 0.22
Rigidity subscore	6.79 ± 3.55	1.15 ± 2.06
Hoehn and Yahr score	2.05 ± 0.62	0

3.2.2 Neurological and motor testing

Prior to MRS, disease severity was assessed in all subjects by a neurologist by administering a health questionnaire and using the motor part of the Modified Parkinson's Disease Rating Scale (MDS UPDRS-III). Sub-scores of rigidity, tremor, and bradykinesia were also recorded (table 1). Motor performance was tested using the Grooved Pegboard test (Lafayette Instrument, IN, USA) which is a sensitive visual-motor coordination test used to assess gross movements of the fingers, hands and arms, as well as fine fingertip dexterity necessary in assembly tasks. In a series of test batteries, subjects were asked to place pegs in the pegboard as quickly as possible with dominant hand and non-dominant hand alternately. The time to complete the task and the number of drops was recorded and scored. The Finger Tapping test, a measure of bilateral psychomotor speed was also included in which subjects were asked to tap as fast as possible using the index finger of their dominant and non-dominant hand alternately for one minute each. The number of finger taps and hand movement was recorded and scored.

Figure 3.1(A) Set-up of finger taping test and (B) Grooved pegboard.

3.2.3 MRS and MRI data acquisition, post-processing and analysis

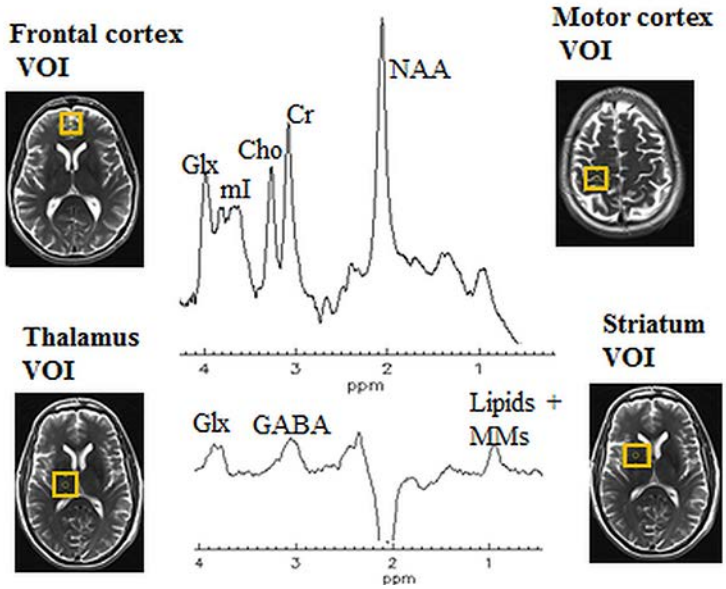

Figure 3.2 Representative placement of volumes of interest (VOI), PRESS spectrum (topcenter) and MEGA-PRESS GABA spectrum (bottom center).

MR scans were performed on a whole body 3-T Siemens Magnetom Tim Trio MR scanner (Siemens Healthcare, Erlangen, Germany) using a standard head coil. Fast T2 weighted images were obtained in the axial plane angled along the anterior commissure – posterior commissure (AC-PC) line, along with orthogonal sagittal and coronal images for planning the MRS volumes of interest (VOIs). Higher order shimming was performed either manually or using FASTMAP (Gruetter, 1993). Single voxel short echo-time (TE) Point RESolved Spectroscopy (PRESS) spectra were obtained from all the VOIs placed in the frontal cortex, motor cortex, right striatum, and right thalamus (refer Figure 3.2) using repetition time (TR) = 2000 ms, TE = 35 ms, averages = 32 (thalamus and striatum) or 96 (frontal and motor), and spectral BW = 1200 Hz. In addition, MEGA-PRESS (R. A. Edden & P. B. Barker, 2007; M Mescher, H Merkle, J Kirsch, M Garwood, & R Gruetter,

1998a) edited GABA spectra were also obtained separately using TR = 2000 ms, TE = 68 ms, averages = 256, edit pulse BW = 44 Hz, and edit ON/OFF pulses at 1.9/7.5 ppm from the thalamus, striatum, and frontal cortex. Following each PRESS and MEGA-PRESS acquisition, a reference spectrum without water suppression was obtained for phase, frequency correction and eddy current correction. In addition, 3D T1-w High resolution T1-weighted Magnetization Prepared RApid Gradient Echo (MPRAGE) images were also obtained for segmentation and co-registration.

All post-processing and quantification of spectra was performed using LCModel (v 6.2-0R) (S. W. Provencher, 1993) . Appropriate basis sets were generated using density matrix simulations obtained by using published values of chemical shifts and coupling constants (L. Kaiser, K. Young, D. Meyerhoff, S. Mueller, & G. Matson, 2008). The parameter “dkntmn” which defines the node spacing of the spline function for estimation of baseline was set to 0.15. The metabolites quantified from PRESS spectra included N-acetyl aspartate (NAA), N-acetylaspartylglutamic acid (NAAG), Cr, myo-inositol (mIns), glutamate (Glu), and glutamine (Gln). Segmentation of the MPRAGE images into grey matter, white matter and cerebrospinal fluid was done using Statistical Parametric Mapping (SPM) and voxel co-registration was implemented using an in-house tool written in MATLAB. Metabolite values were corrected for cerebrospinal fluid content to yield absolute concentrations of metabolites in millimoles (mM) (Chowdhury, O'Gorman, Nashef, & al., 2014). Statistical analysis was done in SPSS (version 22).

The metabolite data was analyzed using a one-way ANOVA with group as a factor and age as a covariate. Post-hoc tests were bonferroni-corrected, when necessary. To assess

the relationship between GABA and motor/cognitive scores, linear regression or correlation analyses was performed with GABA. Results with p values <0.05 were considered to be statistically significant.

3.3 RESULTS

3.3.1 MRS data quality

The quality of spectra obtained in patients and controls was not significantly different between groups, in any region. Representative GABA spectra from both groups are shown in Figure 3.3. The average SNR for thalamus and striatum was 20 and 18 respectively whereas the FWHM was 20 Hz and 24 Hz, respectively. Overall the shims were marginally better in controls than the PD subjects (p=0.05) due to the PD tremor.

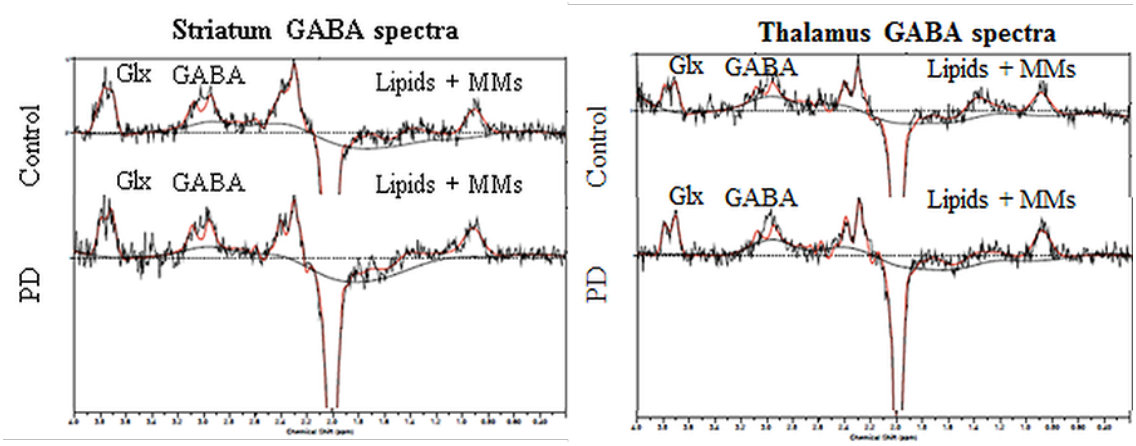

Figure 3.3 Representative LCModel output GABA spectra in the striatum (left) and thalamus (right) of a control and PD subject.

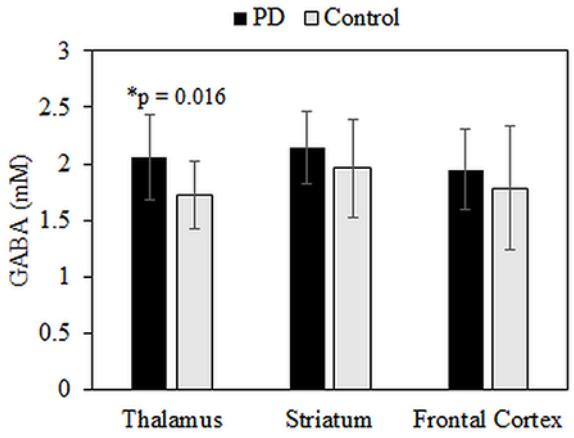

Figure 3.4 Levels of GABA in thalamus, striatum, and frontal cortex in both groups

3.3.2 Neurochemical Differences

Significantly higher GABA was detected in the thalamus of the PD subjects compared to controls (F=6.645, p=0.016, PD=2.06±0.37 mM, controls=1.72±0.30 mM) (Figure 3.4). In contrast, no differences in striatal or frontal GABA were detected between the groups. In the frontal cortex, a trend for lower tNAA was seen in the PD subjects compared to controls (F=3.698, p=0.06). Motor cortex showed no difference in any metabolite levels. Age and tissue-composition of VOI were not significantly different between the groups. Glu and Gln were quantified together as Glx while sum of NAA and NAAG were reported as tNAA.

3.3.3 Motor scores and correlation with GABA

The PD patients had significantly lower finger-tapping scores when using dominant hand (F=5.053, p=0.031) as well as non-dominant hand (F=14.871, p<0.001) compared to controls. Similarly, the pegboard scores for dominant and non-dominant hands of PD

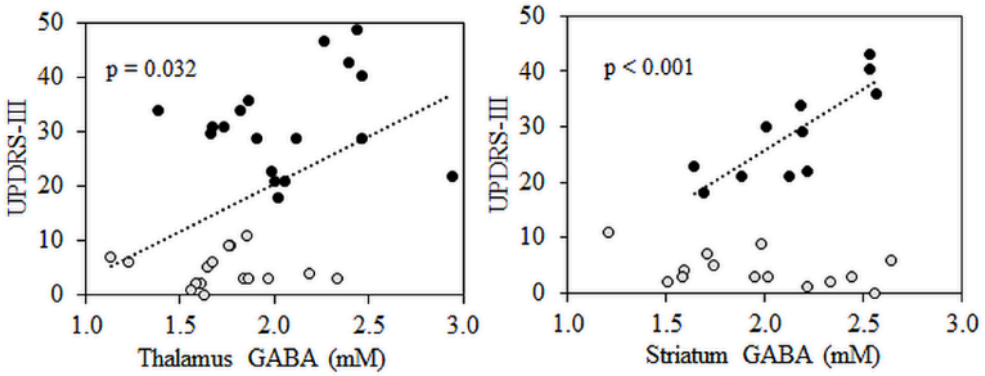

Figure 3.5. Correlation of total UPDRS-III scores with thalamic and striatal GABA

subjects were lower than the scores of controls (dominant: F=14.169 p=0.001, non-dominant: F=29.64, p<0.001).

The regression of thalamic GABA was significant with the UPDRS scores (B=14.57, t=2.25, p=0.032) (Figure 3.5) and rigidity sub-scores (B=3.775, t=2.188, p=0.036) (Figure 3.6). Although striatal GABA was not significantly different between the groups, regression of striatal GABA with total UPDRS scores was significant in the PD group (B=24.825, t=14, p<0.001) (Figure 3.5). The regression of frontal GABA and UPDRS was significant in the PD group (B=-18.299, t=-2.61, p=0.03) (Figure 3.7). The

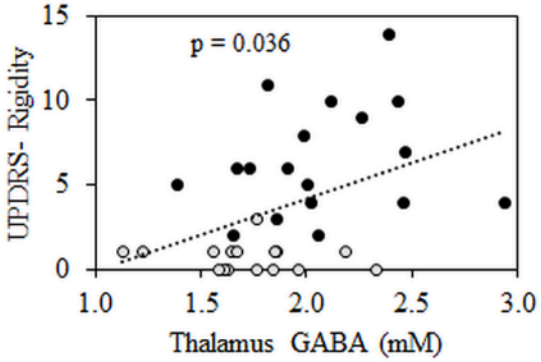

Figure 3.6 Correlation of UPDRS rigidity sub-scores with thalamic GABA

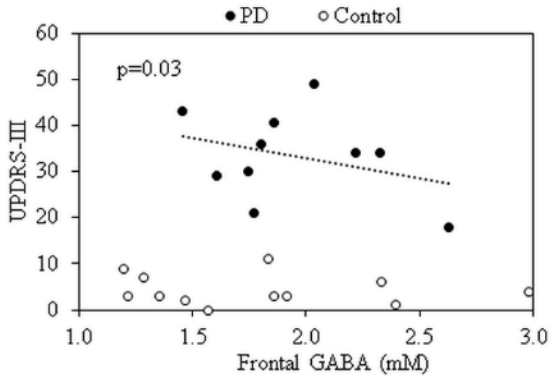

Figure 3.7 Correlation of UPDRS scores with frontal GABA

regression of frontal GABA and the time for pegboard using the dominant hand was also significant in the PD group (B=-0.09, t= -3.38, p=0.01).

3.4 DISCUSSION AND CONCLUSION

Our results indicate that thalamic GABA is elevated in PD patients that are withheld medication for about 12 hours or are medication-naive. In the PD patients, thalamic GABA is specifically associated with worsening rigidity. We further find that within the PD group itself, striatal and frontal GABA levels have strong but opposite association with disease severity as measured by the UPDRS. Thus, disease severity is worse with increasing thalamic and striatal GABA but decreasing frontal GABA which is in agreement with the understood mechanism of hypokinetic symptoms seen in PD. This was also confirmed with lower frontal GABA levels associated with worsening dexterity and motor speed. Lower levels of NAA in the frontal cortex in the PD patients are indicative of neuronal loss.

Recently, thalamic GABA has been of interest in DBS studies of STN. STN which is used for alleviating motor symptoms in advanced PD. Studies have shown that during effective DBS of STN, thalamic levels of GABA are reduced significantly (Alessandro Stefani et al., 2011). This is also the outcome after taking levodopa, during the ON status (Alessandro Stefani et al., 2011; A. Stefani et al., 2011). Thus, our findings support the idea of thalamic dis-inhibition as a therapeutic strategy for motor improvement.

In our study, we do not see significant striatal GABA differences in PD, unlike previous MRS studies (Emir et al., 2012; Öz et al., 2006). Small sample size and a larger VOI (necessary for the GABA scan in order to obtain sufficient signal to noise ratio) are some limitations of this study. Irrespective of that, there is a strong evidence of the role of elevations in striatal and thalamic GABA being related to worsening of PD symptoms. Future studies are planned to investigate the impact of dopaminergic drugs on thalamic and striatal GABA, and sensitivity of GABA to changes over time. Given our findings of altered GABA in asymptomatic welders, however, we hypothesize that GABA MRS may be useful as a non-invasive tool to detect changes in the premotor phase of PD.

CHAPTER 4. CORTICAL GABA AND GLUTAMATE CHANGES IN SLEEP BRUXISM

"GABA and Glutamate Levels in Occlusal Splint-Wearing Males with Possible Bruxism"

Published in Achives of Oral Biology

4.1 INTRODUCTION

The oral parafunction generally known as bruxism (clenching and grinding of teeth during both sleep and while awake) is commonly encountered by clinicians in psychiatry, neurology, and dentistry. Sleep bruxism (SB) has been reclassified in recent years as a sleep-related movement disorder; this category also includes periodic limb movement and rhythmic movement disorders (Medicine). SB has been estimated at 10-20% of the pediatric population, 5-8% of the adult population, with a decrease to 3% in geriatric populations; no sex differences have been documented to date (Laberge, Tremblay, Vitaro, & Montplaisir, 2000; Lavigne & Montplaisir, 1994; Ohayon, Li, & Guilleminault, 2001). Clenching and grinding of teeth parafunctions are often seen in individuals with stress and anxiety disorders (Manfredini, Landi, Fantoni, Segu, & Bosco, 2005; Petit, Touchette, Tremblay, Boivin, & Montplaisir, 2007; Pingitore, Chrobak, & Petrie, 1991) and are comorbid with restless leg syndrome, sleep apnea, and other parasomnias (Kato & Lavigne, 2010; Lavigne, Manzini, & Kato, 2005). Iatrogenic secondary causes of such

oral parafunctions may include delivery/cessation of neuroactive medications (Lavigne, Khoury, Abe, Yamaguchi, & Raphael, 2008), certain dental procedures, and treatment for temporomandibular disorder (TMD) (Baba, Haketa, Sasaki, Ohyama, & Clark, 2005; Lobbezoo, Brouwers, Cune, & Naeije, 2006; Tosun, Karabuda, & Cuhadaroglu, 2003). A high occurrence of TMD pain has been documented in persons exhibiting (1) the behaviors of both SB and daytime clenching (awake bruxism), and (2) the sleep disorders of sleep apnea, insomnia, and bruxism (Lavigne et al., 2008; Lavigne et al., 2005; Lobbezoo & Lavigne, 1997; Manfredini, Cantini, Romagnoli, & Bosco, 2003; Manfredini & Lobbezoo, 2009; Raphael, Marbach, Klausner, Teaford, & Fischoff, 2003; Raphael et al., 2012; Smith et al., 2009).

A link between emotion-induced oral parafunctional behaviors and group I TMD was proposed long ago (Keefe & Dolan, 1988; Kight, Gatchel, & Wesley, 1999; McCreary, Clark, Merril, Flack, & Oakley, 1991), although the mechanism underpinning this association is still unclear. Recent neuroimaging studies of bruxism have identified the involvement of the Hypothalamic–Pituitary–Adrenal (HPA) axis system, which is also implicated in TMD and Post-Traumatic Stress Disorder (PTSD). Currently, it is thought that bruxism, PTSD, and other stress-related psychiatric disorders, are due to a dysfunction of a circuit involving the medial prefrontal/anterior cingulate cortical region, dorsolateral prefrontal cortex (DLPFC), hippocampus, and amygdala.

The role of neurochemicals in anxiety-related parafunctions such as bruxism has been and continues to be of intense interest for some time now (Lavigne et al., 2001; Lobbezoo, Lavigne, Tanguay, & Montplaisir, 1997; Lobbezoo & Naeije, 2001; Lobbezoo, Soucy,

Montplaisir, & Lavigne, 1996; Lobbezoo, van Denderen, Verheij, & Naeije, 2001; Ranjan, P, & Prabhu, 2006; Sjoholm, Lehtinen, & Piha, 1996; Winocur, Gavish, Voikovitch, Emodi-Perlman, & Eli, 2003). The exact neurochemical mechanisms that cause certain selective serotonin reuptake inhibitors (SSRIs) to manifest sleep bruxism is a focus of research efforts (Lobbezoo et al., 2001; Ranjan et al., 2006; Winocur et al., 2003) as are those involved in the important comorbid factors of sleep regulation, endocrine systems, autonomic functions, stress/anxiety, and motor control (Huynh et al., 2006; Jones, 2000; Kato & Lavigne, 2010; Lavigne et al., 2008; Van Cauter, 2005). As demonstrated by the bruxism-ameliorating effects of the drugs GABApentin, tiagabine, gamma-hydroxybutyrate, diazepam, and lorazepam, the major neurotransmitter GABA is suggested to play a critical role in bruxism (Winocur et al., 2003).

MRS techniques allow for a noninvasive examination of *in vivo* brain function by assessing regional concentrations of neurotransmitter metabolites (Bremner, 2007). As determined by recent MRS studies (Cameron et al., 2007; G. Hasler et al., 2008), GABA plays an important role in the pathophysiology of human anxiety disorders such as panic disorder and PTSD (Millan, 2003). A recent study found lower GABA levels in individuals with PTSD (Meyerhoff, Mon, Metzler, & Neylan, 2014). Goddard et al. discovered lower than normal cortical GABA levels in panic disorder individuals (A. W. Goddard et al., 2004; Z. Long et al., 2013). The etiology of oral parafunctions such as bruxism and TMD is multifactorial and psychological factors are considered a major component in the initiation and progression of these disorders (Manfredini & Lobbezoo, 2009), which suggests that GABA neuronal system may also be critical in the

manifestation of bruxism. The increased incidence of anxiety and depression in these patients (Hicks, Conti, & Bragg, 1990; Kight et al., 1999; Mongini, Ciccone, Ceccarelli, Baldi, & Ferrero, 2007; J. W. Park, Clark, Kim, & Chung, 2010) has led to a theory that psychological factors, such as anxiety, predispose patients to TMD/bruxism by increasing tooth grinding and clenching behaviors, which may produce masticatory muscle fatigue and soreness (Keefe & Dolan, 1988; Kight et al., 1999; McCreary et al., 1991).

We hypothesized that the stress-related behavioral disorder of bruxism and anxiety-related disorders share similar underlying mechanisms involving the inhibitory neurotransmitter GABA as well as the metabolites NAA, creatine, choline-containing compounds, myo-inositol, glutamate and glutamine (Maddock & Buonocore, 2012). To study this cross-link between brux-like parafunctions and anxiety-related disorders, we performed a ^{1}H MRS study for metabolite quantification in anxiety-related regions of the brain involved in the HPA axis system. HPA axis dysfunction plays a major role in the anxiety disorders reported by patients who clench and grind their teeth and suffer with TMDs (Burris, Evans, & Carlson, 2010). We focused on two HPA-axis brain regions, the right hippocampus and right thalamus and selected the right hemisphere because of the documented laterality in stress-regulatory components of the HPA axis. In addition, we also investigated the DLPFC because of its role in anxiety-related disorders (Prater, Hosanagar, Klumpp, Angstadt, & Phan, 2013) and a dorsal anterior cingulate cortex/pre-supplementary motor area (dACC/preSMA) involved in motor planning (Byrd, Romito, Dzemidzic, Wong, & Talavage, 2009; Wong, Dzemidzic, Talavage, Romito, & Byrd,

2011). The dACC has also been implicated in anxiety behavioral disorders such as PTSD (Etkin & Wager, 2007; I. M. Rosso et al., 2013).

The specific aims of this study was to identify parallels in metabolic and neurotransmitter changes between the manifestation of brux-like behavior and reported changes in anxiety disorders. The long term goal of this imaging-based, noninvasive research of the neurochemical mechanisms affecting the manifestation of oral parafunctions such as bruxism is to provide improved treatment strategies in the clinical population.

4.2 MATERIALS AND METHODS

4.2.1 Subject Recruitment

Subject group classification was based on an interview that was conducted after self-reported tooth clenching and grinding history, followed up by evaluation of each subject's protective nightguard and positive responses on the TMD history questionnaire (Dworkin & LeResche, 1992). The TMD questionnaire documented subjects' perception of pain, loss of function, and bruxing behavior. Based on this classification, 8 male subjects (age: 28.6±3.0 years) were recruited and classified in the Bx group. Subjects were classified to exhibit bruxing behavior if currently reporting active clenching and grinding of teeth and wearing of a protective nightguard, being right-handed, 20-45 years old, not currently under medication for migraine headaches, without previous history of brain injury or psychiatric problems, magnetic surgical implants, false teeth, retainers, or magnetic braces, having normal hearing sensitivity by self-report, and not being

claustrophobic by self-report. The control (NB) group consisted of 9 age-matched (25.5±1.9 years) healthy men with the inclusion criteria identical to the Bx group except for bruxing behavior and nightguard use. Written informed consent approved by the Indiana University Institutional Review Board was obtained from all subjects prior to participation and all procedures conformed to international STROBE guidelines.

4.2.2 MRS data acquisition and analysis

^{1}H MRS data was acquired on a 3T Siemens Magnetom Tim-Trio MR scanner (Siemens Healthcare, Erlangen, Germany) using a 32-channel head array coil. Both single voxel short echo time Point RESolved Spectroscopy (PRESS) spectra (TE=30 ms, TR=1500 ms, 128 averages) and GABA-edited spectra (TR=1500 ms, TE=68 ms) using MEGA-PRESS (F. A. Chowdhury et al., 2014; R. A. E. Edden & P. B. Barker, 2007; M. Mescher, H. Merkle, J. Kirsch, M. Garwood, & R. Gruetter, 1998) were obtained from four volumes of interest (VOIs): thalamus (25×25×25 mm^3, 392 averages), hippocampus (17×40×17 mm^3, 512 averages), DLPFC (25×30×22 mm^3, 392 averages) and dACC/preSMA (25×35×25 mm^3, 392 averages). A reference spectrum without water suppression was obtained in each brain region for phase and frequency correction. Placements of the VOIs and representative spectra from each brain region are illustrated by Figure 4.1.

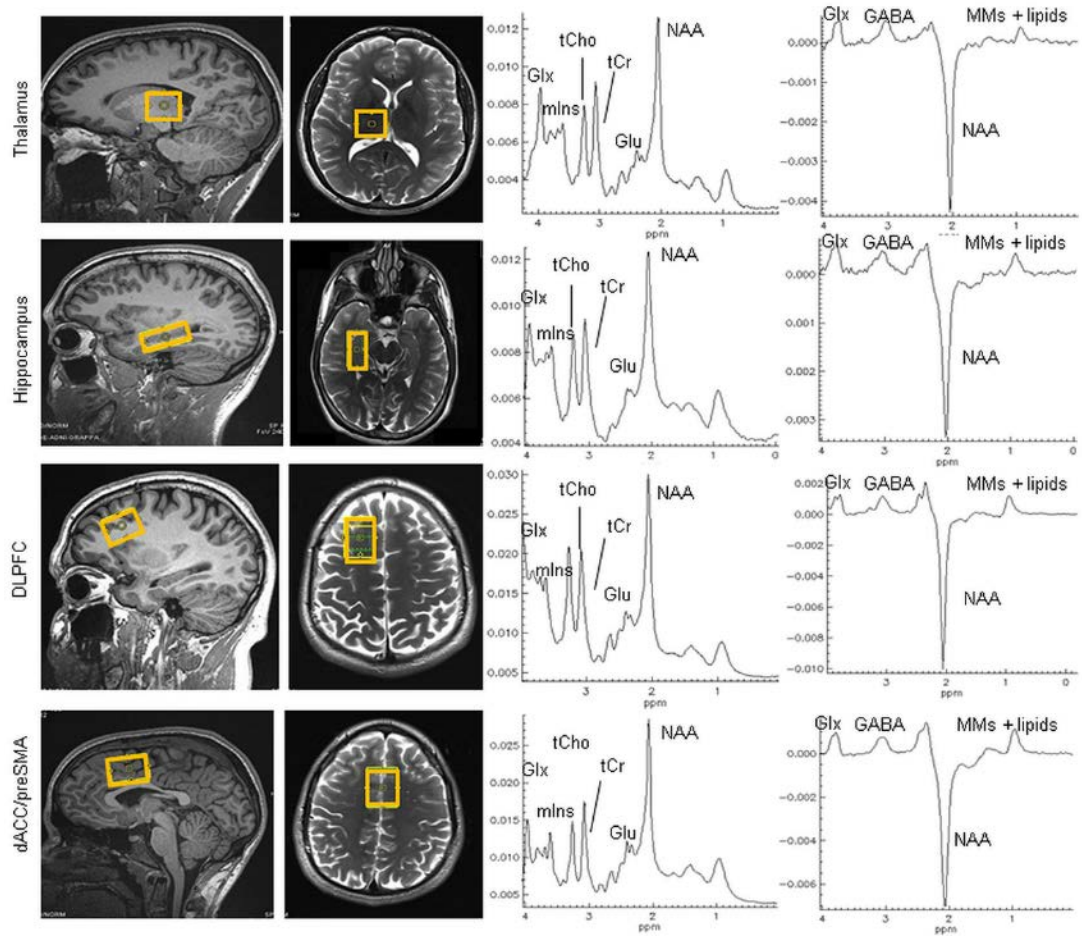

Figure 4.1. Representative voxel placement (left), short echo time PRESS spectra (center) and MEGA-PRESS GABA spectra (right) for all regions of interest.

The post-processing and quantification of all spectra was performed with LCModel (v6.2-0R) (S. Provencher, 1993). Appropriate basis sets for GABA were generated using density matrix simulations with published values of chemical shifts and coupling constants (L. Kaiser et al., 2008). PRESS spectra were analyzed for the major metabolites N-acetyl aspartate (NAA), choline (Cho), total creatine (tCr), myo-inositol (mIns) and glutamate (Glu), whereas GABA levels were obtained from the GABA-edited spectra. Quantification results are expressed in institutional units (i.u.) and only the NAA, tCr,

Glu, and mIns metabolites from the PRESS spectrum with LCModel CRLB below 20% were used for further statistical analysis.

All statistical calculations were performed with SPSS (Version 20.0, IBM Corp.). The questionnaire data were grouped into three categories: depression, anxiety and pain with an overall (summed) score calculated for each category. The scores in each category were compared between groups using the Wilcoxon–Mann–Whitney two-sample rank-sum test. Spearman's rank correlations were computed for the questionnaire scores in each of the categories and regional metabolite estimates. A Group (2; Bx and NB) × Region (4; hippocampus, DLPFC, thalamus and preSMA) × Metabolite (5; NAA, Glu, mIns, tCr, and GABA) repeated measures ANOVA was performed with a post-hoc ANOVA F-test conducted where effects of Group × Region interaction were significant. In addition, questionnaire scores were examined in the regression analysis or as covariates when showing significant effects of Group.

4.3 RESULTS

4.3.1 TMD Questionnaire

Questionnaire data from both groups indicated that all nightguard subjects reported experiencing daytime and night time tooth clenching/grinding, morning jaw soreness /stiffness, and the use of a protective occlusal nightguard obtained from a dentist. Control subjects had negative responses to all of the aforementioned questionnaire items.

Anxiety and depression scores in all subjects were significantly correlated (Spearman's r=0.736, p<0.01, two-sided). There were no significant group differences in the scores of depression (Mann-Whitney U=29, p=0.54, two-tailed) or pain (Mann-Whitney U=24.5, p=0.28, two-tailed), while a trend was present for anxiety (Mann-Whitney U=18.5, Bx mean=3.88, NB mean=1.00, p=0.09, two-tailed). This trend-level anxiety score difference was in the anticipated direction (e.g. higher for the Bx). Therefore, anxiety scores were added as a covariate in the MRS data analysis to test whether anxiety contributed to the metabolite group differences reported below.

4.3.2 GABA and metabolite differences

The multivariate tests in the repeated-measures ANOVA showed significant Group x Region interaction (Wilk's lambda=0.38, F=3.36). In the repeated-measures ANOVA, Group x Region interaction was significant for two metabolites, GABA (F(3,55)=6.66, p=0.001) and Glu (F(3,55)=3.22, p=0.031). Between-group post-hoc ANOVA showed

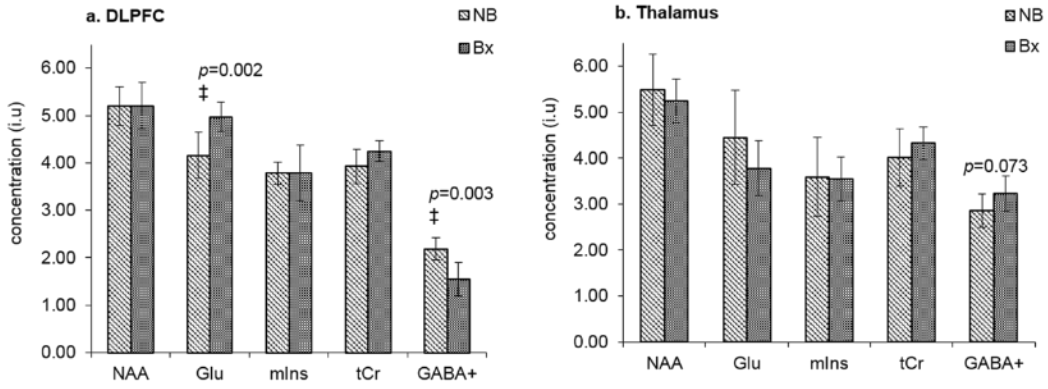

Figure 4.2 Metabolite levels in a) DLPFC and b) thalamus of both groups.

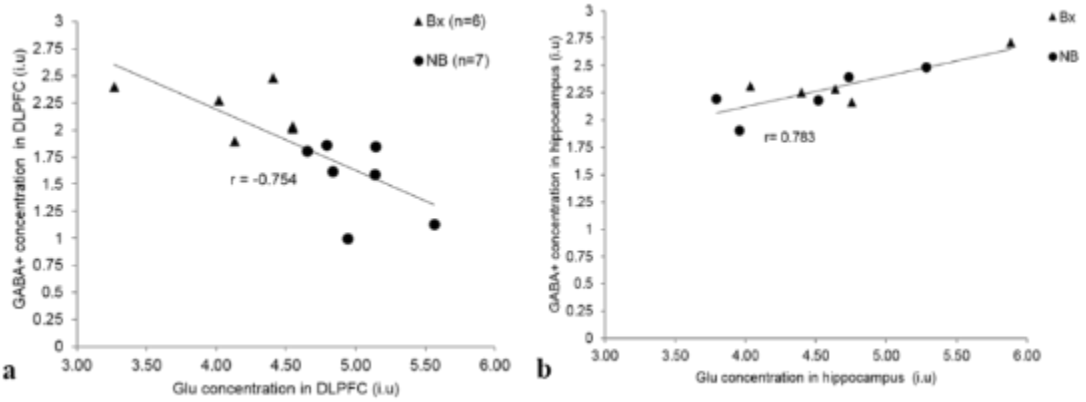

Figure 4.3. Correlation plots of GABA and Glu in a) DLPFC and b) hippocampus

significant effects only in the DLPFC, where lower levels of GABA ($F(1,12)=14.01$, $p=0.003$) and higher levels of Glu ($F(1,13)=14.71$, $p=0.002$) were observed in Bx (Figure 4.2). In the thalamus, compared to controls, Bx showed a trend level increase in GABA+ ($F(1,14)=3.81$, $p=0.07$) (Figure 4.2). These GABA and Glu group differences in the DLPFC were reduced but remained significant (GABA, $F(1,13)=5.17$, $p=0.049$; Glu; $F(1,13)=5.829$, $p=0.039$) after the inclusion of anxiety as a covariate. Furthermore, GABA and Glu levels in the DLPFC showed a significant negative relationship (Pearson's $r=-0.754$, $p=0.003$ two-sided) as illustrated by Figure 4.3. While no group differences in GABA and Glu were present in the hippocampus, these two metabolites did show positive relationship (Pearson's $r=0.783$, $p=0.004$ two-sided; Figure 4.3).

Table 4. Metabolite concentrations (in i.u.) for four brain regions and both groups. Significant (‡, $p<0.01$) differences are highlighted.

	Region	**NAA**	**Glu**	**mIns**	**tCr**	**GABA**
NB	Hippocampus	3.83±0.70	4.64±0.60	4.62±1.02	3.66±0.75	2.32±0.20
	DLPFC	5.20±0.41	**4.15±0.49**‡	3.78±0.23	3.93±0.37	**2.18±0.24**‡
	Thalamus	5.49±0.77	4.45±1.03	3.59±0.86	4.01±0.62	**2.86±0.36***
	PreSMA	5.87±0.57	6.01±0.67	4.68±0.43	4.71±0.17	2.81±0.25
Bx	Hippocampus	3.96±0.94	4.46±0.6	3.40±0.79	3.21±0.92	2.40±0.32
	DLPFC	5.21±0.48	**4.97±0.31**‡	3.80±0.59	4.25±0.22	**1.55±0.35**‡
	Thalamus	5.24±0.48	3.78±0.60	3.55±0.48	4.33±0.36	**3.23±0.38***
	PreSMA	6.10±0.55	6.02±0.66	4.73±0.40	4.84±0.43	2.80±0.10

4.4 CONCLUSION AND DISCUSSION

While the focus of previous neurochemical studies was on sleep bruxism (SB) (Lavigne et al., 2008), there is some evidence that the variability of bruxism symptoms in *both* diurnal and nocturnal forms may have a neurochemical basis, involving different brain regions such as the ventral tegmental area and the distribution of striatal dopaminoceptor-2 (D_{2R}) receptors (Chen, Lu, Lui, & Liu, 2005). In this study, lower GABA levels in DLPFC in nightguard-wearing subjects suggest that anxiety-related circuits (Peers, Simons, & Lawrence, 2013; Prater et al., 2013) that may affect bruxism were less inhibited than in controls. Decreased frontal lobe GABA levels have also been detected in panic disorder individuals (Z. Long et al., 2013) albeit in the medial rather than dorsolateral prefrontal cortex.

A review of earlier studies of DLPFC metabolite levels in anxiety subjects indicates that the DLPFC plays an important role in responses to threatening stimuli, particularly in anxiety disorders (Bar-Haim, Lamy, Pergamin, Bakermans-Kranenburg, & van, 2007; Duncan, 2010; Miller & Cohen, 2001; Peers et al., 2013) . It is currently thought that the DLPFC guides control of tasks by providing excitatory feedback to pools of neurons that process task-relevant aspects of anxiety-provoking stimuli; in this case the DLPFC may enhance the manifestation of bruxism by channeling anxiety-associated stimuli to those brain regions actually causing the behavior. Increased DLPFC activity during an emotional Stroop task suggests that the DLPFC is important for task control mechanisms in the face of emotional distraction (Bishop, Jenkins, & Lawrence, 2007; Compton et al., 2003; Denkova et al., 2010). The documented decrease of bruxism with increased age may also be related to an age-related decrease of DLPFC mechanisms regarding early perceptual features (Schmitz, Cheng, & De Rosa, 2010).

Hippocampus metabolite levels in anxiety subjects have been reported to show higher Glx, myo-inositol, and Cr, and to be correlated with psychiatric symptoms and mitochondrial disorders (Anglin, Rosebush, Noseworthy, Tarnopolsky, & Mazurek, 2012). Alterations in hippocampal activity and volume have also been documented in anxiety disorders (Etkin & Wager, 2007; Gilbertson et al., 2002). In our study, no significant group differences were found for any of the reported metabolites in the hippocampus. However, a significant positive correlation between GABA and Glu emerged. Interestingly, these two metabolites were negatively related in the DLPFC, which may reflect the documented bidirectional interactions between the hippocampus

and the DLPFC (Cho et al., 2012). In this sense, our finding might indicate the presence of a negative feedback circuit between hippocampus and DLPFC, which may play an important role in regulating the manifestation of bruxing behaviors (Ganon-Elazar & Akirav, 2013; Herman, Ostrander, Mueller, & Figueiredo, 2005; Jankord & Herman, 2008). The activity dynamics between the DLPFC and hippocampus in retrieval of facts during problem solving (Cho et al., 2012) and our findings may also suggest a role for both the DLPFC and hippocampus in motor memory systems (Albouy, King, Maquet, & Doyon, 2013; Albouy, Sterpenich, et al., 2013) that might be involved in bruxism behaviors. It has also been suggested that epileptic seizures involving limbic structures within the temporal lobe (hippocampus) may activate masticatory central pattern generators that help cause bruxism behaviors (Meletti et al., 2004). It has been found that DLPFC of idiopathic generalized epilepsy patients demonstrate increased levels of glutamine and GABA compared with controls (F. A. Chowdhury et al., 2014). This differs from our study in that DLPFC of Bx subjects showed significantly lower levels of GABA and higher levels of Glu. The precise neurochemical mechanisms and interactive relationships between epilepsy and brux behaviors need to be investigated further.

In this study, we detected no metabolic group differences in the preSMA/dACC; this despite our earlier fMRI findings that the preSMA/dACC may play an important role in oral parafunctions such as tooth grinding and clenching (Byrd et al., 2009; Wong et al., 2011). This discrepancy may be due to the passive nature of the MRS scans in the present study, while our earlier fMRI studies employed the active, physical tasks of jaw clenching and tooth grinding.

Limitations of this study include: (1) modest sample size, and (2) nightguard wearer inclusion criteria that were based on self-report and were non-specific in bruxing classification. In addition, continuing analysis of oral parafunction and pain data in the nightguard wearers was not performed. In this study, subject gender selection was necessarily driven by a small sample so we focused on males due to the higher incidence of PTSD and TBI in men (Evans et al., 2013; Iverson, Pogoda, Gradus, & Street, 2013). In the future, we intend to include women and make gender ratios similar and more representative of oral parafunctions and bruxing behaviors prevalence. Polysomnography (PSG), the current gold standard for determination of bruxism (Koyano, Tsukiyama, Ichiki, & Kuwata, 2008; Lavigne et al., 2008) was not used in this study because of limited funds. Larger voxel sizes were chosen to compensate for the low signal-to-noise ratio of GABA MRS. The geometric limitations of the MRS VOIs preclude complete sampling of some neuroanatomical regions or include small contributions of adjacent non-targeted regions. The measured GABA levels include some contribution from co-edited macromolecules (MM30) at 3 ppm and a small contribution from homocarnosine and are hence reported together as GABA (GABA+MM30). However, changes in macromolecules have not been reported for anxiety-related disorders to date.

These results in our proof-of-concept study are the first indications of the disturbances in GABAergic and glutamatergic systems of nightguard wearers with oral parafunctions. Future research in larger samples should improve sensitivity of quantifying GABA and other pertinent metabolites and detecting group differences. In addition, results of this study indicate a need for a more comprehensive MRS investigation with an emphasis on

the coupling of anxiety-related and limbic regions with executive control brain networks. The relevance of such research is supported by the observed differences between HPA anxiety-related brain areas as indicated by our finding of negative feedback between the hippocampus and DLPFC. Careful further investigations may reveal not only the neurochemical mechanisms underlying bruxism behaviors and their interactions with other anxiety disorders, but also myofascial TMD as recently documented (Gerstner et al., 2012)

CHAPTER 5. GABA QUANTIFICATION USING LCMODEL – ACCURACY, SENSITIVITY AND SPECIFICITY

5.1 INTRODUCTION

5.1.1 What is LCModel?

LCModel (http://s-provencher.com/pages/lcmodel.shtml) is a tool that enables automatic quantitation of *in vivo* proton MR spectra (S. Provencher, 1993). It utilizes a Linear Combination of Model in vitro / simulated spectra for estimating individual metabolites. The main advantage of using this approach is that the complete model spectra are used for estimation of concentration, in contrast to individual resonances, to incorporate maximum prior information into the analysis. This is particularly helpful to resolve multiplet structures that evolve due to coupling (e.g. GABA) (Stephen W Provencher, 2001). LCModel is not limited to any specific vendor, MRS sequences or localization method, or field strength (up to 16.4 T has been used) as long as the basis spectra (termed ‘basis set’) are also generated using the same scheme.

Some of the key elements/features and parameters of LCModel are briefly outlined below:

- Basis set: Basis sets can be either simulated or obtained using phantoms. It is advisable to include all metabolites that can be expected in the in vivo spectrum.

The basis spectra should have a significantly higher resolution and SNR than in vivo spectra..

- Control file: A control file includes a list of user-selected parameters used for fitting. These can include settings for eddy current correction, water scaling, any optional prior information or constraints (e.g. limiting the peak ratios, omitting certain metabolites from the fit, etc.), settings for the analysis range, display plot details, baseline flexibility settings, etc.
- Baseline estimation: A nearly model-free constrained regularization method is used for estimation of the baseline. It can automatically account for large unexpected distortions, like residual water, susceptibility artifacts and macromolecule or lipid signals.
- Cramér-Rao Lower Bounds (CRLB): CRLB is the lower threshold of the error associated with the model fitting (Kreis, 2015). LCModel outputs these in %SD as estimated standard deviations expressed in percent of the estimated concentrations. %CRLB can be useful reliability indicators if interpreted correctly. Lower %CRLB may be generated using over-simplified models (for instance, fit a linear baseline plus a Lorentzian to each “peak”), and caution must be exercised in interpreting the CRLB estimate. Especially in the case of low concentrations metabolites like GABA, it may not be suitable to use a % CRLB threshold alone to discard any data since the higher % CRLB could be due to smaller concentration (small denominator term).
- Water scaling: Absolute metabolite concentrations can be obtained by scaling metabolite concentrations consistently with the basis set. This is done by using

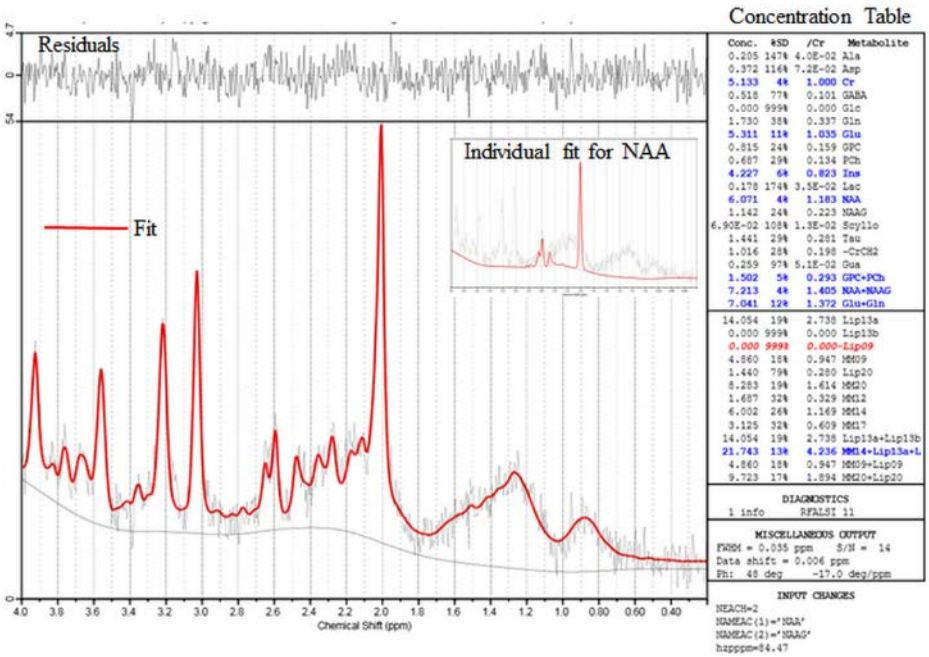

Figure 5.1 Typical LCModel output showing the data, the fit, the residuals, concentration estimates, fit diagnostics and control parameters used for fitting (figure from LCModel manual).Shown inset is the individual fit for the NAA spectrum.

the resonance area of the unsuppressed water peak (reference spectrum) However, due to uncertainties in the exact NMR visible water concentration and the attenuation of the NMR-visible water signal in different tissue types due to relaxation effects, the actual concentrations are given in institutional units (i.u).

- Concentration Ratios: Metabolite concentration ratios can be obtained by specifying a reference metabolite (e.g. creatine). This is useful as ratios are less sensitive to relaxation effects and tissue water concentration.

A typical LCModel output is shown in Figure 5.1.

5.1.2 GABA quantification using LCModel

Earlier versions of LCModel (prior to v 6.3) were mostly suited for short echo time spectra. It has been debated in the literature that the default set of macromolecule resonances and lineshapes in LCModel may not be optimally designed for difference spectra and that better estimation would be possible by including a revised set of macromolecule (MM) functions in the fitting (Murdoch & Dydak, 2011; Schaller et al., 2013). As discussed in chapter 2, handling of baseline is an important step in the accurate quantification of GABA owing to the presence of a co-edited macromolecule (MM30) peak in the TE=68 MEGA-PRESS GABA difference spectra.

An important feature of LCModel that makes it attractive for use with GABA spectra is the customization capability, which allows the user to choose different settings for baseline flexibility and fitting constraints. Stiffer baseline settings have been used in some studies using short TE spectra at 4 T and 7 T or using homonuclear difference editing for detection of ascorbate (Banerjee et al., 2012; Terpstra, Ugurbil, & Tkac, 2010; Tkáč, Öz, Adriany, Uğurbil, & Gruetter, 2009). Moreover, in the latest version of LCModel (v 6.3), the default baseline stiffness has been increased to double the value used in the older versions (v6.2). Exploring firmer baseline settings is of interest also for GABA quantification since the difference spectrum ideally is assumed to have a relatively flat baseline. However, the LCModel User's Manual cautions against using a completely flat baseline; such an approach can yield more reproducible data, but the results may have a systematic bias and can be consistently wrong. Some baseline flexibility is recommended to compensate for the inevitable variability in acquiring in

vivo spectra (S. W. Provencher, 2008). Recently, while comparing different LCModel fitting techniques, Long et al. have shown that a stiffer baseline leads to smaller CRLB values but perhaps an overestimation of GABA, whereas a flexible baseline may lead to slightly higher CRLB values but better GABA estimates (Long, 2013). Long et al. recommended adding a softly constrained MM30 peak to the LCModel fit to explicitly handle the macromolecular portion of the difference spectrum peak at 3.0 ppm and thereby minimize its effect on the measured GABA level. However, their study was done using only one set of in vivo data, of which the "true" GABA concentrations were not known.

The aim of this project was to extend this analysis, by comparing different LCModel fitting techniques using semi-synthetically generated GABA spectra with different noise levels. Different combinations of GABA, other metabolites, MM and noise levels were used to assess the accuracy, sensitivity and specificity of GABA quantification between the different methods.

5.2 MATERIAL AND METHODS

5.2.1 GABA MRS data acquisition

A MEGA-PRESS sequence with an added pre-inversion pulse (O'Gorman, Edden, Michels, Murdoch, & Martin, 2007) (TI=580 ms, TR=2000 ms, TE=68 ms, averages=256, edit pulse BW= 44 Hz, placed at 1.9 and 7.5 ppm in ON and OFF scans) was used to obtain metabolite-nulled spectra on a Siemens 3 T Tim Trio MR scanner

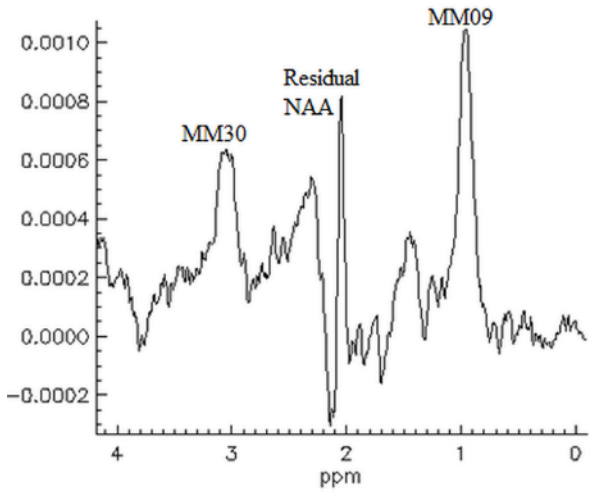

Figure 5.2. Averaged metabolite-nulled spectrum from thalamus of three subjects

using a 32-channel head coil. Metabolite-nulled spectra were obtained from a 25x30x25 mm^3 VOI placed in the right thalamus of three healthy subjects. The metabolite-nulled difference spectra were averaged and apodized using a 1 Hz Gaussian filter to obtain an averaged metabolite-nulled spectrum containing mainly MM30 and MM09 peaks along with some residual NAA, as shown in Figure 5.2.

5.2.2 Simulations

To begin with, MEGA-PRESS difference spectra were generated by adding NAA (60 arbitrary units (a.u.)) and Glu (30 and 36 a.u) with different levels of metabolite line broadening (5 and 7 Hz) to the average metabolite-nulled spectrum. To these spectra, varying levels of GABA were added (0, 2.0, 3.0, and 6.0 a.u.) along with noise that was either artificial/white (A) or realistic (B). Noise type ‘A’ was created with a random number generator and distributed evenly over a -1 to +1 range in the time domain, whereas noise type ‘B’ was real noise from the left-of-water portion of the averaged

metabolite-nulled spectrum. Each type of noise was added using three different scaling factors: 2.0, 4.0, and 6.0. The overall scaling was chosen more-or-less by eye, but the relative scaling was consistent (e.g. the spectrum with noise=A4 had twice as much added noise as the spectrum with noise=A2). A total of 39 spectra (21 with GABA and 18 without GABA) were created. The GABA spectra were generated using a combination of three GABA levels x two noise types x three noise levels + three with no noise, all with one NAA setting (60 a.u.), one Glu setting (30 a.u.), and a metabolite linewidth of 5 Hz. The GABA-free spectra consisted of i) six spectra without additional noise [one NAA level × three Glu levels (0, 30, and 36 a.u.) × two line broadening values] and ii) twelve spectra with added noise [two Glu levels (30 and 36 a.u.) × two noise types × three noise levels]. These were used to determine the sensitivity and specificity of fitting methods.

Furthermore, a few spectra without noise or MMs, i.e., pure simulated metabolites with different GABA, NAA and Glu levels, were generated to compare the accuracy of GABA quantification from all methods.

Finally, for evaluating the sensitivity of the fitting methods in accurately detecting group differences in GABA, two separate cohorts (n=10 each) with GABA levels of 2 (low-GABA group) and 3 (high-GABA group) were generated. Each spectrum in the low-GABA group was replicated for the high-GABA group – the only difference being the GABA level. Three pairs of these simulated spectra were created using the averaged and apodized metabolite-nulled spectrum described previously, but with

differing noise levels. To get more baseline variability for the remaining seven pairs, the three *individual* metabolite-nulled Siemens spectra were used, as well as an average of five metabolite-nulled MEGA-PRESS spectra obtained from the posterior cingulate cortex (PCC) and acquired on a 3T Toshiba Vantage Titan scanner (13-channel head coil, TI=600 ms, TR = 1560-1800 ms, TE = 68 ms, 512 averages, 14 ms editing pulses applied at 1.9 and 7.5 ppm).

5.2.3 LCModel fitting

The basis sets used for fitting GABA spectra were generated from density matrix simulations using published values of chemical shifts and coupling constants (L. G. Kaiser, K. Young, D. J. Meyerhoff, S. G. Mueller, & G. B. Matson, 2008) with an exact treatment of metabolite evolution during the two frequency-selective MEGA inversion pulses. Only those metabolites with differing edit-ON and edit-OFF spectra were included in the basis set: GABA, Glu, Gln, GSH, NAA, and NAAG.

Different LCModel methods (i.e. fitting techniques with customized parameters) were used to analyze the simulated data in LCModel v6.2-0R. The details of the six methods (Murdoch & Dydak, 2011) are as follows:

- Method 1: LCModel's default fully flexible baseline was used to obtain GABA estimates. No special handling of the macromolecular peak at 3.0 ppm was included.

- Method 1M: The baseline was made slightly stiffer using the LCModel control parameter ‘dkntmn,’ which sets the node spacing for the spline baseline function – a larger value yielding a flatter baseline. The default setting for dkntmn in version 6.2-0R is 0.075 ppm (as used in method 1) but a value of 0.15 (same as the default in v6.3) was used for this fitting scheme. The rationale for choosing less flexibility is that a *difference* spectrum should contain a negligible baseline.
- Method 1V: The baseline was fully restricted by setting the LCModel ‘vitro’ parameter to true (corresponds to dkntmn = 0.6). In this technique, the stiff baseline contributes little to fitting the MM component of the peak at 3.0 ppm, so the resulting GABA signal is more accurately “GABA+” (GABA + macromolecules).
- Method 4: A macromolecular peak at 3.0 ppm (“MM30”) was added to the fit using control parameters. Moreover, a soft constraint (MM30/MM09=0.667±0.1) was applied to the ratio of the MM30 and MM09 peaks (Bhagwagar et al., 2007; Murdoch & Dydak, 2011). Because of this extra peak, the resulting GABA values should have minimal contribution from macromolecules at 3.0 ppm.
- Method 4M: Same as Method 4 but with a stiffer baseline (dkntmn=0.15).
- Method 4V: Same as Method 4, but with vitro=true.

5.3 RESULTS

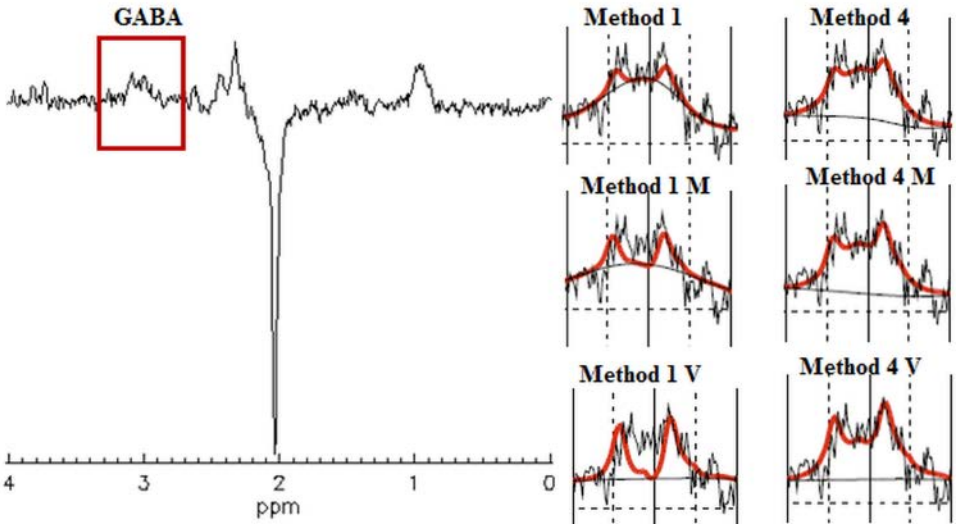

Figure 5.3 A representative simulated GABA spectrum (left) with Glu =30, NAA=60 and GABA=3 amd noise =B4. The GABA fits for all methods are shown on right.

Figure 5.3 shows the LCModel fits of the peak at 3.0 ppm obtained using all six methods for one of the simulated spectra with GABA=3, Glu=30, NAA=60, the averaged MM baseline, and noise level B4.

For the GABA-free input spectra, all methods reported non-zero “phantom” values for GABA, although to a varying degree (Figure 5.4). The smallest amount of GABA was reported by Methods 1 and 4, whereas the highest values were generated by fitting schemes with the vitro option turned on (Methods 1V and 4V). GABA concentrations found by Method 1M were smaller than those of Method 4M. Moreover, all methods reported an increase in “phantom” GABA with increasing noise level for both types of noise (A and B) (Figure 5.4). This effect was more pronounced for Methods 1M and 4M, with a linear increase in the reported GABA value (R^2= 0.98 and R^2=0.96,

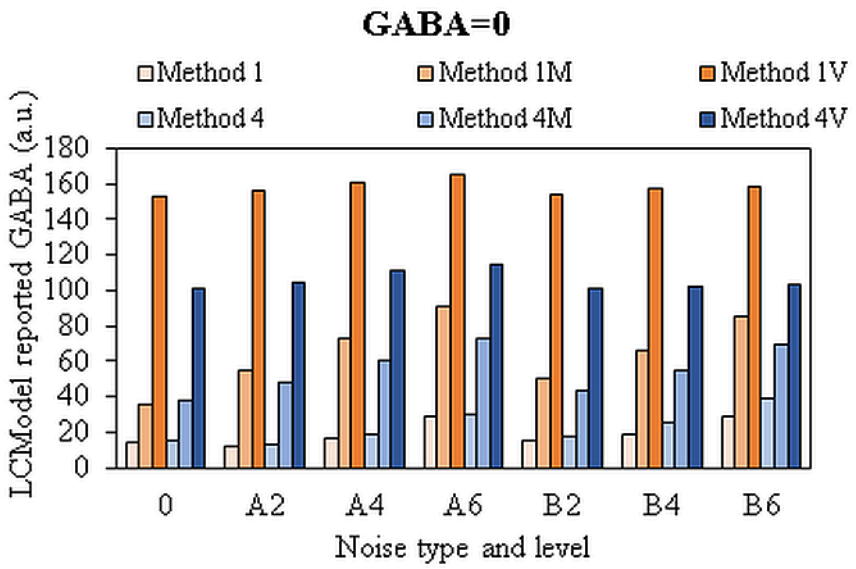

Figure 5.5 LCModel GABA values for a GABA-free input spectrum reported by different methods under different noise conditions

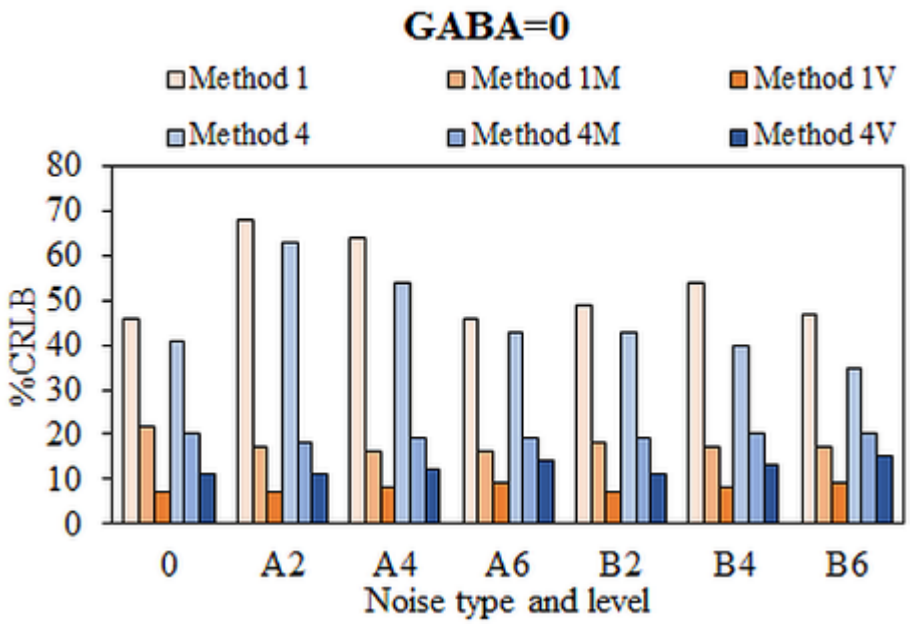

Figure 5.5 LCModel GABA % CRLB values for a GABA-free input spectrum reported by different methods under different noise conditions

respectively, averaged over the two types of noise). In contrast, vitro=T methods

showed the least dependence on noise. In addition, the minimum fit error (%CRLB) for GABA-free spectra was higher for Methods 1 and 4and lowest for vitro methods (Figure 5.5).

For GABA-inclusive spectra, all the methods showed a linear response (R^2>0.98) to

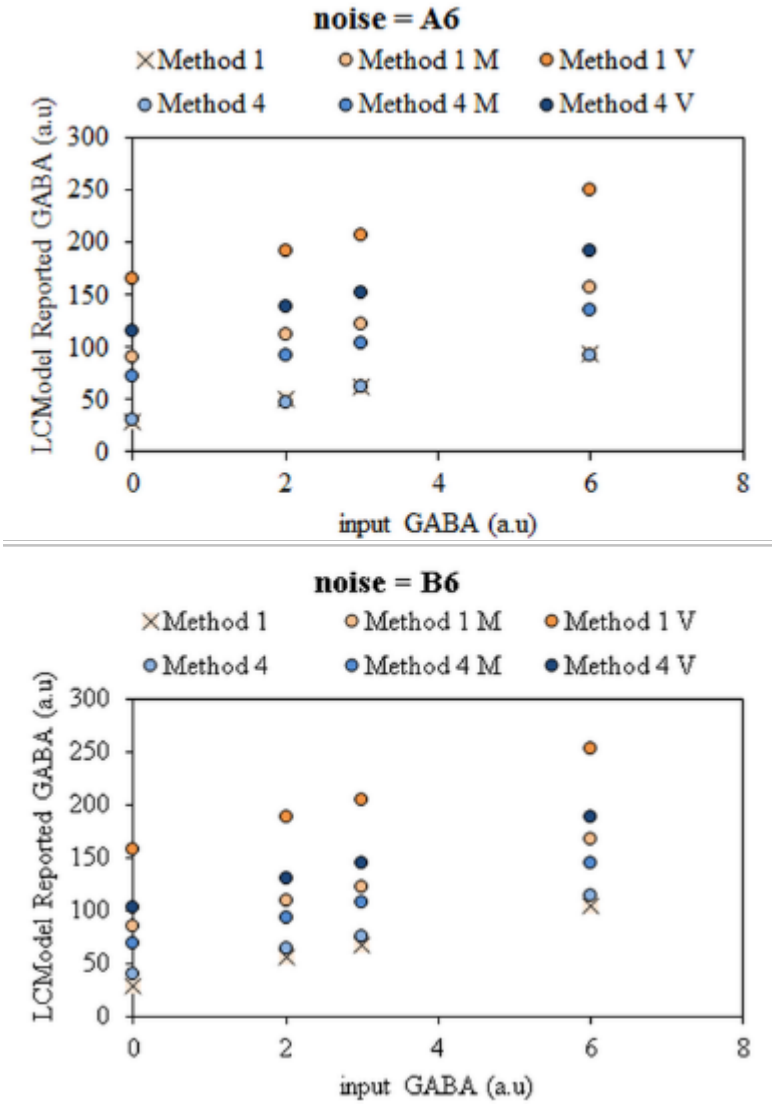

Figure 5.6 Representative charts for noise = A6 (top) and B6 (bottom), showing linear response of all methods to input GABA.

added levels of GABA (2, 3, and 6 a.u.) for all noise levels (Figure 5.6). Moreover, the reported GABA values were very similar for Methods 1 and 4 and somewhat higher, but again similar for Methods 1M and 4M. The % CRLB for all methods improved (i.e., became smaller) with increasing GABA content (Figure 5.7).

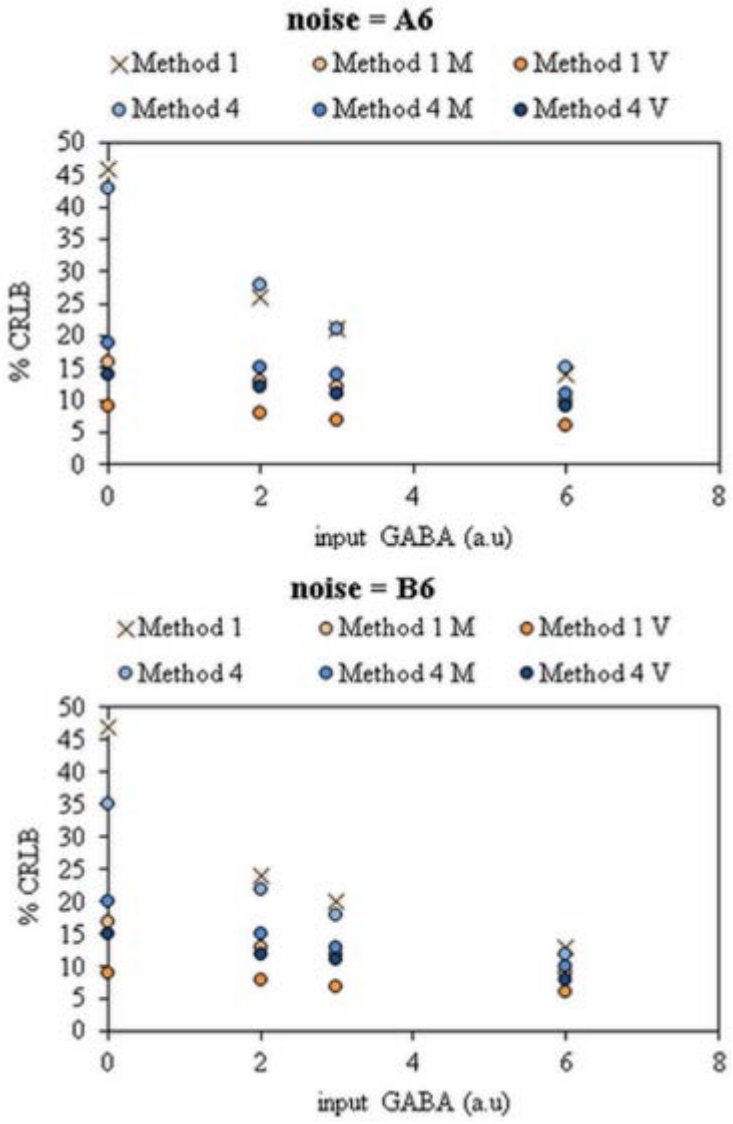

Figure 5.7 Representative charts for noise = A6 (top) and B6 (bottom), showing % CRLB for different methods

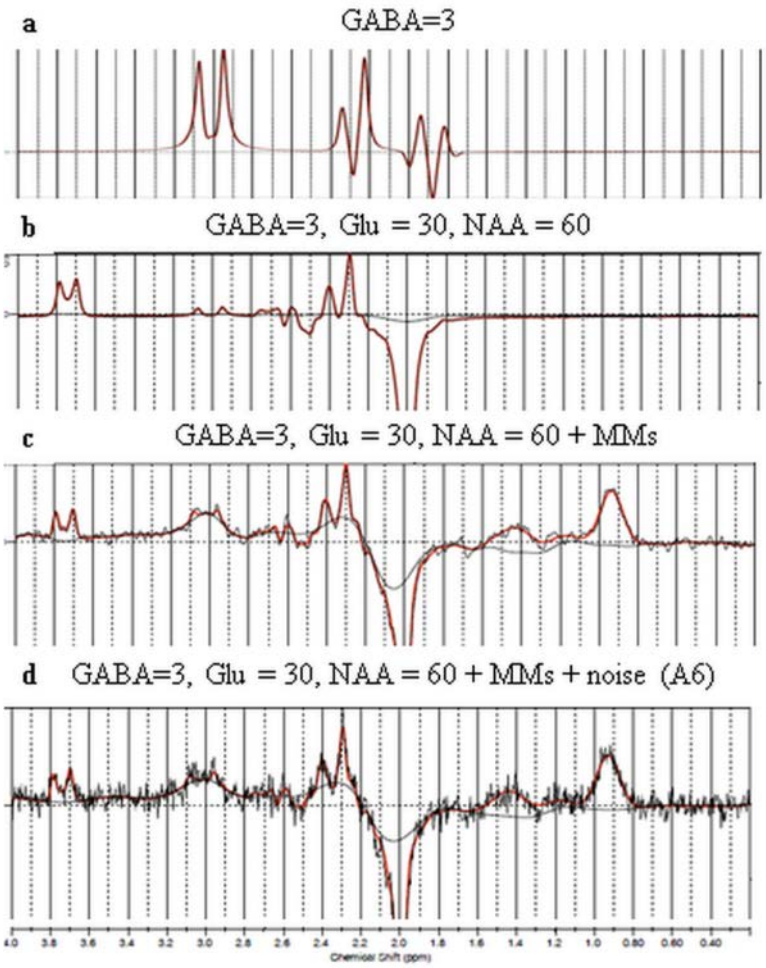

Figure 5.8 LCModel fits using method 1 for spectra with same input GABA but different levels of metabolites, macromolecules and noise

To test the accuracy of the reported GABA levels, the GABA values obtained from the noise-free and MM-free (i.e., pure) simulated spectra (e.g. Figure 5.8 a) were used as a standard to determine how closely the methods estimated GABA in the presence of other metabolites, MMs and noise in the corresponding spectra. Figure 5.8 shows representative LCModel output for spectra generated for a GABA level of 3. In fitting the metabolite-only spectrum in Figure 5.8 b, results from method 1 and 4 were slightly closer to the GABA level reported for the GABA-only spectrum in Figure 5.8a than

were results for methods with stiffer baselines (ratio > 0.8). Methods 1 and 4 also performed better in the presence of increasing noise, reporting values closest to the actual GABA level, whereas all the other variants overestimated the GABA content (Figure 5.9 and Figure 5.10).

Finally, for the two simulated cohorts, only the GABA values from methods 1 and 4

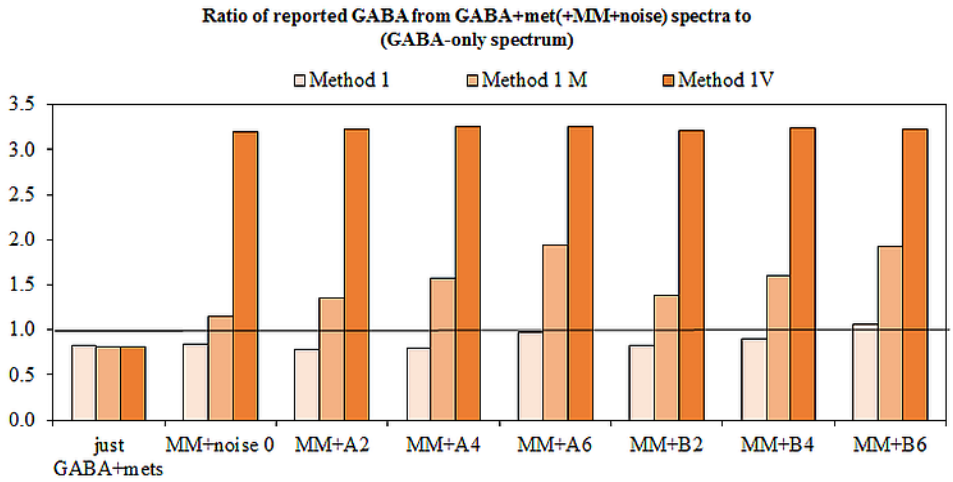

Figure 5.10 Ratio of reported GABA from GABA+met (+MM+noise) spectra to (GABA-only spectrum) for method 1 variants

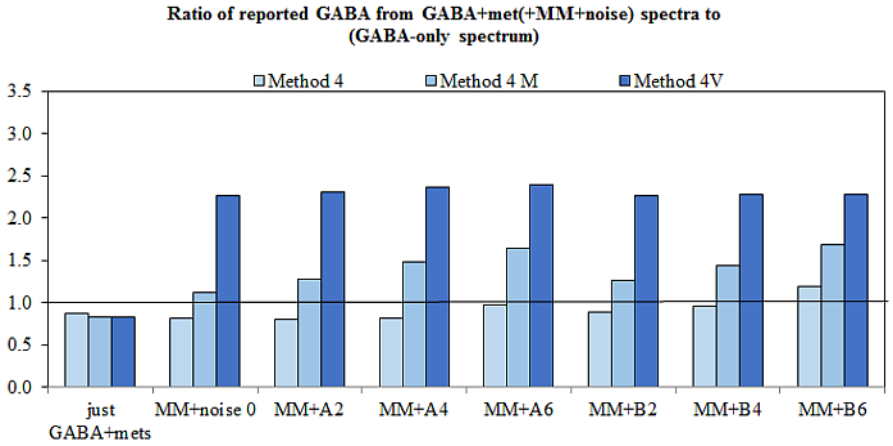

Figure 5.10 Ratio of reported GABA from GABA+met (+MM+noise) spectra to (GABA-only spectrum) for method 4 variants

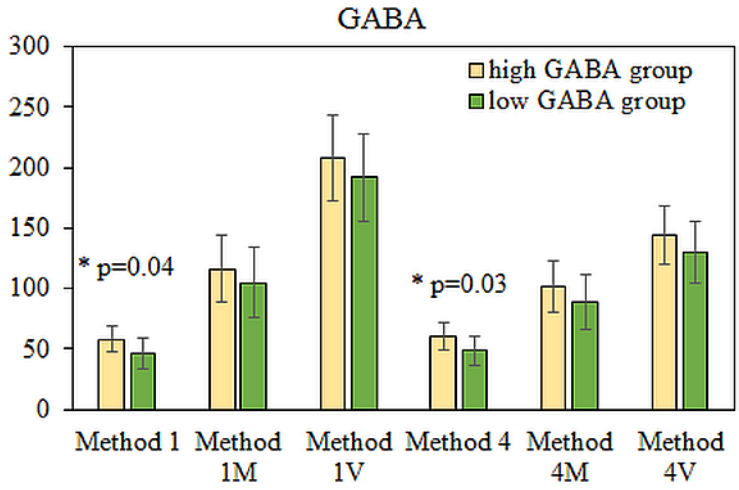

Figure 5.11 Method 1 and 4 detected group difference between low and high GABA cohorts

were found to be significantly different between the two groups ($p<0.05$), even though by design the GABA was 1.5 times higher in one group than the other (Figure 5.11). This illustrates that methods with flexible baseline are perhaps most sensitive for determining group differences.

5.4 CONCLUSION AND DISCUSSION

The closeness in GABA values reported by methods 1and 4 (and the similar results for method 1M vs. method 4M) indicates that the effect of the soft-constrained MM30 peak is much smaller compared to the effect of baseline stiffness. However, with increasing stiffness of the baseline, the GABA values reported by the two types of fitting (i.e., with or without an explicit MM30 peak) differ more. This also indicates that the MM30 peak may be well estimated by the flexible baseline and method 4 may not provide a big advantage over method 1.

For GABA-free spectra, the high %CRLB values on the left side of the plots in Figure 5.7 suggest that the results from Method 1 and 4 estimated negligible amount of GABA. However, since detected GABA was not entirely zero, these were still wrong since no GABA was actually present. On the other hand, the low %CRLB values associated with the vitro=T methods would lead to false positives.

The GABA values reported by methods using a fully flexible baseline were the most accurate in estimating actual GABA concentrations and showed the least variation with addition of noise. These methods were also able to correctly identify a significant group difference between the high-GABA and low-GABA cohorts. These results indicate that the LCModel default baseline may be able to handle the presence of MMs in GABA difference spectra better than thought earlier, resulting in more accurate levels of GABA. Since an increase in noise resulted in an increase in reported GABA by all methods, GABA from smaller voxel locations would likely be overestimated.

If we define sensitivity as the ability to detect real changes in GABA, then the sensitivity of all the fitting methods was similar ($R^2 > 0.98$ for measured GABA vs input GABA). If we define specificity as the ability to correctly identify the absence of GABA, then the specificity of the methods with fully flexible baseline was the highest.

A method with high accuracy, high specificity and high sensitivity is desirable for GABA quantification. Results of the current preliminary simulation study provide indication that a flexible baseline with a small knot spacing of the spline function is, in fact, the most accurate method for estimating GABA content from MEGA-PRESS

difference spectra with high sensitivity and specificity. Hence, it may be reasonable to change the default node spacing setting to the original value in the newer LCModel versions.

REFERENCES

REFERENCES

Albin, R. L., Young, A. B., & Penney, J. B. (1989). The functional anatomy of basal ganglia disorders. *Trends in neurosciences, 12*(10), 366-375.

Albouy, G., King, B. R., Maquet, P., & Doyon, J. (2013). Hippocampus and striatum: Dynamics and interaction during acquisition and sleep-related motor sequence memory consolidation. *Hippocampus*. doi: 10.1002/hipo.22183

Albouy, G., Sterpenich, V., Vandewalle, G., Darsaud, A., Gais, S., Rauchs, G., . . . Maquet, P. (2013). Interaction between hippocampal and striatal systems predicts subsequent consolidation of motor sequence memory. *PLoS One, 8*(3), e59490. doi: 10.1371/journal.pone.0059490 PONE-D-12-28753 [pii]

Anglin, R. E., Rosebush, P. I., Noseworthy, M. D., Tarnopolsky, M., & Mazurek, M. F. (2012). Psychiatric symptoms correlate with metabolic indices in the hippocampus and cingulate in patients with mitochondrial disorders. *Transl Psychiatry, 2*, e187. doi: 10.1038/tp.2012.107 tp2012107 [pii]

ASTM F2182 - 11a Standard Test Method for Measurement of Radio Frequency Induced Heating On or Near Passive Implants During Magnetic Resonance Imaging (2011).

Baba, K., Haketa, T., Sasaki, Y., Ohyama, T., & Clark, G. T. (2005). Association between masseter muscle activity levels recorded during sleep and signs and symptoms of temporomandibular disorders in healthy young adults. *J Orofac Pain, 19*(3), 226-231.

Bagga, P., Chugani, A. N., Varadarajan, K. S., & Patel, A. B. (2013). In vivo NMR studies of regional cerebral energetics in MPTP model of Parkinson's disease: recovery of cerebral metabolism with acute levodopa treatment. *Journal of neurochemistry, 127*(3), 365-377.

Banerjee, A., Ganji, S., Hulsey, K., Dimitrov, I., Maher, E., Ghose, S., . . . Choi, C. (2012). Measurement of glycine in gray and white matter in the human brain in vivo by 1H MRS at 7.0 T. *Magn Reson Med, 68*(2), 325-331. doi: 10.1002/mrm.24368

Bansal, N., & Seshan, V. (1995). Three-dimensional triple quantum-filtered ^{23}Na imaging of rabbit kidney with weighted signal averaging. *J Magn Reson Imaging, 5*(6), 761-767.

Bar-Haim, Y., Lamy, D., Pergamin, L., Bakermans-Kranenburg, M. J., & van, I. M. H. (2007). Threat-related attentional bias in anxious and nonanxious individuals: a meta-analytic study. *Psychol Bull, 133*(1), 1-24. doi: 2006-23058-001 [pii] 10.1037/0033-2909.133.1.1

Bassen, H., Kainz, W., Mendoza, G., & Kellom, T. (2006). MRI induced heating of selected thin wire metallic implants – laboratory and computational studies – findings and new questions raised. *Minim Invasive Ther Allied Technol, 15*(2), 76-84. doi: 10.1080/13645700600640931

Bhagwagar, Z., Wylezinska, M., Jezzard, P., Evans, J., Ashworth, F., Sule, A., . . . Cowen, P. J. (2007). Reduction in occipital cortex γ-aminobutyric acid concentrations in medication-free recovered unipolar depressed and bipolar subjects. *Biological psychiatry, 61*(6), 806-812.

Bishop, S. J., Jenkins, R., & Lawrence, A. D. (2007). Neural processing of fearful faces: effects of anxiety are gated by perceptual capacity limitations. *Cereb Cortex, 17*(7), 1595-1603. doi: bhl070 [pii] 10.1093/cercor/bhl070

Bremner, J. D. (2007). Neuroimaging in posttraumatic stress disorder and other stress-related disorders. *Neuroimaging Clin N Am, 17*(4), 523-538, ix. doi: S1052-5149(07)00066-4 [pii] 10.1016/j.nic.2007.07.003

Brooks, D. J. (2012). Parkinson's disease: diagnosis. *Parkinsonism & related disorders, 18*, S31-S33.

Brown, M. A., & Semelka, R. C. (2011). *MRI: basic principles and applications*: John Wiley & Sons.

Brown, P., & Marsden, C. (1998). What do the basal ganglia do? *The Lancet, 351*(9118), 1801-1804.

Brownell, A.-L., Jenkins, B. G., Elmaleh, D. R., Deacon, T. W., Spealman, R. D., & Isacson, O. (1998). Combined PET/MRS brain studies show dynamic and long-term physiological changes in a primate model of Parkinson disease. *Nature medicine, 4*(11), 1308-1312.

Burris, J. L., Evans, D. R., & Carlson, C. R. (2010). Psychological correlates of medical comorbidities in patients with temporomandibular disorders. *J Am Dent Assoc, 141*(1), 22-31. doi: 141/1/22 [pii]

Byrd, K., Romito, L., Dzemidzic, M., Wong, D., & Talavage, T. (2009). fMRI study of brain activity elicited by oral parafunctional movements. *Journal of Oral Rehabilitation, 36*(5), 346-361.

Cameron, O. G., Huang, G. C., Nichols, T., Koeppe, R. A., Minoshima, S., Rose, D., & Frey, K. A. (2007). Reduced gamma-aminobutyric acid(A)-benzodiazepine binding sites in insular cortex of individuals with panic disorder. *Arch Gen Psychiatry, 64*(7), 793-800. doi: 64/7/793 [pii]10.1001/archpsyc.64.7.793

Cao, Z., Park, J., Cho, Z.-H., & Collins, C. M. (2014). Numerical evaluation of image homogeneity, signal-to-noise ratio, and specific absorption rate for human brain imaging at 1.5, 3, 7, 10.5, and 14T in an 8-channel transmit/receive array. *J Magn Reson Imaging*. doi: 10.1002/jmri.24689

Chassain, C., Bielicki, G., Durand, E., Lolignier, S., Essafi, F., Traoré, A., & Durif, F. (2008). Metabolic changes detected by proton magnetic resonance spectroscopy in vivo and in vitro in a murin model of Parkinson's disease, the MPTP-intoxicated mouse. *Journal of neurochemistry, 105*(3), 874-882.

Chaudhuri, K., Lemmens, G., Williams, S., Ellis, C., Lloyd, C., Dawson, J., . . . Leigh, P. (1996). Proton magnetic resonance spectroscopy of the striatum in Parkinson's disease patients with motor response fluctuations. *Parkinsonism & related disorders, 2*(2), 63-67.

Chaudhuri, K. R., Healy, D. G., & Schapira, A. H. (2006). Non-motor symptoms of Parkinson's disease: diagnosis and management. *The Lancet Neurology, 5*(3), 235-245.

Chen, W. H., Lu, Y. C., Lui, C. C., & Liu, J. S. (2005). A proposed mechanism for diurnal/nocturnal bruxism: hypersensitivity of presynaptic dopamine receptors in the frontal lobe. *J Clin Neurosci, 12*(2), 161-163. doi: S0967-5868(04)00228-0 [pii] 10.1016/j.jocn.2004.07.007

Cho, S., Metcalfe, A. W., Young, C. B., Ryali, S., Geary, D. C., & Menon, V. (2012). Hippocampal-prefrontal engagement and dynamic causal interactions in the maturation of children's fact retrieval. *J Cogn Neurosci, 24*(9), 1849-1866. doi: 10.1162/jocn_a_00246

Choe, B.-Y., Park, J.-W., Lee, K.-s., Son, B.-C., Kim, M.-C., Kim, B.-S., . . . Shinn, K.-S. (1998). Neuronal laterality in Parkinson's disease with unilateral symptom by in vivo 1H magnetic resonance spectroscopy. *Investigative Radiology, 33*(8), 450-455.

Choi, C.-B., Kim, S.-Y., Lee, S.-H., Jahng, G.-H., Kim, H.-Y., Choe, B.-Y., . . . Choi, W.-S. (2011). Assessment of metabolic changes in the striatum of a MPTP-intoxicated canine model: in vivo< sup> 1</sup> H-MRS study of an animal model for Parkinson's disease. *Magn Reson Imaging, 29*(1), 32-39.

Chowdhury, F. A., O'Gorman, R. L., Nashef, L., & al., e. (2014). Investigation of glutamine and GABA levels in patients with idiopathic generalized epilepsy using MEGAPRESS. *J Magn Reson Imaging*. doi: 10.1002/jmri.24611

Chowdhury, F. A., O'Gorman, R. L., Nashef, L., Elwes, R. D., Edden, R. A., Murdoch, J. B., . . . Richardson, M. P. (2014). Investigation of glutamine and GABA levels in patients with idiopathic generalized epilepsy using MEGAPRESS. *J Magn Reson Imaging*. doi: 10.1002/jmri.24611

Ciurleo, R., Di Lorenzo, G., Bramanti, P., & Marino, S. (2014). Magnetic Resonance Spectroscopy: An In Vivo Molecular Imaging Biomarker for Parkinson's Disease? *BioMed Research International, 2014*.

Coman, D., Trubel, H. K., & Hyder, F. (2010). Brain temperature by Biosensor Imaging of Redundant Deviation in Shifts (BIRDS): comparison between TmDOTP5− and TmDOTMA−. *NMR in Biomedicine, 23*(3), 277-285.

Compton, R. J., Banich, M. T., Mohanty, A., Milham, M. P., Herrington, J., Miller, G. A., . . . Heller, W. (2003). Paying attention to emotion: an fMRI investigation of cognitive and emotional stroop tasks. *Cogn Affect Behav Neurosci, 3*(2), 81-96.

Coune, P., Craveiro, M., Gaugler, M., Mlynárik, V., Schneider, B., Aebischer, P., & Gruetter, R. (2013). An in vivo ultrahigh field 14.1 T 1H-MRS study on 6-OHDA and α-synuclein-based rat models of Parkinson's disease: GABA as an early disease marker. *NMR Biomed, 26*(1), 43-50.

de Graaf, R. A. (2014). Chapter 1.4 - Spectral Editing and 2D NMR. In C. Stagg & D. Rothman (Eds.), *Magnetic Resonance Spectroscopy* (pp. 40-48). San Diego: Academic Press.

Denkova, E., Wong, G., Dolcos, S., Sung, K., Wang, L., Coupland, N., & Dolcos, F. (2010). The impact of anxiety-inducing distraction on cognitive performance: a combined brain imaging and personality investigation. *PLoS One, 5*(11), e14150. doi: 10.1371/journal.pone.0014150

Duncan, J. (2010). The multiple-demand (MD) system of the primate brain: mental programs for intelligent behaviour. *Trends Cogn Sci, 14*(4), 172-179. doi: 10.1016/j.tics.2010.01.004 S1364-6613(10)00005-7 [pii]

Dworkin, S. F., & LeResche, L. (1992). Research diagnostic criteria for temporomandibular disorders: review, criteria, examinations and specifications, critique. *Journal of craniomandibular disorders: facial & oral pain, 6*(4), 301.

Dydak, U., Jiang, Y.-M., Long, L.-L., Zhu, H., Chen, J., Li, W.-M., . . . Long, Z. (2010). In vivo measurement of brain GABA concentrations by magnetic resonance spectroscopy in smelters occupationally exposed to manganese. *Environmental health perspectives, 119*(2), 219-224.

Edden, R. A., & Barker, P. B. (2007). Spatial effects in the detection of γ-aminobutyric acid: Improved sensitivity at high fields using inner volume saturation. *Magn Reson Med, 58*(6), 1276-1282.

Edden, R. A. E., & Barker, P. B. (2007). Spatial effects in the detection of γ-aminobutyric acid: Improved sensitivity at high fields using inner volume saturation. *Magn Reson Med, 58*(6), 1276-1282.

Edden, R. A. E., Puts, N. A. J., & Barker, P. B. (2012). Macromolecule-suppressed GABA-edited magnetic resonance spectroscopy at 3T. *Magn Reson Med, 68*(3), 657-661. doi: 10.1002/mrm.24391

Emir, U. E., Tuite, P. J., & Öz, G. (2012). Elevated pontine and putamenal GABA levels in mild-moderate Parkinson disease detected by 7 tesla proton MRS. *PloS one, 7*(1), e30918.

Etkin, A., & Wager, T. D. (2007). Functional neuroimaging of anxiety: a meta-analysis of emotional processing in PTSD, social anxiety disorder, and specific phobia. *Am J Psychiatry, 164*(10), 1476-1488. doi: 10.1176/appi.ajp.2007.07030504

Evans, C. T., St Andre, J. R., Pape, T. L., Steiner, M. L., Stroupe, K. T., Hogan, T. P., . . . Smith, B. M. (2013). An evaluation of the Veterans Affairs traumatic brain injury screening process among Operation Enduring Freedom and/or Operation Iraqi Freedom veterans. *PM R, 5*(3), 210-220; quiz 220. doi: 10.1016/j.pmrj.2012.12.004 S1934-1482(12)01773-X [pii]

FDA, U. (2014). *Criteria for Significant Risk Investigations of Magnetic Resonance Diagnostic Devices - Guidance for Industry and Food and Drug Administration Staff*.

Ferrer, I. (2009). Early involvement of the cerebral cortex in Parkinson's disease: convergence of multiple metabolic defects. *Progress in neurobiology, 88*(2), 89-103.

Galvan, A., & Wichmann, T. (2007). GABAergic circuits in the basal ganglia and movement disorders. *Progress in brain research, 160*, 287-312.

Ganon-Elazar, E., & Akirav, I. (2013). Cannabinoids and traumatic stress modulation of contextual fear extinction and GR expression in the amygdala-hippocampal-prefrontal circuit. *Psychoneuroendocrinology, 38*(9), 1675-1687. doi: 10.1016/j.psyneuen.2013.01.014 S0306-4530(13)00019-X [pii]

Gao, H.-C., Zhu, H., Song, C.-Y., Lin, L., Xiang, Y., Yan, Z.-H., . . . Li, X.-K. (2013). Metabolic changes detected by ex vivo high resolution 1H NMR spectroscopy in the striatum of 6-OHDA-induced Parkinson's rat. *Molecular neurobiology, 47*(1), 123-130.

Gensler, D., Fidler, F., Ehses, P., Warmuth, M., Reiter, T., Düring, M., . . . Nordbeck, P. (2012). MR safety: Fast T1 thermometry of the RF-induced heating of medical devices. *Magn Reson Med, 68*(5), 1593-1599. doi: 10.1002/mrm.24171

Gerlach, M., Gsell, W., Kornhuber, J., Jellinger, K., Krieger, V., Pantucek, F., . . . Riederer, P. (1996). A post mortem study on neurochemical markers of dopaminergic, GABA-ergic and glutamatergic neurons in basal ganglia-thalamocortical circuits in Parkinson syndrome. *Brain research, 741*(1), 142-152.

Gerstner, G. E., Gracely, R. H., Deebajah, A., Ichesco, E., Quintero, A., Clauw, D. J., & Sundgren, P. C. (2012). Posterior insular molecular changes in myofascial pain. *J Dent Res, 91*(5), 485-490. doi: 0022034512443366 [pii] 10.1177/0022034512443366

Gilbertson, M. W., Shenton, M. E., Ciszewski, A., Kasai, K., Lasko, N. B., Orr, S. P., & Pitman, R. K. (2002). Smaller hippocampal volume predicts pathologic vulnerability to psychological trauma. *Nat Neurosci, 5*(11), 1242-1247. doi: 10.1038/nn958nn958 [pii]

Goddard, A. W., Mason, G. F., Almai, A., Rothman, D. L., Behar, K. L., Petroff, O. A., . . . Krystal, J. H. (2001). Reductions in occipital cortex GABA levels in panic disorder detected with 1h-magnetic resonance spectroscopy. *Archives of General Psychiatry, 58*(6), 556-561.

Goddard, A. W., Mason, G. F., Appel, M., Rothman, D. L., Gueorguieva, R., Behar, K. L., & Krystal, J. H. (2004). Impaired GABA neuronal response to acute benzodiazepine administration in panic disorder. *Am J Psychiatry, 161*(12), 2186-2193. doi: 161/12/2186 [pii]10.1176/appi.ajp.161.12.2186

Gorny, K. R., & et al. (2008). Calorimetric calibration of head coil SAR estimates displayed on a clinical MR scanner. *Phys Med Biol, 53*(10), 2565.

Gröger, A., Kolb, R., Schäfer, R., & Klose, U. (2014). Dopamine Reduction in the Substantia Nigra of Parkinson's Disease Patients Confirmed by In Vivo Magnetic Resonance Spectroscopic Imaging. *PloS one, 9*(1), e84081.

Gruetter, R. (1993). Automatic, localized in Vivo adjustment of all first-and second-order shim coils. *Magn Reson Med, 29*(6), 804-811.

Hargreaves, B. A., Worters, P. W., Pauly, K. B., Pauly, J. M., Koch, K. M., & Gold, G. E. (2011). Metal-induced artifacts in MRI. *AJR Am J Roentgenol, 197*(3), 547-555.

Harris, A. D., Puts, N. A. J., Barker, P. B., & Edden, R. A. E. (2014). Spectral-editing measurements of GABA in the human brain with and without macromolecule suppression. *Magn Reson Med*. doi: 10.1002/mrm.25549

Hasler, G., Nugent, A. C., Carlson, P. J., Carson, R. E., Geraci, M., & Drevets, W. C. (2008). Altered cerebral gamma-aminobutyric acid type A-benzodiazepine receptor binding in panic disorder determined by [11C]flumazenil positron emission tomography. *Arch Gen Psychiatry, 65*(10), 1166-1175. doi: 65/10/1166 [pii] 10.1001/archpsyc.65.10.1166

Hasler, G., van der Veen, J. W., Tumonis, T., Meyers, N., Shen, J., & Drevets, W. C. (2007). Reduced prefrontal glutamate/glutamine and γ-aminobutyric acid levels in major depression determined using proton magnetic resonance spectroscopy. *Archives of General Psychiatry, 64*(2), 193-200.

Hattingen, E., Magerkurth, J., Pilatus, U., Mozer, A., Seifried, C., Steinmetz, H., . . . Hilker, R. (2009). Phosphorus and proton magnetic resonance spectroscopy demonstrates mitochondrial dysfunction in early and advanced Parkinson's disease. *Brain, 132*(Pt 12), 3285-3297. doi: 10.1093/brain/awp293

Henry, P. G., Dautry, C., Hantraye, P., & Bloch, G. (2001). Brain GABA editing without macromolecule contamination. *Magn Reson Med, 45*(3), 517-520.

Herman, J. P., Ostrander, M. M., Mueller, N. K., & Figueiredo, H. (2005). Limbic system mechanisms of stress regulation: hypothalamo-pituitary-adrenocortical axis. *Prog Neuropsychopharmacol Biol Psychiatry, 29*(8), 1201-1213. doi: S0278-5846(05)00269-1 [pii]10.1016/j.pnpbp.2005.08.006

Hicks, R. A., Conti, P. A., & Bragg, H. R. (1990). Increases in nocturnal bruxism among college students implicate stress. *Med Hypotheses, 33*(4), 239-240. doi: 0306-9877(90)90134-Z [pii]

Hindman, J. C. (1966). Proton Resonance Shift of Water in the Gas and Liquid States. *J Chem Phys, 44*(12), 4582-4592. doi: 10.1063/1.1726676

Holshouser, B. A., Komu, M., Möller, H. E., Zijlmans, J., Kolem, H., Hinshaw, D. B., . . . Masur, H. (1995). Localized proton NMR spectroscopy in the striatum of patients with idiopathic Parkinson's disease: a multicenter pilot study. *Magn Reson Med, 33*(5), 589-594.

Hu, M., Taylor-Robinson, S. D., Chaudhuri, K. R., Bell, J. D., Morris, R., Clough, C., . . . Turjanski, N. (1999). Evidence for cortical dysfunction in clinically non-demented patients with Parkinson's disease: a proton MR spectroscopy study. *Journal of Neurology, Neurosurgery & Psychiatry, 67*(1), 20-26.

Huynh, N., Kato, T., Rompre, P. H., Okura, K., Saber, M., Lanfranchi, P. A., . . . Lavigne, G. J. (2006). Sleep bruxism is associated to micro-arousals and an increase in cardiac sympathetic activity. *J Sleep Res, 15*(3), 339-346. doi: JSR536 [pii] 10.1111/j.1365-2869.2006.00536.x

IEC. (2010). International standard, medical equipment—part 2: particular requirements for the safety of magnetic resonance equipment for medical diagnosis, 3rd edition (Vol. 601-2-33). Geneva.

Ishihara, Y., Calderon, A., Watanabe, H., Okamoto, K., Suzuki, Y., Kuroda, K., & Suzuki, Y. (1995). A precise and fast temperature mapping using water proton chemical shift. *Magn Reson Med, 34*(6), 814-823.

Iverson, K. M., Pogoda, T. K., Gradus, J. L., & Street, A. E. (2013). Deployment-related traumatic brain injury among Operation Enduring Freedom/Operation Iraqi Freedom veterans: associations with mental and physical health by gender. *J Womens Health (Larchmt), 22*(3), 267-275. doi: 10.1089/jwh.2012.3755

James, J. R., Gao, Y., Miller, M. A., Babsky, A., & Bansal, N. (2009). Absolute temperature MR imaging with thulium 1,4,7,10-tetraazacyclododecane-1,4,7,10-tetramethyl-1,4,7,10-tetraacetic acid (TmDOTMA−). *Magn Reson Med, 62*(2), 550-556. doi: 10.1002/mrm.22039

Jankord, R., & Herman, J. P. (2008). Limbic regulation of hypothalamo-pituitary-adrenocortical function during acute and chronic stress. *Ann N Y Acad Sci, 1148*, 64-73. doi: 10.1196/annals.1410.012 NYAS1148012 [pii]

Jin, J. M., & et al. (1996). Computation of electromagnetic fields for high-frequency magnetic resonance imaging applications. *Phys Med Biol, 41*(12), 2719.

Jones, B. (2000). Basic mechanisms of sleep-wake states. *Principles and practice of sleep medicine, 3*, 134-154.

Kaiser, L., Young, K., Meyerhoff, D., Mueller, S., & Matson, G. (2008). A detailed analysis of localized J-difference GABA editing: theoretical and experimental study at 4 T. *NMR Biomed, 21*(1), 22-32.

Kaiser, L. G., Young, K., Meyerhoff, D. J., Mueller, S. G., & Matson, G. B. (2008). A detailed analysis of localized J-difference GABA editing: theoretical and experimental study at 4 T. *NMR Biomed, 21*(1), 22-32. doi: 10.1002/nbm.1150

Kato, T., & Lavigne, G. J. (2010). Sleep bruxism: A sleep-related movement disorder. *Sleep Medicine Clinics, 5*(1), 9-35.

Keefe, F. J., & Dolan, E. A. (1988). Correlation of pain behavior and muscle activity in patients with myofascial pain-dysfunction syndrome. *J Craniomandib Disord, 2*(4), 181-184.

Kight, M., Gatchel, R. J., & Wesley, L. (1999). Temporomandibular disorders: evidence for significant overlap with psychopathology. *Health Psychol, 18*(2), 177-182.

Kish, S. J., Rajput, A., Gilbert, J., Rozdilsky, B., Chang, L. J., Shannak, K., & Hornykiewicz, O. (1986). Elevated γ-aminobutyric acid level in striatal but not extrastriatal brain regions in Parkinson's disease: Correlation with striatal dopamine loss. *Annals of neurology, 20*(1), 26-31.

Koyano, K., Tsukiyama, Y., Ichiki, R., & Kuwata, T. (2008). Assessment of bruxism in the clinic. *J Oral Rehabil, 35*(7), 495-508. doi: JOR1880 [pii] 10.1111/j.1365-2842.2008.01880.x

Kreis, R. (2015). The trouble with quality filtering based on relative Cramér-Rao lower bounds. *Magn Reson Med*, n/a-n/a. doi: 10.1002/mrm.25568

Laberge, L., Tremblay, R. E., Vitaro, F., & Montplaisir, J. (2000). Development of parasomnias from childhood to early adolescence. *Pediatrics, 106*(1 Pt 1), 67-74.

Lavigne, G. J., Khoury, S., Abe, S., Yamaguchi, T., & Raphael, K. (2008). Bruxism physiology and pathology: an overview for clinicians. *J Oral Rehabil, 35*(7), 476-494. doi: JOR1881 [pii] 10.1111/j.1365-2842.2008.01881.x

Lavigne, G. J., Manzini, C., & Kato, T. (2005). Sleep bruxism. Principles and practice of sleep medicine: Philadelphia: Elsevier Saunders.

Lavigne, G. J., & Montplaisir, J. Y. (1994). Restless legs syndrome and sleep bruxism: prevalence and association among Canadians. *Sleep, 17*(8), 739-743.

Lavigne, G. J., Soucy, J. P., Lobbezoo, F., Manzini, C., Blanchet, P. J., & Montplaisir, J. Y. (2001). Double-blind, crossover, placebo-controlled trial of bromocriptine in patients with sleep bruxism. *Clin Neuropharmacol, 24*(3), 145-149.

Liu, G., Qin, Q., Chan, K. W. Y., Li, Y., Bulte, J. W. M., McMahon, M. T., . . . Gilad, A. A. (2014). Non-invasive temperature mapping using temperature-responsive water saturation shift referencing (T-WASSR) MRI. *NMR Biomed, 27*(3), 320-331. doi: 10.1002/nbm.3066

Lobbezoo, F., Brouwers, J. E., Cune, M. S., & Naeije, M. (2006). Dental implants in patients with bruxing habits. *J Oral Rehabil, 33*(2), 152-159. doi: JOR1542 [pii] 10.1111/j.1365-2842.2006.01542.x

Lobbezoo, F., & Lavigne, G. J. (1997). Do bruxism and temporomandibular disorders have a cause-and-effect relationship? *J Orofac Pain, 11*(1), 15-23.

Lobbezoo, F., Lavigne, G. J., Tanguay, R., & Montplaisir, J. Y. (1997). The effect of catecholamine precursor L-dopa on sleep bruxism: a controlled clinical trial. *Mov Disord, 12*(1), 73-78. doi: 10.1002/mds.870120113

Lobbezoo, F., & Naeije, M. (2001). Bruxism is mainly regulated centrally, not peripherally. *J Oral Rehabil, 28*(12), 1085-1091. doi: 839 [pii]

Lobbezoo, F., Soucy, J. P., Montplaisir, J. Y., & Lavigne, G. J. (1996). Striatal D2 receptor binding in sleep bruxism: a controlled study with iodine-123-iodobenzamide and single-photon-emission computed tomography. *J Dent Res, 75*(10), 1804-1810.

Lobbezoo, F., van Denderen, R. J., Verheij, J. G., & Naeije, M. (2001). Reports of SSRI-associated bruxism in the family physician's office. *J Orofac Pain, 15*(4), 340-346.

Long, Z. (2013). *In vivo quantification of GABA by magnetic resonance spectroscopy and its applications in panic disorder and manganese neurotoxicity.* (Ph.D.), Purdue University.

Long, Z., Li, X.-R., Xu, J., Edden, R. A., Qin, W.-P., Long, L.-L., . . . Dydak, U. (2014). Thalamic GABA Predicts Fine Motor Performance in Manganese-Exposed Smelter Workers. *PloS one, 9*(2), e88220.

Long, Z., Medlock, C., Dzemidzic, M., Shin, Y., Goddard, A. W., & Dydak, U. (2013). Decreased GABA levels in anterior cingulate cortex/medial prefrontal cortex in panic disorder. *Progress in Neuro-Psychopharmacology and Biological Psychiatry, 44*, 131-135.

Long, Z., Medlock, C., Dzemidzic, M., Shin, Y. W., Goddard, A. W., & Dydak, U. (2013). Decreased GABA levels in anterior cingulate cortex/medial prefrontal cortex in panic disorder. *Prog Neuropsychopharmacol Biol Psychiatry, 44*, 131-135. doi: 10.1016/j.pnpbp.2013.01.020 S0278-5846(13)00033-X [pii]

Lu, W., Pauly, K. B., Gold, G. E., Pauly, J. M., & Hargreaves, B. A. (2009). SEMAC: slice encoding for metal artifact correction in MRI. *Magn Reson Med, 62*(1), 66-76.

Maddock, R. J., & Buonocore, M. H. (2012). MR Spectroscopic Studies of the Brain in Psychiatric Disorders. *Curr Top Behav Neurosci*. doi: 10.1007/7854_2011_197

Mader, I., Seeger, U., Weissert, R., Klose, U., Naegele, T., Melms, A., & Grodd, W. (2001). Proton MR spectroscopy with metabolite-nulling reveals elevated macromolecules in acute multiple sclerosis. *Brain, 124*(5), 953-961.

Manfredini, D., Cantini, E., Romagnoli, M., & Bosco, M. (2003). Prevalence of bruxism in patients with different research diagnostic criteria for temporomandibular disorders (RDC/TMD) diagnoses. *Cranio, 21*(4), 279-285.

Manfredini, D., Landi, N., Fantoni, F., Segu, M., & Bosco, M. (2005). Anxiety symptoms in clinically diagnosed bruxers. *J Oral Rehabil, 32*(8), 584-588. doi: JOR1462 [pii] 10.1111/j.1365-2842.2005.01462.x

Manfredini, D., & Lobbezoo, F. (2009). Role of psychosocial factors in the etiology of bruxism. *J Orofac Pain, 23*(2), 153-166.

Mattei, E., Calcagnini, G., Censi, F., Triventi, M., & Bartolini, P. (2010). Numerical Model for Estimating RF-Induced Heating on a Pacemaker Implant During MRI: Experimental Validation. *Biomedical Engineering, IEEE Transactions on, 57*(8), 2045-2052.

Mattei, E., Triventi, M., Calcagnini, G., Censi, F., Kainz, W., Bassen, H. I., & Bartolini, P. (2007). Temperature and SAR measurement errors in the evaluation of metallic linear structures heating during MRI using fluoroptic® probes. *Phys Med Biol, 52*(6), 1633-1646. doi: 10.1088/0031-9155/52/6/006

McCreary, C. P., Clark, G. T., Merril, R. L., Flack, V., & Oakley, M. E. (1991). Psychological distress and diagnostic subgroups of temporomandibular disorder patients. *Pain, 44*(1), 29-34. doi: 0304-3959(91)90143-L [pii]

Medicine, A. A. o. S. Westchester, IL: American Academy of Sleep Medicine; 2005. *International classification of sleep disorders, 2nd ed.: diagnostic and coding manual*, 51-55.

Meletti, S., Cantalupo, G., Volpi, L., Rubboli, G., Magaudda, A., & Tassinari, C. A. (2004). Rhythmic teeth grinding induced by temporal lobe seizures. *Neurology, 62*(12), 2306-2309.

Mescher, M., Merkle, H., Kirsch, J., Garwood, M., & Gruetter, R. (1998a). Simultaneous in vivo spectral editing and water suppression. *NMR Biomed, 11*, 266-272.

Mescher, M., Merkle, H., Kirsch, J., Garwood, M., & Gruetter, R. (1998b). Simultaneous in vivo spectral editing and water suppression. *NMR Biomed, 11*(EPFL-ARTICLE-177509), 266-272.

Mescher, M., Merkle, H., Kirsch, J., Garwood, M., & Gruetter, R. (1998). Simultaneous in vivo spectral editing and water suppression. *NMR in Biomedicine, 11*(6), 266-272.

Meyerhoff, D. J., Mon, A., Metzler, T., & Neylan, T. C. (2014). Cortical gamma-aminobutyric acid and glutamate in posttraumatic stress disorder and their relationships to self-reported sleep quality. *Sleep, 37*(5), 893.

Millan, M. J. (2003). The neurobiology and control of anxious states. *Prog Neurobiol, 70*(2), 83-244. doi: S030100820300087X [pii]

Miller, E. K., & Cohen, J. D. (2001). An integrative theory of prefrontal cortex function. *Annu Rev Neurosci, 24*, 167-202. doi: 10.1146/annurev.neuro.24.1.167
24/1/167 [pii]
Mlynárik, V., Gruber, S., & Moser, E. (2001). Proton T1 and T2 relaxation times of human brain metabolites at 3 Tesla. *NMR Biomed, 14*(5), 325-331.
Mohsin, S. A., Nyenhuis, J. A., & Masood, R. (2010). Interaction of medical implants with the MRI electromagnetic fields. *Prog Electromagn Res B Pier B C, 13*, 195-202.
Monchi, O., Petrides, M., Mejia-Constain, B., & Strafella, A. P. (2007). Cortical activity in Parkinson's disease during executive processing depends on striatal involvement. *Brain, 130*(1), 233-244.
Mongini, F., Ciccone, G., Ceccarelli, M., Baldi, I., & Ferrero, L. (2007). Muscle tenderness in different types of facial pain and its relation to anxiety and depression: A cross-sectional study on 649 patients. *Pain, 131*(1-2), 106-111. doi: S0304-3959(06)00702-0 [pii]
10.1016/j.pain.2006.12.017
Mullins, P. G., McGonigle, D. J., O'Gorman, R. L., Puts, N. A. J., Vidyasagar, R., Evans, C. J., . . . Edden, R. A. E. (2014). Current practice in the use of MEGA-PRESS spectroscopy for the detection of GABA. *NeuroImage, 86*, 43-52. doi: 10.1016/j.neuroimage.2012.12.004
Murdoch, J., & Dydak, U. (2011). *Modeling MEGA-PRESS macromolecules for a better grasp of GABA.* Paper presented at the ISMRM 29th Scientific Meeting & Exhibition, Montreal, Canada.
Near, J., Simpson, R., Cowen, P., & Jezzard, P. (2011). Efficient γ-aminobutyric acid editing at 3T without macromolecule contamination: MEGA-SPECIAL. *NMR Biomed, 24*(10), 1277-1285. doi: 10.1002/nbm.1688
Nie, K., Zhang, Y., Huang, B., Wang, L., Zhao, J., Huang, Z., . . . Wang, L. (2013). Marked N-acetylaspartate and choline metabolite changes in Parkinson's disease patients with mild cognitive impairment. *Parkinsonism & related disorders, 19*(3), 329-334.
O'Gorman, R., Edden, R., Michels, L., Murdoch, J., & Martin, E. (2007). *Precision and repeatability of in vivo GABA and glutamate quantification.* Paper presented at the Proc ISMRM.
O'Neill, J., Schuff, N., Marks, W. J., Feiwell, R., Aminoff, M. J., & Weiner, M. W. (2002). Quantitative 1H magnetic resonance spectroscopy and MRI of Parkinson's disease. *Movement disorders, 17*(5), 917-927.
Obeso, J. A., Rodríguez-Oroz, M. C., Rodríguez, M., Arbizu, J., & Giménez-Amaya, J. M. (2002). The basal ganglia and disorders of movement: pathophysiological mechanisms. *Physiology, 17*(2), 51-55.
Obeso, J. A., Rodriguez-Oroz, M. C., Rodriguez, M., Lanciego, J. L., Artieda, J., Gonzalo, N., & Olanow, C. W. (2000). Pathophysiology of the basal ganglia in Parkinson's disease. *Trends in neurosciences, 23*, S8-S19.
Ohayon, M. M., Li, K. K., & Guilleminault, C. (2001). Risk factors for sleep bruxism in the general population. *Chest, 119*(1), 53-61.

Öngür, D., Prescot, A. P., McCarthy, J., Cohen, B. M., & Renshaw, P. F. (2010). Elevated gamma-aminobutyric acid levels in chronic schizophrenia. *Biological psychiatry, 68*(7), 667-670.

Öz, G., Terpstra, M., Tkáč, I., Aia, P., Lowary, J., Tuite, P. J., & Gruetter, R. (2006). Proton MRS of the unilateral substantia nigra in the human brain at 4 tesla: detection of high GABA concentrations. *Magn Reson Med, 55*(2), 296-301.

Parent, A., & Hazrati, L.-N. (1995). Functional anatomy of the basal ganglia. I. The cortico-basal ganglia-thalamo-cortical loop. *Brain Research Reviews, 20*(1), 91-127.

Park, J. W., Clark, G. T., Kim, Y. K., & Chung, J. W. (2010). Analysis of thermal pain sensitivity and psychological profiles in different subgroups of TMD patients. *Int J Oral Maxillofac Surg, 39*(10), 968-974. doi: S0901-5027(10)00278-X [pii]
10.1016/j.ijom.2010.06.003

Park, S.-M., Kamondetdacha, R., & Nyenhuis, J. A. (2007). Calculation of MRI-induced heating of an implanted medical lead wire with an electric field transfer function. *J Magn Reson Imaging, 26*(5), 1278-1285. doi: 10.1002/jmri.21159

Park, S. M., Kamondetdacha, R., Amjad, A., & Nyenhuis, J. A. (2005). MRI safety: RF-induced heating near straight wires. *IEEE Trans Magn, 41*(10), 4197-4199.

Peers, P. V., Simons, J. S., & Lawrence, A. D. (2013). Prefrontal control of attention to threat. *Front Hum Neurosci, 7*, 24. doi: 10.3389/fnhum.2013.00024

Perry, T. L., Javoy-Agid, F., Agid, Y., & Fibiger, H. C. (1983). Striatal GABAergic neuronal activity is not reduced in Parkinson's disease. *Journal of neurochemistry, 40*(4), 1120-1123.

Petit, D., Touchette, E., Tremblay, R. E., Boivin, M., & Montplaisir, J. (2007). Dyssomnias and parasomnias in early childhood. *Pediatrics, 119*(5), e1016-1025. doi: peds.2006-2132 [pii] 10.1542/peds.2006-2132

Pingitore, G., Chrobak, V., & Petrie, J. (1991). The social and psychologic factors of bruxism. *J Prosthet Dent, 65*(3), 443-446.

Pizzi, S. D., Rossi, C., Di Matteo, V., Esposito, E., Guarnieri, S., Mariggiò, M. A., . . . Onofrj, M. (2013). Morphological and metabolic changes in the nigro-striatal pathway of synthetic proteasome inhibitor (PSI)-treated rats: a MRI and MRS study. *PloS one, 8*(2), e56501.

Poorter, J. D., Wagter, C. D., Deene, Y. D., Thomsen, C., Ståhlberg, F., & Achten, E. (1995). Noninvasive MRI thermometry with the proton resonance frequency (PRF) method: in vivo results in human muscle. *Magn Reson Med, 33*(1), 74-81.

Prater, K. E., Hosanagar, A., Klumpp, H., Angstadt, M., & Phan, K. L. (2013). Aberrant amygdala-frontal cortex connectivity during perception of fearful faces and at rest in generalized social anxiety disorder. *Depress Anxiety, 30*(3), 234-241. doi: 10.1002/da.22014

Provencher, S. (1993). Estimation of metabolite concentrations from localized in vivo proton NMR spectra. *Magn Reson Med: official journal of the Society of Magn Reson Med/Society of Magn Reson Med, 30*(6), 672.

Provencher, S. W. (1993). Estimation of metabolite concentrations from localized in vivo proton NMR spectra. *Magn Reson Med, 30*(6), 672-679.

Provencher, S. W. (2001). Automatic quantitation of localized in vivo1H spectra with LCModel. *NMR Biomed, 14*(4), 260-264.

Provencher, S. W. (2008). LCModel Manual for v6.2-0R.

Puts, N. A. J., & Edden, R. A. E. (2012). In vivo magnetic resonance spectroscopy of GABA: A methodological review. *Progress in Nuclear Magnetic Resonance Spectroscopy, 60*, 29-41. doi: 10.1016/j.pnmrs.2011.06.001

Qian, D., El-Sharkawy, A.-M. M., Bottomley, P. A., & Edelstein, W. A. (2013). An RF dosimeter for independent SAR measurement in MRI scanners. *Med Phys, 40*(12), -. doi: 10.1118/1.4829527

Ranjan, S., P, S. C., & Prabhu, S. (2006). Antidepressant-induced bruxism: need for buspirone? *Int J Neuropsychopharmacol, 9*(4), 485-487. doi: S1461145705005985 [pii] 10.1017/S1461145705005985

Raphael, K. G., Marbach, J. J., Klausner, J. J., Teaford, M. F., & Fischoff, D. K. (2003). Is bruxism severity a predictor of oral splint efficacy in patients with myofascial face pain? *J Oral Rehabil, 30*(1), 17-29. doi: 1117 [pii]

Raphael, K. G., Sirois, D. A., Janal, M. N., Wigren, P. E., Dubrovsky, B., Nemelivsky, L. V., . . . Lavigne, G. J. (2012). Sleep bruxism and myofascial temporomandibular disorders: A laboratory-based polysomnographic investigation. *J Am Dent Assoc, 143*(11), 1223-1231. doi: 143/11/1223 [pii]

Regatte, R. R., Akella, S. V. S., Borthakur, A., Kneeland, J. B., & Reddy, R. (2003). In Vivo Proton MR Three-dimensional T1ρ Mapping of Human Articular Cartilage: Initial Experience1. *Radiology, 229*(1), 269-274. doi: 10.1148/radiol.2291021041

Rieke, V., & Butts Pauly, K. (2008). MR thermometry. *J Magn Reson Imaging, 27*(2), 376-390.

Rosso, I. M., Weiner, M. R., Crowley, D. J., Silveri, M. M., Rauch, S. L., & Jensen, J. E. (2013). Insula and Anterior Cingulate Gaba Levels in Posttraumatic Stress Disorder: Preliminary Findings Using Magnetic Resonance Spectroscopy. *Depress Anxiety*. doi: 10.1002/da.22155

Rosso, I. M., Weiner, M. R., Crowley, D. J., Silveri, M. M., Rauch, S. L., & Jensen, J. E. (2013). Insula and anterior cingulate gaba levels in posttraumatic stress disorder: preliminary findings using magnetic resonance spectroscopy. *Depression and anxiety*.

Rothman, D. L., Behar, K. L., Hetherington, H. P., & Shulman, R. G. (1984). Homonuclear 1H double-resonance difference spectroscopy of the rat brain in vivo. *Proceedings of the National Academy of Sciences, 81*(20), 6330-6334.

Rothman, D. L., Behar, K. L., Prichard, J. W., & Petroff, O. A. C. (1997). Homocarnosine and the measurement of neuronal pH in patients with epilepsy. *Magn Reson Med, 38*(6), 924-929. doi: 10.1002/mrm.1910380611

Rothman, D. L., Petroff, O. A., Behar, K. L., & Mattson, R. H. (1993). Localized 1H NMR measurements of gamma-aminobutyric acid in human brain in vivo. *Proc Natl Acad Sci U S A, 90*(12), 5662-5666.

Schaller, B., Xin, L., Cudalbu, C., & Gruetter, R. (2013). Quantification of the neurochemical profile using simulated macromolecule resonances at 3 T. *NMR Biomed, 26*(5), 593-599. doi: 10.1002/nbm.2896

Schmitz, T. W., Cheng, F. H., & De Rosa, E. (2010). Failing to ignore: paradoxical neural effects of perceptual load on early attentional selection in normal aging. *J Neurosci, 30*(44), 14750-14758. doi: 10.1523/JNEUROSCI.2687-10.2010 30/44/14750 [pii]

Schneider, W. G., Bernstein, H. J., & Pople, J. A. (1958). Proton Magnetic Resonance Chemical Shift of Free (Gaseous) and Associated (Liquid) Hydride Molecules. *J Chem Phys, 28*(4), 601-607. doi: doi:http://dx.doi.org/10.1063/1.1744199

Seraji-Bozorgzad, N., Bao, F., Shneyder, N., George, E., Martinez, C. S., Gorden, V., . . . Khan, O. (2014). Quantitative MRI Biomarker Study in Parkinson's Disease: High-field 1H-MR Spectroscopic and Multi-Modal MRI Longitudinal Study of the Substantia Nigra (P6. 069). *Neurology, 82*(10 Supplement), P6. 069-P066. 069.

Shapiro, E. M., Borthakur, A., & Reddy, R. (2000). MR imaging of RF heating using a paramagnetic doped agarose phantom. *MAGMA, 10*(2), 114-121.

Shellock, F. (2001). *Magnetic Resonance Procedures: Health effects and safety*: CRC Press.

Sjoholm, T. T., Lehtinen, I., & Piha, S. J. (1996). The effect of propranolol on sleep bruxism: hypothetical considerations based on a case study. *Clin Auton Res, 6*(1), 37-40.

Smith, M. T., Wickwire, E. M., Grace, E. G., Edwards, R. R., Buenaver, L. F., Peterson, S., . . . Haythornthwaite, J. A. (2009). Sleep disorders and their association with laboratory pain sensitivity in temporomandibular joint disorder. *Sleep, 32*(6), 779-790.

Stagg, C., & Rothman, D. L. (2013). *Magnetic Resonance Spectroscopy: Tools for Neuroscience Research and Emerging Clinical Applications*: Academic Press.

Stefani, A., Fedele, E., Pierantozzi, M., Galati, S., Marzetti, F., Peppe, A., . . . Stanzione, P. (2011). Reduced GABA Content in the Motor Thalamus during Effective Deep Brain Stimulation of the Subthalamic Nucleus. *Frontiers in Systems Neuroscience, 5*, 17. doi: 10.3389/fnsys.2011.00017

Stefani, A., Fedele, E., Vitek, J., Pierantozzi, M., Galati, S., Marzetti, F., . . . Stanzione, P. (2011). The clinical efficacy of L-DOPA and STN-DBS share a common marker: reduced GABA content in the motor thalamus. *Cell Death and Dis, 2*, e154.

Sun, Y., Sugawara, M., Mulkern, R. V., Hynynen, K., Mochizuki, S., Albert, M., & Zuo, C. S. (2000). Simultaneous measurements of temperature and pH in vivo using NMR in conjunction with TmDOTP5−. *NMR in Biomedicine, 13*(8), 460-466. doi: 10.1002/nbm.676

Terpstra, M., Ugurbil, K., & Tkac, I. (2010). Noninvasive quantification of human brain ascorbate concentration using (1)H NMR spectroscopy at 7 T. *NMR Biomed, 23*(3), 227-232. doi: 10.1002/nbm.1423

Tkáč, I., Öz, G., Adriany, G., Uğurbil, K., & Gruetter, R. (2009). In vivo 1H NMR spectroscopy of the human brain at high magnetic fields: Metabolite quantification at 4T vs. 7T. *Magn Reson Med, 62*(4), 868-879. doi: 10.1002/mrm.22086

Tosun, T., Karabuda, C., & Cuhadaroglu, C. (2003). Evaluation of sleep bruxism by polysomnographic analysis in patients with dental implants. *Int J Oral Maxillofac Implants, 18*(2), 286-292.

Twelves, D., Perkins, K. S., & Counsell, C. (2003). Systematic review of incidence studies of Parkinson's disease. *Mov Disord, 18*(1), 19-31.

Van Cauter, E. (2005). Endocrine physiology. *Principles and practice of sleep medicine, 4*, 266-282.

Wheaton, A. J., Borthakur, A., Corbo, M., Charagundla, S. R., & Reddy, R. (2004). Method for reduced SAR T1ρ-weighted MRI. *Magn Reson Med, 51*(6), 1096-1102. doi: 10.1002/mrm.20141

Wichmann, T., & Delong, M. R. (2007). Anatomy and physiology of the basal ganglia: relevance to Parkinson's disease and related disorders. *Handbook of clinical neurology, 83*, 1.

Winocur, E., Gavish, A., Voikovitch, M., Emodi-Perlman, A., & Eli, I. (2003). Drugs and bruxism: a critical review. *J Orofac Pain, 17*(2), 99-111.

Wolf, S., Diehl, D., Gebhardt, M., Mallow, J., & Speck, O. (2013). SAR simulations for high-field MRI: How much detail, effort, and accuracy is needed? *Magn Reson Med, 69*(4), 1157-1168. doi: 10.1002/mrm.24329

Wong, D., Dzemidzic, M., Talavage, T. M., Romito, L. M., & Byrd, K. E. (2011). Motor control of jaw movements: An fMRI study of parafunctional clench and grind behavior. *Brain Res, 1383*, 206-217. doi: S0006-8993(11)00204-6 [pii] 10.1016/j.brainres.2011.01.096

Yeo, D. T., Wang, Z., Loew, W., Vogel, M. W., & Hancu, I. (2011). Local SAR in High Pass Birdcage and TEM Body Coils for Multiple Human Body Models in Clinical Landmark Positions at 3T. *J Magn Reson Imaging: JMRI, 33*(5), 1209.

Yoon, J. H., Maddock, R. J., Rokem, A., Silver, M. A., Minzenberg, M. J., Ragland, J. D., & Carter, C. S. (2010). GABA concentration is reduced in visual cortex in schizophrenia and correlates with orientation-specific surround suppression. *The Journal of neuroscience, 30*(10), 3777-3781.

Zhou, B., Yuan, F., He, Z., & Tan, C. (2014). Application of proton magnetic resonance spectroscopy on substantia nigra metabolites in Parkinson’s disease. *Brain Imaging Behav, 8*(1), 97-101.

Zuo, C. S., Bowers, J. L., Metz, K. R., Nosaka, T., Sherry, A. D., & Clouse, M. E. (1996). TmDOTP5−: A substance for NMR temperature measurements in vivo. *Magn Reson Med, 36*(6), 955-959. doi: 10.1002/mrm.1910360619

Zuo, C. S., Mahmood, A., & Sherry, A. D. (2001). TmDOTA−: A sensitive probe for MR thermometry in vivo. *Journal of Magnetic Resonance, 151*(1), 101-106.

Zuo, C. S., Metz, K. R., Sun, Y., & Sherry, A. D. (1998). NMR Temperature Measurements Using a Paramagnetic Lanthanide Complex. *J Magn Reson, 133*(1), 53-60. doi: DOI: 10.1006/jmre.1998.1429

VITA

VITA

Shalmali Dharmadhikari

Education

- Purdue University — W. Lafayette, IN, USA
  CAMPEP Accredited
  Doctor of Philosophy, Medical Physics
  GPA: 3.99/4.0
  (08/09 – present)

- University of Iowa — Iowa City, IA, USA
  Master of Science, Biomedical Engineering
  GPA: 3.71/4.0
  (08/06 – 12/08)

- University of Pune — Pune, India
  Bachelor of Engineering, Instrumentation and Process Control
  (06/02 – 06/06)

Research Experience

- Purdue University — W. Lafayette, IN, USA
  Research Assistant
  (08/09 – present)

  A. Gamma-aminobutyric acid (GABA) MR Spectroscopy (MRS) of brain: Setup and optimization of novel J-edited single voxel GABA MRS pulse sequences on different MRI scanners and researching methods for reliable post-processing and quantification of GABA.

  Projects:
  - Brain metabolite changes in patients with mild to moderate Parkinson's Disease
  - Effects of chronic manganese exposure on neurotransmitters in non-human primates
  - Neurochemical changes in bruxing individuals
  - Role of striatal neurotransmitters in predicting action cascading and response inhibition

B. MR thermometry for evaluating radio-frequency safety in MRI:
Developed a novel MR thermometry technique on 9 T MRI using paramagnetic lanthanide complexes to determine RF-induced heating.

Other projects:

- In vivo MRI detection of super-paramagnetic nanoparticles for photo-thermal therapy:
  Setup and optimization of pulse sequences on 9 T MRI for imaging of nanoparticles uptake in mice breast tumors

- Indiana University School of Medicine — Indianapolis, IN, USA
  Research Technician — (12/08 – 08/09)
  Provided research support (from acquisition to analysis) for 9 T and 3 T MRI scanners. Also assisted the faculty in writing research grants.

- University of Iowa — Iowa City, IA, USA
  Research Assistant — (08/07 – 08/08)
  Developed a C++ code to improve the intra-patient airway tree matching accuracy of an automated program.

Other training and experience

- Indiana University School of Medicine — Indianapolis, IN, USA
  Radiological Imaging Quality Assurance Internship — (08/14 – present)

- Indiana University School of Medicine — Indianapolis, IN, USA
  MRI-Physicist Intern — (01/10 – 12/10)

- Harbor Branch Oceanographic Institute — Fort Pierce, FL, USA
  Summer Intern — (05/07 – 08/07)

- University of Iowa — Iowa City, IA, USA
  Teaching Assistant — (01/07 – 05/07)

Honors and Awards

2015 Trainee Education Stipend award for Joint Annual Meeting ISMRM-ESMRMB 2015, Toronto, Canada
2014 Kessler Graduate Student Award for best graduate student in Health Sciences (based on academic and research achievements)
2014 Trainee Education Stipend award for Joint Annual Meeting ISMRM-ESMRMB 2014, Milan, Italy

2014 Student Travel Award for Society of Toxicology 53rd Annual Meeting, Phoenix, AZ, USA
2013 Second award for an oral presentation at the 38th Campbell-Klatte Annual Oration by Indiana University School of Medicine Department of Radiology and Imaging Sciences, Indianapolis, USA
2013 Recipient of the Purdue Research Fund Grant for academic year 2013-2014
2013 Trainee Education Stipend award for ISMRM 21st Annual Meeting and Exhibition, Salt Lake City, USA
2012 Recipient of the Purdue Research Fund Grant for academic year 2012-2013
2011 Trainee Education Stipend award for ISMRM 19th Annual Meeting and Exhibition, Montreal, Canada
2008 Best Poster Award Engineering Research Open House Poster Competition at the University of Iowa, IA, USA

PUBLICATIONS

PUBLICATIONS

Peer-Reviewed Journal Publications

- **Dharmadhikari S**, Romito L, Dzemidzic M, Dydak U, Xu J, Bodkin C L, Manchanda S, Byrd K. GABA and Glutamate Levels in Occlusal Splint-Wearing Males with Possible Bruxism. Published online in March 2015, Archives of Oral Biology. doi:10.1016/j.archoralbio.2015.03.006.

- Yildiz A*, C Quetscher C*, **Dharmadhikari S**, Chmielewski W, Glaubitz B, Schmidt-Wilcke T, Edden R, Dydak U, Beste C. Feeling safe in the plane: neural mechanisms underlying superior action control in airplane pilot trainees – a combined EEG/MRS study. Published online in April 2014, Hum. Brain Mapp. *2014 35(10):5040-51. PMID: 24753040*.doi: 10.1002/hbm.22530.

- Quetscher C, Yildiz A, **Dharmadhikari S**, Glaubitz B, Schmidt-Wilcke T, Dydak U, and Beste C. Striatal GABA levels predict response inhibition performance and its cortical electrophysiological correlates. Brain Structure and Function, Aug 2014. doi:10.1007/s00429-014-0873-y.

- Reinhardt J, Ding K, Cao K, Christensen G, Hoffman E, **Bodas S**. Registration-based estimates of local lung tissue expansion compared to xenon-CT measures of specific ventilation. Medical Image Analysis 2008 Dec; 12(6):752-63.

Publications under review/in preparation

- **Dharmadhikari S**, James J R, Nyenhuis J, Bansal N. Evaluation of RF safety by high temperature resolution MR thermometry using a paramagnetic lanthanide complex. Minor revision in preparation for Magnetic Resonance in Medicine.

- **Dharmadhikari S**, Ma R, Yeh C, Snyder S, Zauber E Z, Dydak U. Thalamic GABA elevation in Parkinson patients correlates with worsening disease severity. In preparation for submission to Movement Disorders.

- **Dharmadhikari S**, Ma R, Yeh C, Stock A, Dydak U, Beste C. Striatal and thalamic GABA level concentrations play differential roles for the modulation of response selection processes by proprioceptive information. Submitted to NeuroImage.

- **Dharmadhikari S**, James J R, Pakin K, Bansal N**.** Book chapter titled **"**MR Thermometry Using Paramagnetic Lanthanide Complexes" in the book "RF Safety for MRI" to be published by Wiley Publication. In preparation.

Presentations at International Conferences

- **Dharmadhikari S**, Ma R, Yeh CL, Snyder S, Zauber SE, Dydak U. ^{1}MRS of Basal-Ganglia in Parkinson's Disease Reveals Higher GABA Levels. Accepted for poster presentation at the Joint Annual Meeting ISMRM-ESMRMB 2015, Toronto, Canada.

- Zauber SE, **Dharmadhikari S**, Snyder S, Dydak U. Elevated Thalamic GABA Levels in Parkinson disease, measured by 3 Tesla MR spectroscopy, correlate with disease severity. Accepted for presentation at the American Academy of Neurology 67th Annual Meeting, Washington, DC, USA.

- Dydak U, **Dharmadhikari S**, Snyder Zauber SE. Increased Thalamic GABA levels correlate with disease severity. Presented at the 12th International Conference on Alzheimer's and Parkinson's Diseases AD/PD 2015, Nice, France.

- **Dharmadhikari S**, Casjens S, Glaubitz B, Lehnert M, Quetscher C, Lotz A, Brüning T, Schmidt-Wilcke T, Beste C, Pesch B, Woitalla D, Dydak U. Correlation of GABA Levels and Motor Performance in Parkinson's disease. Presented at Joint Annual Meeting ISMRM-ESMRMB 2014, Milan, Italy. Proc. Intl. Soc. Mag. Reson. Med. 22. May 2014.

- **Dharmadhikari S**, Yildiz A, Quetscher C, Chmielewski W, Dydak U, Beste U. Higher Striatal GABA Relates To A More Serial And Efficient Mode Of Action Cascading And Stronger Attentional Gating In Airplane Pilots. Presented at Joint Annual Meeting ISMRM-ESMRMB 2014, Milan, Italy. Proc. Intl. Soc. Mag. Reson. Med. 22. May 2014.

- **Dharmadhikari S**, Ma R, Long Z, Yeh CL, et al. Manganese Neurotoxicity: In Vivo GABA Levels Correlate with Motor Deficits in US Welders.Presented at Society of Toxicology 53rd annual meeting at Phoenix, AZ, USA. March 2014.

- **Dharmadhikari S**, Romito L, Dydak U, Dzemidzic M, and Byrd K. Single voxel MEGA-edited GABA and short TE ^{1}H MRS in hippocampus and other brain regions implicated in bruxism. Presented at ISMRM 21^{s}t Annual Meeting and Exhibition, Salt Lake City, UT, USA. April 2013.

- **Dharmadhikari S**, McGlothan J, Edden R, Barker P, Schneider J, Dydak U, Guilarte TR. Neurochemical alterations in the non-human primate brain during chronic exposure to Manganese: A ^{1}H MRS study. Presented at Society of Toxicology 52nd annual meeting at San Antonio, TX, USA. March 2013.

- **Dharmadhikari S**, Dydak U, Dzemidzic M, Romito L, Byrd K. Quantification of GABA and other metabolite levels in brain regions implicated in PTSD, temporomandibular disorder, and traumatic brain injury. Presented at Society for Neuroscience 2012 meeting, New Orleans, LA, USA. Oct 2012.

- **Dharmadhikari S,** Xu J, Epur A, Zheng W, Dydak U. Increased cortical GABA levels in Manganese treated rats. Presented at Society of Toxicology 51st Annual Meeting, San Francisco, CA, USA. March 2012.

- **Dharmadhikari S**, Bansal N. Evaluation of SAR using MR Thermometry with Thulium 1,4,7,10-tetraazacyclododecane-1,4,7,10-tetrakis(Methylene Phosphonate) (TmDOTP^{5-}) for RF Safety in MRI. Presented at RSNA 97th Scientific Assembly and Annual Meeting, Chicago, IL, USA. Nov 2011.

- **Dharmadhikari S**, Bansal N. MR Thermometry using a paramagnetic lanthanide complex for evaluation of RF safety. Presented at ISMRM 19th Annual Meeting and Exhibition, Montreal, Canada. May 2011.

- **Dharmadhikari S**, Choi M, Bansal N, Clare S and Halas N. MR Imaging Detection of bifunctional super-paramagnetic nanoparticles for photothermal therapy of hypoxic tumors. Oral presentation at RSNA 96th Scientific Assembly and Annual Meeting, Chicago, IL, USA. Nov 2010.

Presentations at local/national meetings

- **Dharmadhikari S**, Yeh CL, McGlothan JL, Edden R, Barker P, Schneider J, Dydak U, Guilarte TR. MRI and ^{1}H MRS evaluation of chronic manganese exposure in non-human primates. Presented at the AAPM Ohio River Valley Chapter Spring Symposium 2013, Erlanger, KY, USA. March 2013.

- Clare SE, Choi M, Badve S, Nakshatri H, **Dharmadhikari S**, Bansal N, Bardhan R and Halas N J. Delivery of Nanotherapeutics Using a Cellular Trojan Horse. Presented at 2010 Material Research Society Fall meeting: Symposium QQ: Nanofunctional Materials, Nanostructures, and Nanodevices for Biomedical Applications II, Boston, MA, USA. Nov 2010.

• **Dharmadhikari S**, Bansal N. A novel method for calorimetric SAR measurement using hyperfine-shifted resonance from $TmDOTP^{5-}$. Presented at the 2010 ISMRM MR-safety Workshop, Stillwater, MN, USA. Oct 2010.

• Choi M, Bardhan R, Badve S, Nakshatri H, **Dharmadhikari S**, Bansal N, Halas N, Clare S. Delivery of Therapeutic Nanoshells to Hypoxic areas of Tumors Using a Cellular Trojan Horse. Presented at San Antonio Breast Cancer Symposium, San Antonio, TX, USA. Dec 2009.

• **Bodas S**, Reinhardt J. Matching intra-patient airway trees using association graph: the effects of labels on matching accuracy. Presented at International Summit: Future of Quantitative and Functional Lung Imaging, IA, USA**.** Oct 2008.

• **Bodas S**, Reinhardt J. Effect of anatomical labels on label-guided Airway Tree Matching. Presented at Engineering Research Open House Poster Competition, University of Iowa, IA, USA**.** April 2008.